Coherent exclusive exponentiation for precision Monte Carlo calculations

S. Jadach
Department of Physics and Astronomy, The University of Tennessee, Knoxville, Tennessee 37996-1200 and Institute of Nuclear Physics, ul. Kawiory 26a, 30-055 Cracow, Poland

B. F. L. Ward
Department of Physics and Astronomy, The University of Tennessee, Knoxville, Tennessee 37996-1200 and SLAC, Stanford University, Stanford, California 94309

Z. Wąs
Institute of Nuclear Physics, ul. Kawiory 26a, 30-055 Cracow, Poland and CERN, Theory Division, CH-1211 Geneva 23, Switzerland

(Received 5 July 2000; published 1 May 2001)

We present the new coherent exclusive exponentiation (CEEX), the older exclusive exponentiation (EEX), and the semianalytical inclusive exponentiation (IEX) for the process $e^-e^+ \to f\bar{f}+n\gamma$, where $f=\mu,\tau,d,u,s,c,b$, which are valid for center-of-mass energies from the τ lepton threshold to 1 TeV, that is, for CERN LEP1, LEP2, the SLC, future linear colliders, and b,c,τ factories, etc. The approaches are based on Yennie-Frautschi-Suura exponentiation. In CEEX, the effects due to photon emission from initial beams and outgoing fermions are calculated in QED up to second order, including all interference effects. Electroweak corrections are included to first order, at the amplitude level. Beams can be polarized longitudinally and transversely, and all spin correlations are incorporated in an exact manner. The EEX is more primitive, lacks initial-final interferences, but it is valuable for testing the newer CEEX. The IEX provides us with a set of sophisticated semianalytical formulas for the total cross section and selected inclusive distributions, which are mainly used for cross-checks of the Monte Carlo results. We analyze numerical results at the Z peak, 189 GeV and 500 GeV for simple kinematical cuts (comparisons with inclusive exponentiation) and for realistic experimental cuts. The physical precision and technical precision are determined for the total cross section and for the charge asymmetry.

DOI: 10.1103/PhysRevD.63.113009 PACS number(s): 12.15.Ji, 13.10.+q, 13.38.Dg, 14.70.Hp

I. INTRODUCTION

At the end of the CERN e^+e^- collider LEP2 operation, the total cross section for the process $e^-e^+ \to f\bar{f}+n\gamma$ will have to be calculated with the precision 0.2–1 %, depending on the event selection. The arbitrary differential distributions also have to be calculated with the corresponding precision. In future linear colliders (LCs) the precision requirement can be even more demanding. This is especially true for the high-luminosity linear colliders, such as in the case of the DESY TeV Energy Superconducting Linear Accelerator (TESLA). The above new requirements necessitate the development of a new calculational framework for the QED corrections and the construction of new dedicated Monte Carlo (MC) programs. The present work is a part of the effort made in this direction.

The main limiting factor preventing us from getting more precise theoretical predictions for the $e^-e^+ \to f\bar{f}+n\gamma$ process is higher-order QED radiative corrections (the QED part of the electroweak standard model). In order to achieve the 0.2% precision tag, the virtual corrections have to be calculated up to two or three loops and the multiple bremsstrahlung up to two or three hard photons, integrating exactly the multiphoton phase-space for the arbitrary event selection (phase-space limits).

For any realistic kinematical cuts, one cannot get the precise theoretical predictions for $e^-e^+ \to f\bar{f}+n\gamma$ at the above ambitious precision level without Monte Carlo event generators. It is therefore mandatory to formulate perturbative standard model (SM) calculations in a way that facilitates their use within a Monte Carlo event generator.

Let us stress that the Monte Carlo method is for us nothing more (or less) than the numerical integration over the Lorentz invariant phase-space. It is therefore an exercise in applied mathematics. In the present work we shall not, however, elaborate on the methods of the Monte Carlo phase-space integration and construction of the Monte Carlo event generator. This is delegated to Ref. [1], which describes the new Monte Carlo event generator $\mathcal{KK}$ in which the matrix element of the present paper is implemented. All numerical results presented here are calculated using the version 4.13 of $\mathcal{KK}$.

In the present work we concentrate on the definition and construction of the matrix element for the process $e^-e^+ \to f\bar{f}$ within the standard model. We shall especially address the problem of the higher-order QED corrections. This work is a continuation of two recent papers [2,3].

A. Two types of QED matrix elements and exponentiations

In the $\mathcal{KK}$ Monte Carlo and in this paper, we use two types of matrix element, with two types of exponentiation: exclusive exponentiation, nicknamed EEX, and coherent ex-

 ©2001 The American Physical Society

clusive exponentiation, referred to as CEEX. Both are termed ''exclusive'' as opposed to ''inclusive,'' see also the discussion in [4]. Exclusivity means that the procedure of exponentiation, that is summing up the infrared (IR) real and virtual contribution, within the standard perturbative scheme of quantum field theory, is done at the level of the fully differential (multiphoton) cross section or, even better, at the level of the scattering matrix element (spin amplitudes), *before any phase-space integration over photon momenta is done*.

The other ''inclusive'' exponentiation is an *ad hoc* procedure of summing up IR corrections *after phase-space integration over photon momenta*, that is, for inclusive distributions. In spite of its weak theoretical basis the inclusive exponentiation is very commonly done routinely in all semianalytical approaches such as that in Ref. [5]. In Sec. V A we shall come back to inclusive exponentiation and show how to justify it theoretically.

The two exclusive exponentiations EEX and CEEX are well suited for the fully exclusive Monte Carlo event generators in which the four momenta of all final-state particles are available. Historically EEX was formulated for the first time in Ref. [6] for the initial-state radiation (ISR) and an improved version was presented in Ref. [7]. It follows very closely the Yennie-Frautschi-Suura (YFS) exponentiation of the classical Ref. [8]. The extension of EEX to the final-state radiation (FSR) was done shortly thereafter [9], but it was actually never fully published. The computer program YFS3, in which EEX for FSR was implemented, was incorporated in KORALZ [10] and some numerical results were published in [9], without actually giving the details of the QED matrix element. The present work gives in fact the first full account of the EEX matrix element for ISR and FSR for the process $e^-e^+ \to f\bar{f}+n\gamma, f\neq e$. This is to be contrasted with the situation for small-angle Bhabha scattering [the well-known LEP or SLAC Linear Collider (SLC) luminosity process], for which the EEX-type matrix element was fully documented in Refs. [11–13].

CEEX is a new version of the exclusive exponentiation, generally more efficient for calculations beyond first order, facilitating inclusion of full spin polarization, narrow resonances, and any kind of interferences. Its first version, limited to first order, was presented in Ref. [3]. In the present work we extend it to (still incomplete) second order.

Let us characterize briefly the main features of EEX and CEEX. EEX is formulated in terms of spin summed or averaged differential distributions; this is the source of some advantages and disadvantages that may be summarized as follows.

The differential distributions in practice are given analytically in terms of Mandelstam variables and scattering angles; they are therefore easily inspected by looking and the correctness of certain important limits, such as the leading-logarithmic and soft limits, is quickly recognized.

The analytical representation of the differential distributions allows for analytical phase-space integration and development of the semianalytical formulas, which are useful for cross-checking with the MC results.

The spin effects are difficult to add already at $\mathcal{O}(\alpha^1)$, because one is forced to calculate radiative corrections to spin density matrices, not an easy task.

The squaring of the sums of spin amplitudes from groups of Feynman diagrams leads to many interference terms, which in the exponentiation procedure are handled analytically and individually. The interference terms can therefore be dealt with efficiently in EEX only for simple processes dominated by a small number of Feynman diagrams and only up to first order.

CEEX is formulated in terms of spin amplitudes, and this is also the source of some advantages and disadvantages.

The differential distributions are calculated out of spin amplitudes numerically—spin amplitudes are generally simpler/smaller objects, especially beyond $\mathcal{O}(\alpha^1)$.

Since an analytical representation for the differential distributions is not available, the semianalytical integration over the phase-space is practically impossible.

The spin effects are added relatively easily, during numerical evaluation of the differential distributions calculated out of the spin amplitudes. The addition of the higher-order corrections does not make the treatment of spin polarization more difficult.

The inclusion of all kinds of interference effects (among which are real photon emissions, many Feynman diagrams, etc.) comes almost for free—it is done numerically in the process of summing and squaring the various contributions to the spin amplitudes.

As we see, CEEX has many advantages over EEX, so why do we keep EEX? There are important reasons.

Generally, CEEX is a relatively new invention; the older and more primitive but well-established EEX is a useful reference for numerical tests of CEEX.

EEX is better suited for semianalytical integration over the phase-space, and can be tested with these semianalytical results.

In the present $\mathcal{KK}$ MC the $\mathcal{O}(\alpha^3)$ leading logarithmic corrections are available for EEX and are not yet available for CEEX.

Summarizing, we see that it makes sense to keep EEX as a backup solution, even if we already rely on CEEX as a default and leading solution.

B. Notation, terminology

It is useful to introduce certain notations and terminology already at this stage. In particular, the most common perturbative calculation (no exponentiation) is ''order-by-order.'' This means that all of the terms beyond a certain order are set to zero. In Fig. 1, it means that we end at a certain row—at $\mathcal{O}(\alpha^2)$ we include the first three rows. Exponentiation blurs this picture because a certain class of terms is summed up to infinite order and the meaning of the rth order exponentiation is that we truncate to $\mathcal{O}(\alpha^r)$ the infrared finite components, the so-called $\bar{\beta}$'s. On the other hand, in the leading-logarithmic (LL) approximation the focus is on summing up first the contributions like $\alpha^n L^n$ and later those like $\alpha^n L^{n-1}$, that is in Fig. 1 we sum up columnwise, neglecting terms far away from the first column, which represents the

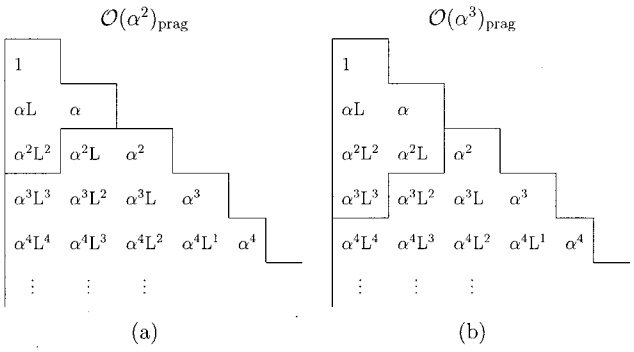

FIG. 1. QED perturbative leading and subleading corrections. The rows represent the corrections in consecutive perturbative orders; the first row is the Born contribution. The first column represents the leading-logarithmic (LL) approximation and the second column the next-to-leading (NLL) approximation. In the figure, the terms selected for the (a) second- and (b) third-order pragmatic expansions are limited by an additional line. Here, $L=\ln(s/m_f^2)$ for the respective fermion mass m_f.

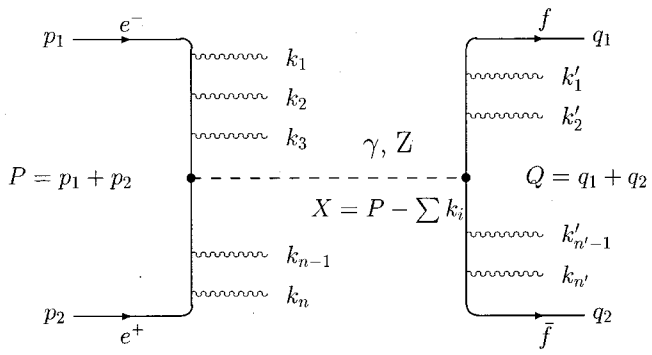

FIG. 2. The kinematics of the process with multiple photon emission from the initial- and final-state fermions in the annihilation process.

so-called LL approximation. Taking the actual value of $\alpha/\pi\sim 1/400$ and of the big logarithm $L=\ln(s/m_f^2)\sim 10$, we discover quickly that in Fig. 1 the limiting line following the numerical importance of the terms is neither row-wise nor columnwise but diagonalwise. This is why we shall often use the $\mathcal{O}(\alpha^r)_{prag}$, $r=1,2,3$ approximation, depicted also in Fig. 1, wherein we use (exponentiated or not) the $\mathcal{O}(\alpha^r)$ calculation in which we use incomplete subleading terms, in the sense of the LL approximation. Note that for the LL approximation we shall never use the strict collinear (zero p_T) approximation. The LL approximation will be done at the level of the differential distributions (or spin amplitudes) without forcing $p_T=0$ on the photons. Just to give the reader a rough idea, the precision level of order 0.5–1% corresponds to the $\mathcal{O}(\alpha^1)_{prag}$, 0.1–0.5 % to the $\mathcal{O}(\alpha^2)_{prag}$, and going below 0.05% will require the $\mathcal{O}(\alpha^3)_{prag}$. The above is true for the exponentiated calculation. The lack of exponentiation makes the calculation less precise by a factor of 2–5. The pure nonlogarithmic terms of the $\mathcal{O}(\alpha^2)$ are negligible ($<10^{-5}$) for any foreseeable practical application.

C. Outline

The outline of the paper is the following. In Sec. II we describe in detail the SM/QED matrix element for the exclusive exponentiation based on the Yennie-Frautschi-Suura work of Ref. [8], that is, for the type of matrix element defined for the first time in Ref. [6]. In Sec. II we describe the new second-order matrix element with coherent exclusive exponentiation, which is the default matrix element in $\mathcal{KK}$ MC. Its first-order variant was given in [3], and is also defined here for the sake of completeness. In Sec. III we elaborate on how we combine the electroweak corrections of Refs. [5,14] with the QED corrections within EEX and CEEX. In Sec. IV we discuss the differences between EEX and CEEX. In Sec. V we integrate analytically over the phase-space for the EEX matrix element in the case of very simple kinematical cuts. The resulting analytical results are used in Sec. VI, where numerical results from the $\mathcal{KK}$ MC are presented. The most important task presented in Sec. VI is, however, the determination of the physical and technical precisions for the total cross section and charge asymmetry at the Z peak, LEP2, and 500 GeV. In particular we discuss the contribution from the initial-final state interference (IFI), which is included in our new CEEX matrix element (IFI is neglected in EEX). In the last section we summarize our work. In the Appendix we define the Weyl-spinor techniques used in the construction of the CEEX multiphoton spin amplitudes.

II. AMPLITUDES FOR EXCLUSIVE EXPONENTIATION

As was already indicated, the role of the EEX matrix element described in this section is to provide a testing environment for the new, more sophisticated matrix element of the CEEX class, which will be defined in the next section.

The kinematics of the process $e^-e^+\to f\bar{f}+n\gamma$ is depicted in Fig. 2. In the case of the EEX matrix element presented here, we neglect the initial-final state interference. Consequently, we are allowed in the following to distinguish between photons emitted from the initial-state fermions and those emitted from the final-state fermions. The four-momentum

$$X=p_1+p_2-\sum_{j=1}^{n} k_j=q_1+q_2+\sum_{l=1}^{n'} k_l' \tag{1}$$

of the s-channel virtual boson $Z+\gamma$ is then well defined. Let us denote the rest frame of X as XMS (the X zero momentum system).

A. Master formula

Denoting the Lorentz-invariant phase-space by

$$d^n\mathrm{Lips}(P;p_1,p_2,\ldots,p_n)=\prod_{j=1}^{n}\frac{d^3p_j}{p_j^0}\,\delta^{(4)}\left(P-\sum_{j=1}^{n}p_j\right), \tag{2}$$

we define, for the process $e^-(p_1)+e^+(p_2)\to f(q_1)+\bar{f}(q_2)+n\gamma(k_j)+n'\gamma(k_l')$, the $\mathcal{O}(\alpha^r)$ total cross section:

$$\sigma^{(r)}_{EEX}=\sum_{n=0}^{\infty}\sum_{n'=0}^{\infty}\frac{1}{n!}\frac{1}{n'!}\int d^{n+n'+2}\mathrm{Lips}(p_1+p_2;q_1,q_2,k_1\ldots,k_n,k'_1\ldots,k'_{n'})\rho^{(r)}_{EEX},\quad r=0,1,2,3, \tag{3}$$

in terms of the fully differential multiphoton distribution

$$\begin{aligned}
&\rho^{(r)}_{EEX}(p_1,p_2,q_1,q_2,k_1\ldots,k_n,k'_1\ldots,k'_n)\\
&\quad=\exp[Y_e(\Omega_I;p_1,p_2)+Y_f(\Omega_F;q_1,q_2)]\prod_{j=1}^{n}\tilde{S}_I(k_j)\bar{\Theta}(\Omega_I;k_j)\prod_{l=1}^{n'}\tilde{S}_F(k'_l)\bar{\Theta}(\Omega_F;k'_l)\Bigg\{\bar{\beta}^{(r)}_0(X,p_1,p_2,q_1,q_2)\\
&\quad+\sum_{j=1}^{n}\frac{\bar{\beta}^{(r)}_{1I}(X,p_1,p_2,q_1,q_2,k_j)}{\tilde{S}_I(k_j)}+\sum_{l=1}^{n'}\frac{\bar{\beta}^{(r)}_{1F}(X,p_1,p_2,q_1,q_2,k'_l)}{\tilde{S}_F(k'_l)}+\sum_{n\geqslant j>k\geqslant 1}\frac{\bar{\beta}^{(r)}_{2II}(X,p_1,p_2,q_1,q_2,k_j,k_k)}{\tilde{S}_I(k_j)\tilde{S}_I(k_k)}\\
&\quad+\sum_{n'\geqslant l>m\geqslant 1}\frac{\bar{\beta}^{(r)}_{2FF}(X,p_1,p_2,q_1,q_2,k'_l,k'_m)}{\tilde{S}_F(k'_l)\tilde{S}_F(k'_m)}+\sum_{j=1}^{n}\sum_{l=1}^{n'}\frac{\bar{\beta}^{(r)}_{2IF}(X,p_1,p_2,q_1,q_2,k_j,k'_l)}{\tilde{S}_I(k_j)\tilde{S}_F(k'_l)}\\
&\quad+\sum_{n\geqslant j>k>l\geqslant 1}\frac{\bar{\beta}^{(r)}_{3III}(X,p_1,p_2,q_1,q_2,k_j,k_k,k_l)}{\tilde{S}_I(k_j)\tilde{S}_I(k_k)\tilde{S}_I(k_l)}\Bigg\}.
\end{aligned} \tag{4}$$

Let us explain the notation and physics content in the above expression. The YFS soft factors for real photons emitted from the initial- and final-state fermions read

$$\tilde{S}_I(k_j)=-Q_e^2\frac{\alpha}{4\pi^2}\left(\frac{p_1}{k_jp_1}-\frac{p_2}{k_jp_2}\right)^2,$$

$$\tilde{S}_F(k'_l)=-Q_f^2\frac{\alpha}{4\pi^2}\left(\frac{q_1}{k'_lq_1}-\frac{q_2}{k'_lq_2}\right)^2, \tag{5}$$

where the electric charges of the electron and fermion f are Q_e and Q_f. The Y function in the exponential YFS form factor is defined as in Ref. [6]:

$$\begin{aligned}
&Y_f(\Omega,p,\bar{p})\\
&\quad\equiv 2Q_f^2\alpha\tilde{B}(\Omega,p,\bar{p})+2Q_f^2\alpha\Re B(p,\bar{p})\\
&\quad\equiv -2Q_f^2\alpha\frac{1}{8\pi^2}\int\frac{d^3k}{k^0}\Theta(\Omega;k)\left(\frac{p}{kp}-\frac{\bar{p}}{k\bar{p}}\right)^2\\
&\qquad+2Q_f^2\alpha\Re\int\frac{d^4k}{k^2}\frac{i}{(2\pi)^3}\left(\frac{2p-k}{kp-k^2}-\frac{2\bar{p}-k}{2k\bar{p}-k^2}\right)^2.
\end{aligned} \tag{6}$$

The above form factor is IR finite and depends explicitly on the soft-photon domains $\Omega=\Omega_I,\Omega_F$, which include (surround) the IR divergence point $k=0$. We define $\Theta(\Omega;k)=1$ for $k\in\Omega$ and $\Theta(\Omega;k)=0$ for $k\notin\Omega$. Contributions from the real photons inside Ω are summed to infinite order and combined with the analogous virtual contributions, forming the exponential YFS form factor. In the Monte Carlo calculation we generate photons $k\notin\Omega$ characterized by the function $\bar{\Theta}(\Omega,k)=1-\Theta(\Omega,k)$. We require, as usual, that Ω_I and Ω_F be small enough (they can be chosen arbitrarily small) for the total cross section, as defined in Eq. (4), and any other physically meaningful observable not to depend on how we choose them; in other words, we require that $\Omega_{I,F}$ be dummy parameters in the calculation. If we neglect the initial-final state interference, then we may choose $\Omega_I\neq\Omega_F$. Let us define Ω_I with the $k^0<E_{\min}$ condition in the center-of-mass system of the incoming $e^{\pm}$ beams and Ω_F with $k^0<E'_{\min}$ in the center of mass of the outgoing fermions $f\bar{f}$. The two domains differ because the Lorentz frames in which they are defined are different. The above choice is the easiest for the Monte Carlo generation, but in the later discussion we shall describe in detail how we implement the $\Omega_I=\Omega_F$ option in our Monte Carlo calculation. The actual YFS form factors for the above choices are well known [6–8]:

$$\begin{aligned}
Y_e(\Omega_I;p_1,p_2)&=\gamma_e\ln\frac{2E_{\min}}{\sqrt{2p_1p_2}}+\frac{1}{4}\gamma_e+Q_e^2\frac{\alpha}{\pi}\left(-\frac{1}{2}+\frac{\pi^2}{3}\right),\\
Y_f(\Omega_F;q_1,q_2)&=\gamma_f\ln\frac{2E_{\min}}{\sqrt{2q_1q_2}}+\frac{1}{4}\gamma_f+Q_f^2\frac{\alpha}{\pi}\left(-\frac{1}{2}+\frac{\pi^2}{3}\right),
\end{aligned} \tag{7}$$

where

$$\begin{aligned}
\gamma=\gamma_e&=2Q_e^2\frac{\alpha}{\pi}\left(\ln\frac{2p_1p_2}{m_e^2}-1\right),\\
\gamma_f&=2Q_f^2\frac{\alpha}{\pi}\left(\ln\frac{2q_1q_2}{m_f^2}-1\right).
\end{aligned} \tag{8}$$

B. Pure virtual corrections

The perturbative QED matrix element is located in the $\overline{\beta}$ functions. The $\overline{\beta}_0$ function is ''proportional'' to the Born $e^-e^+\to f\bar{f}$ differential cross section $d\sigma^{\rm Born}(s,\vartheta)/d\Omega$ and it contains (IR-finite) corrections calculable order by order. According to our general strategy we shall calculate $\overline{\beta}_0$ and other $\overline{\beta}$'s in the $\mathcal{O}(\alpha^i)_{prag}$, $i=0,1,2$.

The $\mathcal{O}(\alpha^i)_{prag}$ expressions for $\overline{\beta}_0^{(i)}, i=0,1,2$, read[1]

$$\overline{\beta}_0^{(r)}(X,p_1,p_2,q_1,q_2)=(1+\delta_I^{(r)})(1+\delta_F^{(r)}) \times\frac{1}{4}\sum_{k,l=1,2}\frac{d\sigma^{\rm Born}}{d\Omega}(X^2,\vartheta_{kl}), \quad (9)$$

$$\delta_I^{(0)}=0, \quad \delta_I^{(1)}=\frac{1}{2}\gamma, \quad \delta_I^{(2)}=\delta_I^{(1)}+\frac{1}{8}\gamma^2,$$

$$\delta_I^{(3)}=\delta_I^{(2)}+\frac{1}{48}\gamma^3, \quad (10)$$

$$\delta_F^{(0)}=0, \quad \delta_F^{(1)}=\frac{1}{2}\gamma_f, \quad \delta_F^{(2)}=\delta_F^{(1)}+\frac{1}{8}\gamma_f^2,$$

$$\delta_F^{(3)}=\delta_F^{(2)}+\frac{1}{48}\gamma_f^3, \quad (11)$$

where

$$\vartheta_{11}=\angle(\vec{p}_1,\vec{q}_1), \quad \vartheta_{12}=\angle(\vec{p}_1,-\vec{q}_2),$$

$$\vartheta_{21}=\angle(-\vec{p}_2,\vec{q}_1), \quad \vartheta_{22}=\angle(-\vec{p}_2,-\vec{q}_2), \quad (12)$$

with all three-vectors taken in the rest frame of the four-momentum X, that is in the frame XMS.

Let us first explain why, instead of having a single $d\sigma^{\rm Born}/d\Omega(\vartheta)$ with a single ϑ, we take an average over four ϑ_{kl}. In fact we could adopt one ϑ, for example $\vartheta_0=\angle(\vec{p}_1-\vec{p}_2,\vec{q}_1-\vec{q}_2)$ where all three-momenta are taken in XMS. The main reason for our apparently more complicated choice is related to the implementation of the first- and higher-order real photon contributions in the next subsections. More precisely, it is well known [15,16] that the exact single-photon ISR matrix element can be cast as a linear combination of the two $d\sigma^{\rm Born}/d\Omega(\vartheta_k), k=1,2$, distributions. The same is true for the FSR [16]. (Our implementation of the LL matrix element for two and three real photons will also involve the linear combination of this type.) It is therefore logical and practical to use a similar solution already for $\overline{\beta}_0$. One should also keep in mind that in the soft limit, when all photons are soft, then all four angles ϑ_{kl} are identical and averaging over them is a spurious operation anyway.

[1]It may look as though we miss a pure (α/π) term in $\delta_{I,F}^{(1)}$. The calculation shows [6] that such a nonlogarithmic contribution is accidentally equal to zero.

The reader who is not familiar with exponentiation may have an even more elementary question: Why do we have the freedom of defining ϑ in $d\sigma^{\rm Born}/d\Omega(\vartheta)$ in the first place? Is this ambiguity dangerous? These questions are already discussed in Refs. [7,11]. The answer is the following: strictly speaking, the differential cross section $d\sigma^{\rm Born}(s,\vartheta)/d\Omega$ and $\overline{\beta}_0^{(i)}$ are defined within the two-body phase-space. Later on they are used, however, in Eq. (4) and in the definitions of $\overline{\beta}^{(i)}, i=1,2,\ldots$, all over the phase-space with additional soft and/or hard photons. This requires some kind of extrapolation of $\overline{\beta}_0$ and $d\sigma^{\rm Born}(s,\vartheta)/d\Omega$ beyond the two-body phase-space. In Ref. [7], this extrapolation was done by manipulating the four-momenta and, in Ref. [11], it was done as an extrapolation in the Mandelstam variables s,t,u. Here we present another solution, which is somewhere in between the previous two. What is really important, however, is that the effect due to changing from one particular choice of extrapolation to another is always, for the entire calculation, a kind of ''higher-order effect.'' For instance, at the $\mathcal{O}(\alpha^1)$ changing the type of extrapolation is an $\mathcal{O}(\alpha^2)$ effect. Of course, it is always wise to use some kind of ''smooth'' extrapolation, which is able to minimize the higher-order effects.

Another possible question is: Why did we not write down the second-order virtual correction factor in an *additive* way, such as $(1+\delta_I^{(2)}+\delta_F^{(2)}+\delta_I^{(1)}\delta_F^{(1)})$? We have opted for the *factorized* form because it is generally known that the factorized form is closer to reality at higher perturbative orders. Another important reason is that the factorized form is easier for the semianalytical integrations over the phase-space, see the discussion in Sec. V.

C. One real photon with virtual corrections

The contributions $\overline{\beta}_1^{(2)}$ are needed directly in Eq. (4) and the $\mathcal{O}(\alpha^1)_{prag}$ version of $\overline{\beta}_1^{(2)}$ enters indirectly as a construction element in $\overline{\beta}_2$. They are constructed from the QED distributions with a single real-photon emission and up to one virtual-photon contribution. They are defined separately for the initial- and final-state photons:

$$\overline{\beta}_{1I}^{(i)}(X,p_1,p_2,q_1,q_2,k_j)=D_{1I}^{(i)}(X,p_1,p_2,q_1,q_2,k_j) -\tilde{S}_I(k_j)\overline{\beta}_0^{(i-1)}(X,p_1,p_2,q_1,q_2), \quad (13)$$

$$\overline{\beta}_{1F}^{(i)}(X,p_1,p_2,q_1,q_2,k_l')=D_{1F}^{(i)}(X,p_1,p_2,q_1,q_2,k_l') -\tilde{S}_F(k_l')\overline{\beta}_0^{(i-1)}(X,p_1,p_2,q_1,q_2),$$

where $i=1,2$. Let us first define all the ingredients for the initial-state contribution. The single initial-state photon emission differential distribution at the $\mathcal{O}(\alpha^r)$, $r=1,2,3$, with the eventual additional, up to two-loop virtual correction, from the initial- and/or final-state photon reads

$$
\begin{aligned}
&D_{1I}^{(r)}(X,p_1,p_2,q_1,q_2,k_j)\\
&\quad=Q_e^2\frac{\alpha}{4\pi^2}\frac{2p_1p_2}{(k_jp_1)(k_jp_2)}W_e(\hat{\alpha}_j,\hat{\beta}_j)\\
&\quad\times\left\{\frac{(1-\hat{\alpha}_j)^2}{2}\sum_{r=1,2}\frac{d\sigma^{\mathrm{Born}}}{d\Omega}(X^2,\vartheta_{1r})\right.\\
&\quad\left.+\frac{(1-\hat{\beta}_j)^2}{2}\sum_{r=1,2}\frac{d\sigma^{\mathrm{Born}}}{d\Omega}(X^2,\vartheta_{2r})\right\}\\
&\quad\times[1+\Delta_I^{(r-1)}(z_j)](1+\delta_F^{(r-1)}),
\end{aligned}
\tag{14}
$$

where

$$
\hat{\alpha}_j=\frac{k_jp_2}{p_1p_2},\quad \hat{\beta}_j=\frac{k_jp_1}{p_1p_2},\quad z_j=(1-\hat{\alpha}_j)(1-\hat{\beta}_j),
$$

$$
\Delta_I^{(0)}(z)\equiv 0,\quad \Delta_I^{(1)}(z)\equiv\frac{1}{2}\gamma-\frac{1}{4}\gamma\ln(z),
\tag{15}
$$

$$
\Delta_I^{(2)}(z)\equiv\Delta_I^{(1)}(z)+\frac{1}{8}\gamma^2-\frac{1}{8}\gamma^2\ln(z)+\frac{1}{24}\gamma^2\ln^2(z),
$$

$$
W_e(a,b)\equiv 1-\frac{m_e^2}{2p_1p_2}\frac{(1-a)(1-b)}{(1-a)^2+(1-b)^2}\left(\frac{a}{b}+\frac{b}{a}\right).
$$

Again the question arises as to why is the averaging over r in ϑ_{kr} introduced? In the case of just one ISR hard photon the averaging trivially disappears because $\vartheta_{k1}=\vartheta_{k2}$; our formula then coincides with the exact $\mathcal{O}(\alpha^1)$ result, see [15,17], as it should. In the less trivial case of the presence of additional hard photons, there is an ambiguity in defining $D_{1I}^{(r)}$ which is reflected in our ''averaging'' procedure; however, it is harmless, i.e., the effect is of $\mathcal{O}(\alpha^2)$.

It is necessary and interesting to check the soft limit. In the presence of many additional photons ($n>1$), if we take the soft limit $k_j\to 0$, keeping the momenta of the other photons constant, then ϑ_{kr} are in general all different. However, in Eq. (14) the sums over $d\sigma^{\mathrm{Born}}/d\Omega$ combine into a simple average over all four angles, as in Eq. (9); in fact the single photon distribution reduces to

$$
D_{1I}^{(2,1)}(X,p_1,p_2,q_1,q_2,k_j)\sim\widetilde{S}_I(k_j)\overline{\beta}_0^{(1,0)}(X,p_1,p_2,q_1,q_2)
$$

and therefore $\overline{\beta}_{1I}^{(2,1)}(X,p_1,p_2,q_1,q_2,k_j)$ is IR finite as required. The above argument shows that the extrapolations for $\overline{\beta}_0$ and $\overline{\beta}_1$ have to be of the same type. If we had opted for another extrapolation in Eq. (14), for example without averaging, with a single angle $\vartheta_{kr}\to\vartheta_k$, then the extrapolation in Eq. (9) would need to be changed appropriately.

Another interesting limit is the collinear limit. If all of the (possibly hard) photons are collinear to the initial or final fermions, then all of the angles $\vartheta_{sr},s,r=1,2$, are identical and equal to the familiar LL effective scattering angle for the hard process in the ''reduced frame'' XMS. This will facilitate the introduction of the higher-order LL corrections in the following.

Another remark on Eq. (14) is in order: there are many equivalent ways, modulo a term of $\mathcal{O}(m^2/s)$, of writing the single-bremsstrahlung spin-summed differential distribution [17]. Our choice follows the representation implemented in the Monte Carlo programs YFS2 [7], KORALZ [10], and MUSTRAAL [16], because it minimizes the machine rounding errors (which are quite important in view of the smallness of the electron mass), and it is explicitly expressed in terms of the Born differential cross sections: this feature facilitates the introduction of electroweak corrections.

The virtual correction $[1+\Delta_I^{(1)}(\hat{\alpha}_j,\hat{\beta}_j)]$ is taken in the LL approximation [sufficient for our $\mathcal{O}(\alpha^2)_{prag}$ approach] and it agrees with the corresponding distribution in Ref. [18]. In the $k_j\to 0$ limit we have $\Delta_I^{(1)}(\hat{\alpha}_j,\hat{\beta}_j)\to\delta_I^{(1)}$ as expected, and as required for the infrared finiteness of $\overline{\beta}_{1F}^{(2)}$. The other factor $(1+\delta_F^{(1)})$ represents the contribution from the simultaneous emission of the real initial and the virtual final photons. We again prefer the factorized form over an additive one $(1+\Delta_I^{(1)}+\delta_F^{(1)})$.

The essential ingredients for the $\mathcal{O}(\alpha^r)$ final state $\overline{\beta}_{1F}^{(r)},r=1,2$, is the single final-state photon-emission matrix element, with up to one-loop virtual initial- or final-state photon corrections:

$$
\begin{aligned}
&D_{1F}^{(r)}(X,p_1,p_2,q_1,q_2,k_l')\\
&\quad=Q_f^2\frac{\alpha}{4\pi^2}\frac{2q_1q_2}{(k_l'q_1)(k_l'q_2)}W_f(\hat{\eta}_l,\hat{\zeta}_l)\\
&\quad\times\left\{\frac{(1-\hat{\eta}_l)^2}{2}\sum_{r=1,2}\frac{d\sigma^{\mathrm{Born}}}{d\Omega}(X^2,\vartheta_{r1})\right.\\
&\quad\left.+\frac{(1-\hat{\zeta}_l)^2}{2}\sum_{r=1,2}\frac{d\sigma^{\mathrm{Born}}}{d\Omega}(X^2,\vartheta_{r2})\right\}\\
&\quad\times[1+\Delta_F^{(r-1)}(z_l)](1+\delta_I^{(r-1)}),
\end{aligned}
\tag{16}
$$

where

$$
\eta_l=\frac{k_l'q_2}{q_1q_2},\quad \zeta_l=\frac{k_l'q_1}{q_1q_2},\quad \hat{\eta}_l=\frac{\eta_l}{1+\eta_l+\zeta_l},
$$

$$
\hat{\zeta}_l=\frac{\zeta_l}{1+\eta_l+\zeta_l},\quad z_l=(1-\hat{\eta}_l)(1-\hat{\zeta}_l)
\tag{17}
$$

$$
\Delta_F^{(0)}(z)\equiv 0,\quad \Delta_F^{(1)}(z)\equiv\frac{1}{2}\gamma_f+\frac{1}{4}\gamma_f\ln(z).
$$

$$
W_f(a,b)\equiv 1-\frac{m_f^2}{2q_1q_2}\frac{(1-a)(1-b)}{(1-a)^2+(1-b)^2}\left(\frac{a}{b}+\frac{b}{a}\right).
$$

Any discussion on the ISR distribution of Eq. (14) also applies to the above FSR distribution.

D. Two real photons with virtual corrections

The contributions $\overline{\beta}^{(2)}_{2II}$, $\overline{\beta}^{(2)}_{2FF}$, and $\overline{\beta}^{(2)}_{2IF}$ are related to the emission of real photons, two initial, two final, and one initial and one final, respectively. They are genuine $\mathcal{O}(\alpha^2)$ objects because they appear in this order for the first time. For the same reason they do not include any virtual contributions. They are defined formally in the usual way:

$$\begin{aligned}\overline{\beta}^{(r)}_{2II}(X,p_1,p_2,q_1,q_2,k_j,k_k)&=D^{(r)}_{2II}(X,p_1,p_2,q_1,q_2,k_j,k_k)\\&-\widetilde{S}_I(k_j)\overline{\beta}^{(r-1)}_{1I}(X,p_1,p_2,q_1,q_2,k_k)\\&-\widetilde{S}_I(k_k)\overline{\beta}^{(r-1)}_{1I}(X,p_1,p_2,q_1,q_2,k_j)\\&-\widetilde{S}_I(k_j)\widetilde{S}_I(k_k)\overline{\beta}^{(r-2)}_{0}(X,p_1,p_2,q_1,q_2),\quad r=2,3,\end{aligned}\tag{18}$$

$$\begin{aligned}\overline{\beta}^{(r)}_{2FF}(X,p_1,p_2,q_1,q_2,k'_l,k'_m)&=D^{(r)}_{2FF}(X,p_1,p_2,q_1,q_2,k'_l,k'_m)\\&-\widetilde{S}_F(k'_l)\overline{\beta}^{(r-1)}_{1F}(X,p_1,p_2,q_1,q_2,k'_m)\\&-\widetilde{S}_F(k'_m)\overline{\beta}^{(r-1)}_{1F}(X,p_1,p_2,q_1,q_2,k'_l)\\&-\widetilde{S}_F(k'_l)\widetilde{S}_F(k'_m)\overline{\beta}^{(r-2)}_{0}(X,p_1,p_2,q_1,q_2),\quad r=2,3,\end{aligned}\tag{19}$$

$$\begin{aligned}\overline{\beta}^{(r)}_{2IF}(X,p_1,p_2,q_1,q_2,k_j,k'_l)&=D^{(r)}_{2IF}(X,p_1,p_2,q_1,q_2,k_j,k'_l)\\&-\widetilde{S}_I(k_j)\overline{\beta}^{(r-1)}_{1F}(X,p_1,p_2,q_1,q_2,k'_l)\\&-\widetilde{S}_F(k'_l)\overline{\beta}^{(r-1)}_{1I}(X,p_1,p_2,q_1,q_2,k_j)\\&-\widetilde{S}_I(k_j)\widetilde{S}_F(k'_l)\overline{\beta}^{(r-2)}_{0}(X,p_1,p_2,q_1,q_2),\quad r=2,3.\end{aligned}\tag{20}$$

The new objects in the above expressions are the differential distributions $D^{(2)}_{2II}$, $D^{(2)}_{2FF}$, and $D^{(2)}_{2IF}$ for double bremsstrahlung. They are not taken directly from Feynman diagrams but they are *constructed* in such a way that if one photon is hard and one is soft, then the single bremsstrahlung expressions of Eqs. (14) and (16) are recovered, if both photons are hard and collinear, then the proper LL limit, which we know from the double or triple convolution of the Altarelli-Parisi kernels, is also recovered. The resulting expressions are rather compact and the LL limit is manifest, which is not necessarily true for the exact double-bremsstrahlung spin amplitudes (see next section). The method is similar to that of Refs. [7,12]. In the case of ISR, we shall also include the one-loop virtual corrections read from the triple convolution of the Altarelli-Parisi kernels, see Ref. [12].

Our construction in the case of the double real ISR reads as follows:

$$\begin{aligned}D^{(2)}_{2II}(X,p_1,p_2,q_1,q_2,k_1,k_2)\equiv Q_e^4\frac{\alpha}{4\pi^2}\frac{2p_1p_2}{(k_1p_1)(k_1p_2)}\frac{\alpha}{4\pi^2}\frac{2p_1p_2}{(k_2p_1)(k_2p_2)}W_e(\hat{\alpha}_1,\hat{\beta}_1)W_e(\hat{\alpha}_2,\hat{\beta}_2)\\\times\Bigg\{\Theta(v_1-v_2)[1+\Delta^{(r-1)}_{II}(z_1,z_{12})](1+\delta^{(r-1)}_F)\Bigg[\chi_2(\hat{\alpha}_1;\hat{\alpha}'_2,\hat{\beta}'_2)\sum_{r=1,2}\frac{d\sigma^{\rm Born}}{d\Omega}(X^2,\vartheta_{1r})\\+\chi_2(\hat{\beta}_1;\hat{\alpha}'_2,\hat{\beta}'_2)\sum_{r=1,2}\frac{d\sigma^{\rm Born}}{d\Omega}(X^2,\vartheta_{2r})\Bigg]+\Theta(v_2-v_1)[1+\Delta^{(r-1)}_{II}(z_2,z_{21})](1+\delta^{(r-1)}_F)\\\times\Bigg[\chi_2(\hat{\alpha}_2;\hat{\alpha}'_1,\hat{\beta}'_1)\sum_{r=1,2}\frac{d\sigma^{\rm Born}}{d\Omega}(X^2,\vartheta_{1r})+\chi_2(\hat{\beta}_2;\hat{\alpha}'_1,\hat{\beta}'_1)\sum_{r=1,2}\frac{d\sigma^{\rm Born}}{d\Omega}(X^2,\vartheta_{2r})\Bigg]\Bigg\},\end{aligned}\tag{21}$$

where

$$\hat{\alpha}'_1=\frac{\hat{\alpha}_1}{1-\hat{\alpha}_2},\quad \hat{\alpha}'_2=\frac{\hat{\alpha}_2}{1-\hat{\alpha}_1},\quad \hat{\beta}'_1=\frac{\hat{\beta}_1}{1-\hat{\beta}_2},\quad \hat{\beta}'_2=\frac{\hat{\beta}_2}{1-\hat{\beta}_1},\tag{22}$$

$$v_i=\hat{\alpha}_i+\hat{\beta}_i,\quad z_i=(1-\hat{\alpha}_i)(1-\hat{\beta}_i),$$

$$z_{ij}=(1-\hat{\alpha}_i-\hat{\alpha}_j)(1-\hat{\beta}_i-\hat{\beta}_j),$$

$$\chi_2(u;a,b)\equiv\frac{1}{4}(1-u)^2[(1-a)^2+(1-b)^2],$$

$$\Delta^{(0)}_{II}=0,\quad \Delta^{(1)}_{II}(z_i,z_{ij})=\frac{1}{2}\gamma-\frac{1}{6}\gamma\ln(z_i)-\frac{1}{6}\gamma\ln(z_{ij}).$$

The variables $\hat{\alpha}_i,\hat{\beta}_i$ for the ith photon are defined as in Eq. (14).

In order to understand our construction, let us examine how the LL collinear limit is realized in the exact single-bremsstrahlung matrix element of Eq. (14). If the photon

carrying the fraction x_1 of the beam energy is collinear, let us say, with p_1, then $\hat{\alpha}_1 \sim x$, $\hat{\beta}_1 \sim 0$, all four angles are the same $\vartheta_{sr} \to \vartheta^*$ and we immediately recover the correct LL formula

$$\frac{1}{2}(1-\hat{\alpha}_1)^2 \sum_{r=1,2} \frac{d\sigma^{\rm Born}}{d\Omega}(\vartheta_{1r}) + \frac{1}{2}(1-\hat{\beta}_1)^2 \sum_{r=1,2} \frac{d\sigma^{\rm Born}}{d\Omega}(\vartheta_{2r}) \to \frac{1}{2}[1+(1-x)^2]\frac{d\sigma^{\rm Born}}{d\Omega}(\vartheta^*).$$

It is therefore natural to employ for the double emission the *angular-dependent* Altarelli-Parisi (AP) factors of the kind

$$\frac{1}{2}[(1-\hat{\alpha}_2)^2+(1-\hat{\beta}_2)^2]\frac{1}{2}[(1-\hat{\alpha}_1)^2+(1-\hat{\beta}_1)^2].$$

The above formula is too simple, however, to reproduce correctly the result of the double convolution of the AP kernels in the case when both photons are collinear with the same fermion

$$\frac{1}{2}[1+(1-x_1)^2]\frac{1}{2}(1+\{1-[x_2/(1-x_1)]\}^2)\frac{d\sigma^{\rm Born}}{d\Omega}(\vartheta^*),$$

where $x_2' = x_2/(1-x_1)$ reflects the loss of energy in the emission cascade due to the emission of k_1. In order to match the above cascade limit, we construct a better angular-dependent AP factor as

$$\frac{1}{2}[(1-\hat{\alpha}_1)^2+(1-\hat{\beta}_1)^2]\frac{1}{2}[(1-\hat{\alpha}_2')^2+(1-\hat{\beta}_2')^2].$$

The above fulfills both types of the LL collinear limit, when two photons are collinear with a single beam or each of them follows a different beam. Finally, let us reproduce the limit in which one photon, let us say the first, is hard and the other, the second, is soft, $v_2 = \hat{\alpha}_2 + \hat{\beta}_2 \to 0$. In this case it is logical to split the above double-bremsstrahlung angular-dependent AP factor into two pieces

$$\chi_2(\hat{\alpha}_1;\hat{\alpha}_2',\hat{\beta}_2') = \frac{1}{2}(1-\hat{\alpha}_1)^2\frac{1}{2}[(1-\hat{\alpha}_2')^2+(1-\hat{\beta}_2')^2],$$

$$\chi_2(\hat{\beta}_1;\hat{\alpha}_2',\hat{\beta}_2') = \frac{1}{2}(1-\hat{\beta}_1)^2\frac{1}{2}[(1-\hat{\alpha}_2')^2+(1-\hat{\beta}_2')^2],$$

and associate each one with the corresponding $d\sigma^{\rm Born}/d\Omega$, following Eq. (14). The order in the cascade does not matter. We simply symmetrize over the two orderings in the cascade—it is essentially a Bose-Einstein symmetrization.

The above construction clearly provides the correct limit $D_{2II}^{(2)}(k_1,k_2) \to \tilde{S}(k_2) D_{1I}^{(1)}(k_2)$ for $v_1 = {\rm const}$ and $v_2 \to 0$. As a consequence $\overline{\beta}_{II}^{(2)}(X,p_1,p_2,q_1,q_2,k_1,k_2)$ is finite in the limit of one or both photon momenta tending to zero.

The construction of Eq. (21) will be inadequate if both photons are hard and at least one has high transverse momentum. It reflects the fact that we do not control fully in EEX the second-order next-to-leading logarithmic (NLL), $\mathcal{O}(\alpha^2 L)$, contributions. However, we have known for a long time that a construction of the type of Eq. (21) agrees rather well with the exact double-bremsstrahlung matrix element calculated using spinor techniques, see [19]. When both photons have high transverse momenta, there is only about 20% disagreement between the approximate and exact results (integrated over the double-photon phase-space). This result is confirmed in the present work by the numerical comparisons of EEX and CEEX, where the double-bremsstrahlung matrix element is exact.

The double final-state bremsstrahlung distribution is defined/constructed in an analogous way:

$$\begin{aligned} D_{2FF}^{(r)}(X,p_1,p_2,q_1,q_2,k_1',k_2') = Q_f^4 \frac{\alpha}{4\pi^2}\frac{2q_1p_2}{(k_1'q_1)(k_1'p_2)}\frac{\alpha}{4\pi^2}\frac{2q_1p_2}{(k_2'q_1)(k_2'p_2)} W_f(\hat{\eta}_1,\hat{\zeta}_1) W_f(\hat{\eta}_2,\hat{\zeta}_2) \Bigg\{ \Theta(v_1'-v_2') \\ \times \left[\chi_2(\eta_1;\eta_2',\zeta_2') \sum_{r=1,2} \frac{d\sigma^{\rm Born}}{d\Omega}(X^2,\vartheta_{1r}) + \chi_2(\zeta_1;\eta_2',\zeta_2') \sum_{r=1,2} \frac{d\sigma^{\rm Born}}{d\Omega}(X^2,\vartheta_{2r}) \right] \\ + \Theta(v_2'-v_1') \left[\chi_2(\eta_2;\eta_1',\zeta_1') \sum_{r=1,2} \frac{d\sigma^{\rm Born}}{d\Omega}(X^2,\vartheta_{1r}) + \chi_2(\zeta_2;\eta_1',\zeta_1') \sum_{r=1,2} \frac{d\sigma^{\rm Born}}{d\Omega}(X^2,\vartheta_{2r}) \right] \Bigg\} \\ \times [1+\Delta_I^{(r-1)}(z_j)], \end{aligned} \tag{23}$$

where

$$\eta_1' = \frac{\eta_1}{1+\eta_2}, \quad \eta_2' = \frac{\eta_2}{1+\eta_1}, \quad \zeta_1' = \frac{\zeta_1}{1+\zeta_2}, \quad \zeta_2' = \frac{\zeta_2}{1+\zeta_1}. \tag{24}$$

The definition of the ''primed'' Sudakov variables is done here in a way different from that in the ISR case, because the fermion momenta $q_{1,2}$ get affected by photon emission. The virtual corrections are absent because we restrict the FSR to $\mathcal{O}(\alpha^2)_{LL}$. The above expression is tagged with $r=2,3$ for

$\mathcal{O}(\alpha^r)$; however, we implement the FSR essentially only in $\mathcal{O}(\alpha^2)$, and the only correction in $\mathcal{O}(\alpha^3)$ is the ISR one-loop correction.

The distribution for one photon from the initial-state and one photon from the final-state at $\mathcal{O}(\alpha^r)$, $r=1,2$, we construct as follows:

$$
\begin{aligned}
D^{(r)}_{2IF}(X,p_1,p_2,q_1,q_2,k_j,k'_l) = Q_e^2 \frac{\alpha}{4\pi^2} \frac{2p_1p_2}{(k_jp_1)(k_jp_2)} W_e(\hat{\alpha}_j,\hat{\beta}_j) Q_f^2 \frac{\alpha}{4\pi^2} \frac{2q_1q_2}{(k'_lq_1)(k'_lq_2)} W_f(\hat{\eta}_l,\hat{\xi}_l) \\
\times \Bigg\{ \frac{(1-\hat{\alpha}_j)^2}{2} \frac{(1-\hat{\eta}_l)^2}{2} \frac{d\sigma^{\mathrm{Born}}}{d\Omega}(X^2,\vartheta_{11}) + \frac{(1-\hat{\alpha}_j)^2}{2} \frac{(1-\hat{\xi}_l)^2}{2} \frac{d\sigma^{\mathrm{Born}}}{d\Omega}(X^2,\vartheta_{12}) \\
+ \frac{(1-\hat{\beta}_j)^2}{2} \frac{(1-\hat{\eta}_l)^2}{2} \frac{d\sigma^{\mathrm{Born}}}{d\Omega}(X^2,\vartheta_{21}) + \frac{(1-\hat{\beta}_j)^2}{2} \frac{(1-\hat{\xi}_l)^2}{2} \frac{d\sigma^{\mathrm{Born}}}{d\Omega}(X^2,\vartheta_{22}) \Bigg\} \\
\times [1+\Delta_I^{(r-1)}(z_1)][1+\Delta_F^{(r-1)}(z'_2)],
\end{aligned} \tag{25}
$$

where the variables $\hat{\alpha}_j,\hat{\beta}_j,\hat{\eta}_l,\hat{\xi}_l$ and the other components are defined as in Eqs. (14) and (16). The above construction is in fact the easiest, because two photons cannot be emitted in a cascade from one line and we fully exploit the four scattering angles in the Born differential cross sections. It is trivial to check that all soft and collinear limits are correct.

E. Three real photons

The differential distribution for three real ISR photons is essentially obtained by the triple convolution of the AP kernel, for each beam separately; the two results are combined with the help of an additional convolution. This exercise was done for the collinear subgenerator of BHLUMI [12] and we exploit these results here. Even though the collinear limit is of primary importance, we have to be very careful, in the construction of the fully differential triple-photon distribution, to preserve all soft limits: when all three photons are soft, when two of them are soft, and when only one of them is soft. In these limits the three-photon differential distribution has to reproduce smoothly the previously defined Born, single-, and double-bremsstrahlung distributions times the appropriate soft factor(s). Otherwise we may have a problem with the IR finiteness of

$$
\begin{aligned}
\overline{\beta}^{(3)}_{3III}(X,p_i,q_j,k_1,k_2,k_3) = D^{(3)}_{3III}(X,p_i,q_j,k_1,k_2,k_3) - \widetilde{S}_I(k_1)\overline{\beta}^{(2)}_{2II}(X,p_i,q_j,k_2,k_3) - \widetilde{S}_I(k_2)\overline{\beta}^{(2)}_{2II}(X,p_i,q_j,k_1,k_3) \\
- \widetilde{S}_I(k_3)\overline{\beta}^{(2)}_{2II}(X,p_i,q_j,k_1,k_2) - \widetilde{S}_I(k_1)\widetilde{S}_I(k_2)\overline{\beta}^{(1)}_{1I}(X,p_i,q_j,k_3) - \widetilde{S}_I(k_3)\widetilde{S}_I(k_1)\overline{\beta}^{(1)}_{1I}(X,p_i,q_j,k_2) \\
- \widetilde{S}_I(k_2)\widetilde{S}_I(k_3)\overline{\beta}^{(1)}_{1I}(X,p_i,q_j,k_1) - \widetilde{S}_I(k_1)\widetilde{S}_I(k_2)\widetilde{S}_I(k_3)\overline{\beta}^{(0)}_{0}(X,p_i,q_j).
\end{aligned} \tag{26}
$$

It is therefore not completely straightforward to turn the strictly collinear expression for the three real-photon distributions of Ref. [12] into the fully differential (finite-p_T) triple-photon distribution that we need. As in the case of the double real ISR, the guiding principle is that (i) the hardest photon decides which of the angles is used in $d\sigma^{\mathrm{Born}}/d\Omega(X^2,\vartheta_{lr})$ and (ii) we have to perform Bose symmetrization, that is, to sum over all orderings in a cascade emission of several photons from one beam. For three real photons there are no virtual corrections.

Our construction in the case of the triple real ISR reads as follows:

$$
\begin{aligned}
D^{(3)}_{3III}(X,p_1,p_2,q_1,q_2,k_1,k_2,k_3) \equiv \prod_{l=1,3} Q_e^2 \frac{\alpha}{4\pi^2} \frac{2p_1p_2}{(k_lp_1)(k_lp_2)} W_e(\hat{\alpha}_l,\hat{\beta}_l) \\
\times \Bigg\{ \Theta(v_1-v_2)\Theta(v_2-v_3) \Bigg[\chi_3(\hat{\alpha}_1;\hat{\alpha}'_2,\hat{\beta}'_2,\hat{\alpha}''_3,\hat{\beta}''_3) \sum_{r=1,2} \frac{d\sigma^{\mathrm{Born}}}{d\Omega}(X^2,\vartheta_{1r}) \\
+ \chi_3(\hat{\beta}_1;\hat{\alpha}'_2,\hat{\beta}'_2,\hat{\alpha}''_3,\hat{\beta}''_3) \sum_{r=1,2} \frac{d\sigma^{\mathrm{Born}}}{d\Omega}(X^2,\vartheta_{2r}) \Bigg] \\
+ \text{remaining five permutations of } (1,2,3) \Bigg\},
\end{aligned} \tag{27}
$$

where

$$\chi_3(u_1;a_2,b_2,a_3,b_3)\equiv\frac{1}{8}(1-u_1)^2[(1-a_2)^2+(1-b_2)^2]\times[(1-a_3)^2+(1-b_3)^2],$$

$$\hat{\alpha}_3''=\frac{\hat{\alpha}_3}{1-\hat{\alpha}_1-\hat{\alpha}_2},\quad \hat{\beta}_3''=\frac{\hat{\beta}_3}{1-\hat{\beta}_1-\hat{\beta}_2}. \tag{28}$$

In most cases, such an approach should be sufficient; however, in some special cases with two hard photons explicitly tagged, it may not be so. We have programmed and run special tests (unpublished) relying on ISR amplitudes with up to three hard photons [20], constructed with methods similar to those in Ref. [21], in order to get additional confidence in the approximate real emission distributions presented in this section.

III. AMPLITUDES FOR COHERENT EXCLUSIVE EXPONENTIATION

The coherent exclusive exponentiation was introduced for the first time in Ref. [3]. It is deeply rooted in the YFS exponentiation [8]. It applies in particular to processes with narrow resonances, where it is related also to the works of Greco *et al.* [22,23]. The exponentiation procedure, that is a reorganization of the QED perturbative series such that the IR divergences are summed up to infinite order, is done at the spin-amplitude level for both real and virtual IR singularities. This is to be contrasted with traditional YFS exponentiation, on which our EEX is based, where isolating the *real* IR divergences is done for squared spin-summed spin amplitudes, that is, for differential distributions and spin density matrices.[2]

Our calculations of the spin amplitudes for fermion-pair production in electron-positron scattering is done with the help of the powerful Weyl spinor (WS) techniques. There are several variants of the WS techniques. We have opted for the method of Kleiss and Stirling (KS) [24,25], which we found the best suited for our CEEX. In Ref. [2] the KS spinor technique for massless and massive fermions was reviewed and appended with the rules for controlling their complex phases or, equivalently, the fermion rest frame (all three axes) in which the fermion spin is quantized—this is a critical point if we want to control fully the spin density matrix of the fermions. We call the global positioning of spin (GPS) frame this fermion rest frame and the rule for finding it we call the GPS rule. For the sake of completeness, we include the definitions of the KS spinors, photon polarization vectors, and our GPS rules in the Appendix.

The very interesting feature of CEEX is that, although it is formulated entirely in terms of the spin amplitudes, the IR cancellations in CEEX occur for the integrated cross sections (probabilities), as usual; in practice they are realized *numerically*. There is no contradiction in the above statement. In order to avoid any confusion on this point, we shall provide a new detailed proof of the IR cancellations in the CEEX scheme in one of the following subsections.

[2]The realization of EEX for spin density matrices is an obvious generalization of the EEX/YFS exponentiation which, however, was never fully implemented in practice.

A. Master formula

Defining the Lorentz-invariant phase-space as

$$\int d\,\mathrm{Lips}_n(P;p_1,p_2,\ldots,p_n)=\int(2\pi)^4\delta\left(P-\sum_{i=1}^n p_i\right)\prod_{i=1}^n\frac{d^3p}{(2\pi)^3 2p_i^0}, \tag{29}$$

we write the CEEX total cross section for the process

$$e^-(p_a)+e^+(p_b)\to f(p_c)+\overline{f}(p_d)+\gamma(k_1)+\gamma(k_2)+\cdots+\gamma(k_n),\quad n=0,1,2,\ldots,\infty \tag{30}$$

with polarized beams and decays of unstable final fermions sensitive to fermion spin polarizations, following Ref. [3], as follows:

$$\sigma^{(r)}=\frac{1}{\mathrm{flux}(s)}\sum_{n=0}^{\infty}\times\int d\,\mathrm{Lips}_{n+2}(p_a+p_b;p_c,p_d,k_1,\ldots,k_n)\times\rho^{(r)}_{\mathrm{CEEX}}(p_a,p_b,p_c,p_d,k_1,\ldots,k_n), \tag{31}$$

where, in the CMS (center of mass) $\mathrm{flux}(s)=2s+\mathcal{O}(m_e^2)$,

$$\rho^{(r)}_{\mathrm{CEEX}}(p_a,p_b,p_c,p_d,k_1,k_2,\ldots,k_n)=\frac{1}{n!}\exp[Y(\Omega;p_a,\ldots,p_d)]\overline{\Theta}(\Omega)\times\sum_{\sigma_i=\pm1}\sum_{\lambda_i,\lambda_i=\pm1}\sum_{i,j,l,m=0}^{3}\hat{\varepsilon}^i_a\hat{\varepsilon}^j_b\sigma^i_{\lambda_a\bar{\lambda}_a}\sigma^j_{\lambda_b\bar{\lambda}_b}\times\mathfrak{M}^{(r)}_n\left(\begin{matrix}pk_1k_2\\ \lambda\sigma_1\sigma_2\end{matrix}\cdots\begin{matrix}k_n\\ \sigma_n\end{matrix}\right)\left[\mathfrak{M}^{(r)}_n\left(\begin{matrix}pk_1k_2\\ \bar{\lambda}\sigma_1\sigma_2\end{matrix}\cdots\begin{matrix}k_n\\ \sigma_n\end{matrix}\right)\right]^*\times\sigma^l_{\bar{\lambda}_c\lambda_c}\sigma^m_{\bar{\lambda}_d\lambda_d}\hat{h}^l_c\hat{h}^m_d, \tag{32}$$

and assuming the domination of the s-channel exchanges, including resonances, we define the complete set of spin amplitudes for the emission of n photons, in $\mathcal{O}(\alpha^r)_{\mathrm{CEEX}}$, $r=0,1,2$, as follows:

$$\mathfrak{M}^{(0)}_n\left(\begin{matrix}pk_1\\ \lambda\sigma_1\end{matrix}\cdots\begin{matrix}k_n\\ \sigma_n\end{matrix}\right)=\sum_{\wp\in\{I,F\}^n}\prod_{i=1}^n\mathfrak{s}^{\{\wp_i\}}_{[i]}\hat{\beta}^{(0)}_0\left(\begin{matrix}p\\ \lambda\end{matrix};X_\wp\right), \tag{33}$$

$$\mathfrak{M}_n^{(1)}\left(\begin{matrix} pk_1\cdots k_n \\ \lambda\sigma_1\cdots\sigma_n\end{matrix}\right)=\sum_{\wp\in\{I,F\}^n}\prod_{i=1}^{n}\mathfrak{s}_{[i]}^{\{\wp_i\}}\Bigg\{\hat{\beta}_0^{(1)}\left(\begin{matrix}p\\ \lambda\end{matrix};X_\wp\right)+\sum_{j=1}^{n}\frac{\hat{\beta}_{1\{\wp_j\}}^{(1)}\left(\begin{matrix}pk_j\\ \lambda\sigma_j\end{matrix};X_\wp\right)}{\mathfrak{s}_{[j]}^{\{\wp_j\}}}\Bigg\}, \tag{34}$$

$$\mathfrak{M}_n^{(2)}\left(\begin{matrix} pk_1\cdots k_n \\ \lambda\sigma_1\cdots\sigma_n\end{matrix}\right)=\sum_{\wp\in\{I,F\}^n}\prod_{i=1}^{n}\mathfrak{s}_{[i]}^{\{\wp_i\}}\Bigg\{\hat{\beta}_0^{(2)}\left(\begin{matrix}p\\ \lambda\end{matrix};X_\wp\right)+\sum_{j=1}^{n}\frac{\hat{\beta}_{1\{\wp_j\}}^{(2)}\left(\begin{matrix}pk_j\\ \lambda\sigma_j\end{matrix};X_\wp\right)}{\mathfrak{s}_{[j]}^{\{\wp_j\}}}+\sum_{1\leqslant j<l\leqslant n}\frac{\hat{\beta}_{2\{\wp_j\wp_l\}}^{(2)}\left(\begin{matrix}pk_jk_l\\ \lambda\sigma_j\sigma_l\end{matrix};X_\wp\right)}{\mathfrak{s}_{[j]}^{\{\wp_j\}}\mathfrak{s}_{[l]}^{(\wp_l)}}\Bigg\}. \tag{35}$$

In the following subsections we shall explain all of the basic notations, then in the next section we shall discuss in detail the IR structure in CEEX, effectively deriving all of the above formulas. At $\mathcal{O}(\alpha^r)$ we have to provide the functions $\hat{\beta}_k^{(r)}, k=0,1,\ldots,r$, from the Feynman diagrams, which are IR finite by construction [8]. Their actual precise definitions will be given in the following. We shall define/calculate them explicitly up to $\mathcal{O}(\alpha^2)$.

1. Spin notation

In order to shorten our many formulas, we use a compact collective notation:

$$\left(\begin{matrix}p\\ \lambda\end{matrix}\right)=\left(\begin{matrix}p_ap_bp_cp_d\\ \lambda_a\lambda_b\lambda_c\lambda_d\end{matrix}\right)$$

for fermion four-momenta $p_A, A=a,b,c,d$ (i.e., $p_1=p_a$, $p_2=p_b$, $q_1=p_c$, $q_2=p_d$) and helicities $\lambda_A, A=a,b,c,d$. For $k=1,2,3$, σ^k are the Pauli matrices and $\sigma^0_{\lambda,\mu}=\delta_{\lambda,\mu}$ is the unit matrix. The components $\hat{\varepsilon}_1^j, \hat{\varepsilon}_2^k$, where $j,k=1,2,3$, are the components of the conventional spin-polarization vectors of the e^- and e^+, respectively, defined in the so-called GPS fermion rest frames (see the Appendix and Ref. [2] for the exact definition of these frames). We define $\hat{\varepsilon}_A^0=1$ in a nonstandard way (i.e., $p_A\cdot\hat{\varepsilon}_A=m_e, A=a,b$). The *polarimeter* vectors $\hat{h}_C$ are similarly defined in the appropriate GPS rest frames of the final unstable fermions ($p_C\cdot\hat{h}_C=m_f, C=c,d$). Note that, in general, $\hat{h}_C$ may depend in a nontrivial way on the momenta of all decay products, see Refs. [2,26–28] for more details. We did not introduce polarimeter vectors for the bremsstrahlung photons, i.e., we take advantage of the fact that luckily all high-energy experiments are completely blind to photon-spin polarizations.

2. IR regulators and the YFS form factor

Here we introduce and explain our notation for the IR integration limits for the real photons in Eqs. (31) and (32) and in the following sections. In general, the factor $\overline{\Theta}(\Omega)$ in Eq. (31) defines the IR integration limits for all real photons. More precisely for a single photon, Ω is the domain surrounding the IR divergence point $k=0$, which is in fact *excluded* from the MC phase-space. In CEEX there is no real distinction between ISR and FSR photons, and Ω is therefore necessarily the same for all photons. We define a characteristic function $\Theta(\Omega,k)$ of the IR domain Ω as $\Theta(\Omega,k)=1$ for $k\in\Omega$ and $\Theta(\Omega,k)=0$ for $k\notin\Omega$. The characteristic function for the part of the phase-space *included* in the MC integration for a single real photon is $\overline{\Theta}(\Omega,k)=1-\Theta(\Omega,k)$. The analogous characteristic function for *all* real photons is, of course, the following product:

$$\overline{\Theta}(\Omega)=\prod_{i=1}^{n}\overline{\Theta}(\Omega,k). \tag{36}$$

In the present calculation corresponding to the $\mathcal{KK}$ Monte Carlo program we opt for Ω defined traditionally with the photon-energy cut condition $k^0<E_{\min}$.

The YFS form factor [8] for Ω defined with the condition $k^0<E_{\min}$ reads

$$\begin{aligned}Y(\Omega;p_a,\ldots,p_d)=&Q_e^2Y_\Omega(p_a,p_b)+Q_f^2Y_\Omega(p_c,p_d)\\&+Q_eQ_fY_\Omega(p_a,p_c)+Q_eQ_fY_\Omega(p_b,p_d)\\&-Q_eQ_fY_\Omega(p_a,p_d)-Q_eQ_fY_\Omega(p_b,p_c),\end{aligned} \tag{37}$$

where

$$\begin{aligned}Y_\Omega(p,q)\equiv&2\alpha\tilde{B}(\Omega,p,q)+2\alpha\Re B(p,q)\\\equiv&-2\alpha\frac{1}{8\pi^2}\int\frac{d^3k}{k^0}\Theta(\Omega;k)\left(\frac{p}{kp}-\frac{q}{kq}\right)^2\\&+2\alpha\Re\int\frac{d^4k}{k^2}\frac{i}{(2\pi)^3}\left(\frac{2p-k}{2kp-k^2}-\frac{2q-k}{2kq-k^2}\right)^2\end{aligned} \tag{38}$$

is given analytically in terms of logarithms and Spence functions. As we see, the above YFS form factor includes terms due to the initial-final state interference. The above form-factor will be derived in the following. The additional contribution to the YFS form-factor due to the narrow Z resonance will be discussed in detail separately.

3. Partitions and $\mathfrak{s}$ factors

The *coherent* sum is taken over the set $\{\wp\}=\{I,F\}^n$ of all 2^n partitions—the single partition $\wp$ is defined as a vector $(\wp_1,\wp_2,\ldots,\wp_n)$ where $\wp_i=I$ for an ISR photon and $\wp_F=F$ for an FSR photon, see the analogous construction in Refs. [22,23]. The set of all partitions is explicitly the following:

$$\{\wp\}=\{(I,I,I,\ldots,I),(F,I,I,\ldots,I),(I,F,I,\ldots,I),(F,F,I,\ldots,I),\ldots(F,F,F,\ldots,F)\}.$$

The s-channel four-momentum in the (possibly) resonant s-channel propagator is $X_\wp=p_a+p_b-\Sigma_{\wp_i=I}k_i$.

The soft (eikonal) amplitude factors $\mathfrak{s}_{[i]}^{\{\omega\}},\omega=I,F$, are complex numbers, and they are defined as follows:

$$\mathfrak{s}_{[i]}^{\{I\}}\equiv\mathfrak{s}_{\sigma_i}^{\{I\}}(k_i)=-eQ_e\frac{b_\sigma(k,p_a)}{2k_ip_a}+eQ_e\frac{b_\sigma(k_i,p_b)}{2k_ip_b},$$

$$|\mathfrak{s}_{[i]}^{\{I\}}|^2=-\frac{e^2Q_e^2}{2}\left(\frac{p_a}{k_ip_a}-\frac{p_b}{k_ip_b}\right)^2, \tag{39}$$

$$\mathfrak{s}_{[i]}^{\{F\}}\equiv\mathfrak{s}_{\sigma_i}^{\{F\}}(k_i)=+eQ_f\frac{b_\sigma(k_i,p_c)}{2kp_c}-eQ_f\frac{b_\sigma(k_i,p_d)}{2k_ip_d},$$

$$|\mathfrak{s}_{[i]}^{\{F\}}|^2=-\frac{e^2Q_f^2}{2}\left(\frac{p_c}{k_ip_c}-\frac{p_d}{k_ip_d}\right)^2, \tag{40}$$

$$b_\sigma(k,p)=\sqrt{2}\frac{\overline{u}_\sigma(k)\not{p}u_\sigma(\zeta)}{\overline{u}_{-\sigma}(k)u_\sigma(\zeta)}=\sqrt{2}\sqrt{\frac{2\zeta p}{2\zeta k}}s_\sigma(k,\hat{p}); \tag{41}$$

see also the Appendix for more details. As indicated above, the moduli squared of the CEEX soft factors coincide up to a normalization constant with the corresponding EEX real-photon soft factors $\tilde{S}(k_i)$.

4. Born

The simplest IR-finite $\hat{\beta}$ function $\hat{\beta}_0^{(0)}$ is just the Born spin amplitude times a certain kinematical factor (see the next subsection):

$$\hat{\beta}_0^{(0)}\left(\begin{matrix}p\\ \lambda\end{matrix};X\right)=\mathfrak{B}\left(\begin{matrix}p\\ \lambda\end{matrix};X\right)\frac{X^2}{(p_c+p_d)^2}. \tag{42}$$

The Born spin amplitude $\mathfrak{B}(\begin{smallmatrix}p\\ \lambda\end{smallmatrix};X)$ is a basic building block in the construction of all of our spin amplitudes, so let us define it at this point. The many equivalent notations for $\mathfrak{B}$ will be introduced for flexibility, in view of its role as a basic building block in the calculation of the multi-bremsstrahlung amplitudes. Using the Feynman rules and our basic massive spinors with the definite GPS helicities of the Appendix, the Born spin amplitudes for[3] the $e^-(p_a)e^+(p_b)\to f(p_c)\overline{f}(p_d)$ process are given by

$$\begin{aligned}\mathfrak{B}\left(\begin{matrix}p\\ \lambda\end{matrix};X\right)&=\mathfrak{B}\left(\begin{matrix}p_ap_bp_cp_d\\ \lambda_a\lambda_b\lambda_c\lambda_d\end{matrix};X\right)=\mathfrak{B}\left[\begin{matrix}p_bp_a\\ \lambda_b\lambda_a\end{matrix}\right]\left[\begin{matrix}p_cp_d\\ \lambda_c\lambda_d\end{matrix}\right](X)\\&=\mathfrak{B}_{[ba][cd]}(X)\\&=ie^2\sum_{B=\gamma,Z}\Pi_B^{\mu\nu}(X)(G_{e,\mu}^B)_{[ba]}(G_{f,\nu}^B)_{[cd]}H_B\\&=\sum_{B=\gamma,Z}\mathfrak{B}_{[ba][cd]}^B(X),\\(G_{e,\mu}^B)_{[ba]}&\equiv\overline{v}(p_b,\lambda_b)G_{e,\mu}^Bu(p_a,\lambda_a),\\(G_{f,\mu}^B)_{[cd]}&\equiv\overline{u}(p_c,\lambda_c)G_{f,\mu}^Bv(p_d,\lambda_d),\\G_{e,\mu}^B&=\gamma_\mu\sum_{\lambda=\pm}\omega_\lambda g_\lambda^{B,e},\\G_{f,\mu}^B&=\gamma_\mu\sum_{\lambda=\pm}\omega_\lambda g_\lambda^{B,f},\quad\omega_\lambda=\frac{1}{2}(1+\lambda\gamma_5),\\\Pi_B^{\mu\nu}(X)&=\frac{g^{\mu\nu}}{X^2-M_B^2+i\Gamma_BX^2/M_B},\end{aligned} \tag{43}$$

where $g_\lambda^{B,f}$ are the usual chiral ($\lambda=+1,-1=R,L$) coupling constants of the vector boson $B=\gamma,Z$ to the fermion f in units of the elementary charge e. If not specified otherwise, the ''*hook function*'' H_B is trivial: $H_\gamma=H_Z=1$. It will be used to introduce special effects into Born spin amplitudes, such as running coupling constants or an additional form factor due to a narrow resonance.

Spinor products are reorganized with the help of the Chisholm identity, see Eq. (A11) in the Appendix, which applies assuming that the electron spinors are massless, and the inner product of Eq. (A8):

$$\mathfrak{B}_{[ba][cd]}^B(X)=2ie^2\frac{\delta_{\lambda_a,-\lambda_b}[g_{\lambda_a}^{B,e}g_{-\lambda_a}^{B,f}T_{\lambda_c\lambda_a}T'_{\lambda_b\lambda_d}+g_{\lambda_a}^{B,e}g_{\lambda_a}^{B,f}U'_{\lambda_c\lambda_b}U_{\lambda_a\lambda_d}]}{X^2-M_B^2+i\Gamma_BX^2/M_B}, \tag{44}$$

[3]For the moment we require $f\neq e$.

where

$$T_{\lambda_c\lambda_a}=\overline{u}(p_c,\lambda_c)u(p_a,\lambda_a)=S(p_c,m_c,\lambda_c,p_a,0,\lambda_a),$$

$$T'_{\lambda_b\lambda_d}=\overline{v}(p_b,\lambda_b)v(p_d,\lambda_d)$$
$$=S(p_b,0,-\lambda_b,p_d,-m_d,-\lambda_d),$$

$$U'_{\lambda_c\lambda_b}=\overline{u}(p_c,\lambda_c)v(p_b,-\lambda_b)=S(p_c,m_c,\lambda_c,p_b,0,\lambda_b),$$

$$U_{\lambda_a\lambda_d}=\overline{u}(p_a,-\lambda_a)v(p_d,\lambda_d)$$
$$=S(p_a,0,-\lambda_a,p_d,-m_d,-\lambda_d). \quad (45)$$

Note that the use of the Chisholm identity is a technical detail, which should not obscure the generality of our approach. What we need in practice is *any* numerical method of evaluation of the Born spin amplitudes defined in Eq. (43), and the Chisholm identity is just one possibility.

5. Off-space extrapolation

In Eq. (31) the Born spin amplitudes are obviously used for the p_i which *do not necessarily obey* the four-momentum conservation $p_a+p_b=p_c+p_d$. In the exclusive exponentiation, this is natural and necessary because, in the presence of the bremsstrahlung photons, the relation $X=p_a+p_b=p_c+p_d$ may not hold. In Eq. (31) only the fermion momenta enter as an argument of the Born spin amplitudes. The photon momenta play only an indirect role; they disturb the fermion momenta through energy and momentum conservation (this is sometimes referred to as a ''recoil effect''). The natural questions are: Is this acceptable? Is this dangerous? Can this be avoided? The clear answer is as follows: It is an unavoidable and natural feature of the exclusive exponentiation that certain scattering matrix elements, originally defined within *n*-body phase-space, are in fact used in the phase-space with more particles. Let us call it *off-space extrapolation*, analogously to off-shell extrapolation.[4] It surely makes sense, and in principle it is not dangerous, provided it is done with a little bit of care.

A technical remark is in order: In the actual calculations of the multiphoton spin amplitudes, the fermion momenta p_i in Eq. (44) may be replaced, and occasionally will be replaced, by the momentum k of one of the photons. This will be due to purely technical reasons (specific to the method of calculating multiphoton spin amplitudes). In such a case, the spinor into which k enters as an argument is always understood to be massless.

6. Pseudoflux factor

One demonstration of the ''off-space extrapolation'' is the presence of the auxiliary factor $X_\varphi^2/(p_c+p_d)^2$. In the framework of CEEX, its presence is not really mandatory and it disappears in the ''in-space'' situation $p_a+p_b=p_c+p_d$. In other words, this factor does not affect the soft limit; it really matters if at least one hard FSR photon is present. It is not related to narrow resonances, but rather to the LL structure of the higher orders. Nevertheless, the above factor is useful, because it is already implicitly present in the photon emission matrix element at $\mathcal{O}(\alpha^1)$ and at all higher orders, as can be seen in the LL approximation. It is therefore natural to include it at the early stage, already in the $\mathcal{O}(\alpha^0)$ exponentiation. If we do not include it at the $\mathcal{O}(\alpha^0)$, then it will be included order by order anyway. However, in such a case, the convergence of perturbative expansion will deteriorate. As we shall see below, the introduction of the above factor will slightly complicate the higher-order exponentiation and construction of the $\hat{\beta}$ functions, but the gain is worth the effort. Furthermore, the above factor also has always been present in the ''crude distribution'' in our YFS-type Monte Carlo generators, see for instance Ref. [7], so that its presence also improves the variance of the MC weight, especially for $\mathcal{O}(\alpha^0)_{\rm CEEX}$.

B. IR structure in CEEX

Let us discuss in detail the origin of the $\mathcal{O}(\alpha^r)_{\rm CEEX}$ expressions of Eqs. (31) and (32) and the mechanism of the IR cancellations. Our real starting point is the infinite-order perturbative expression for the total cross section given by the standard quantum-mechanical expression of the type ''matrix element squared modulus times phase-space'':

$$\sigma^{(\infty)}=\sum_{n=0}^{\infty}\frac{1}{n!}\int d\tau_n(p_a+p_b;p_c,p_d,k_1,\ldots,k_n)$$
$$\times\frac{1}{4}\sum_{\lambda,\sigma_i,\ldots,\sigma_n=\pm}\left|\mathcal{M}_n\begin{pmatrix}pk_1k_2\cdots k_n\\ \lambda\sigma_1\sigma_2\cdots\sigma_n\end{pmatrix}\right|^2, \quad (46)$$

where $d\tau_n$ is the respective $n\gamma+2f$ Lorentz-invariant phase-space, and $\mathcal{M}_n$ are the corresponding spin amplitudes. To simplify the discussion we take the unpolarized case, without narrow resonances.

1. IR virtual factorization to infinite order

According to the YFS fundamental factorization theorem [8], all virtual IR corrections can be relocated into an exponential form factor[5] order by order and in infinite order

$$\mathcal{M}_n^{(\infty)}=\exp[\alpha B_4(p_a,p_b,p_c,p_d)]\mathfrak{M}_n^{(\infty)}. \quad (47)$$

As the convergence of the perturbative series is questionable, the above equation is in practice treated as a symbolic representation of the order-by-order relation, which reads at $\mathcal{O}(\alpha^r)$,

[4]In the off-shell case, particles do not obey $p^2=m^2$; here we also modify the dimension of the phase-space.

[5]In the LL approximation it is, of course, the doubly-logarithmic Sudakov form factor.

$$\mathcal{M}_n^{(r)}=\sum_{l=0}^{r-n}\frac{(\alpha B_4)^{r-l}}{(r-l)!}\mathfrak{M}_n^{[l+n]}\quad (n\leqslant r), \tag{48}$$

where the index l is the number of loops in $\mathfrak{M}_n^{[l+n]}$. The above identity is quite powerful because the $\mathfrak{M}_n^{[l+n]}$ are not only free of the *virtual* IR divergences, they are also universal: they are the same in every perturbative order r; for example, for one photon, the one-loop (IR-subtracted) component $\mathfrak{M}_1^{(1)}$ is the same in the fifth order and, let us say, in the second order, where it appears for the first time. The above identity can also be reformulated as follows:

$$\begin{aligned}\mathfrak{M}_n^{(r)}&=\sum_{l=0}^{r-n}\mathfrak{M}_n^{[l+n]}\\&=\{\exp[-\alpha B_4(p_a,p_b,p_c,p_d)]\mathcal{M}_n^{(r)}\}|_{\mathcal{O}(\alpha^r)},\end{aligned} \tag{49}$$

where $\mathcal{M}_n^{(r)}$ has to be calculated from the Feynman diagrams in at least[6] $\mathcal{O}(\alpha^r)$. The above steps are exactly the same as in [8].

The YFS form factor B_4 for $e^-(p_a)+e^+(p_b)\to f(p_c)+\bar{f}(p_d)+n\gamma$ reads

$$\begin{aligned}&\alpha B_4(p_a,p_b,p_c,p_d)\\&\quad=\int\frac{d^4k}{k^2-m_\gamma^2+i\epsilon}\frac{i}{(2\pi)^3}|J_I(k)-J_F(k)|^2,\end{aligned} \tag{50}$$

$$J_I=eQ_e[\hat{J}_a(k)-\hat{J}_b(k)],$$

$$J_F=eQ_f[\hat{J}_c(k)-\hat{J}_d(k)],\quad \hat{J}_f^\mu(k)=\frac{2p_f^\mu+k^\mu}{k^2+2k\cdot p_f+i\epsilon}.$$

Using the identity $(\Sigma_k Z_k J_k)^2=-\Sigma_{i>k}Z_iZ_k(J_i-J_k)^2$, valid for $\Sigma Z_k=0$, where Z_k is the charge or minus charge of the particle in the initial or final state, respectively, we may cast (see Ref. [8]) B_4 into a sum of the simpler dipole components

$$\begin{aligned}B_4(p_a,p_b,p_c,p_d)&=Q_e^2B_2(p_a,p_b)+Q_f^2B_2(p_c,p_b)\\&\quad+Q_eQ_fB_2(p_a,p_c)+Q_eQ_fB_2(p_b,p_d)\\&\quad-Q_eQ_fB_2(p_a,p_d)-Q_eQ_fB_2(p_b,p_c),\end{aligned} \tag{51}$$

$$\begin{aligned}B_2(p_i,p_j)\equiv&\int\frac{d^4k}{k^2-m_\gamma^2+i\epsilon}\frac{i}{(2\pi)^3}\\&\times[\hat{J}(p_i,k)-\hat{J}(p_j,k)]^2.\end{aligned} \tag{52}$$

[6]The use of $\mathfrak{M}_n^{(r+m)}$ at $\mathcal{O}(\alpha^{(r+m)})$, $m>0$, will yield the same result, which is another way of stating the universality property.

In the above we assume that IR singularities are regularized with a finite photon mass m_γ that enters into all of the B_2's and implicitly into the $\mathfrak{s}$ factors (and into the real photon phase-space integrals, see the following discussion).

2. IR real factorization to infinite order

The next step is the isolation of the *real* IR singularities and it is well worth elaborating on this point, because here the CEEX method differs in essential details from the original YFS method [8]. We use again the results of the basic analysis of the real IR singularities of Ref. [8], the essential difference being that we do not square the amplitudes immediately—it is done numerically at a later stage. The validity of the whole basic analysis of the IR cancellations in Ref. [8] remains, however, useful because it is done in terms of the currents

$$j_f^\mu(k)=\frac{2p_f^\mu}{2p_f\cdot k},\quad f=a,b,c,d. \tag{53}$$

The above currents are simply related to our $\mathfrak{s}$ factors:

$$\begin{aligned}\mathfrak{s}_\sigma^{\{I\}}(k)&=\text{const}\times Q_e(j_a-j_b)\cdot\epsilon_\sigma(\beta),\\\mathfrak{s}_\sigma^{\{F\}}(k)&=\text{const}\times Q_f(j_c-j_d)\cdot\epsilon_\sigma(\beta).\end{aligned} \tag{54}$$

It is important to remember that the whole structure of the real IR divergences is entirely controlled by the squares of the currents $|j(k)|^2$, for $j=j_a-j_b$ or $j=j_c-j_d$, independently of whether we prefer to work with the amplitudes or their squares, because only the squares $|j(k)|^2$ are IR divergent and the other contractions do not matter (as was already stressed in Ref. [8]). Similarly, if we express spin amplitudes in terms of $\mathfrak{s}$ factors, only the squares $|\mathfrak{s}(k)|^2$ are IR divergent and not the interference terms such as $\Re\{\mathfrak{s}(k)(\cdots)^*\}$.

Having the above in mind, we may proceed using the results of Ref. [8] and we see that for instance the most IR-divergent part of $\mathcal{M}_n$ is proportional to the products of n $\mathfrak{s}$ factors

$$\mathfrak{M}_n\begin{pmatrix}pk_1k_2\cdots k_n\\ \lambda\sigma_1\sigma_2\cdots\sigma_n\end{pmatrix}\sim\hat{\beta}_0\begin{pmatrix}p\\ \lambda;X\end{pmatrix}\mathfrak{s}_{\sigma_1}(k_1)\mathfrak{s}_{\sigma_2}(k_2)\cdots\mathfrak{s}_{\sigma_n}(k_n), \tag{55}$$

where the function $\hat{\beta}_0$ is no longer IR divergent, and we assumed for the moment the absence of any narrow resonances, using the sum of the ISR and FSR $\mathfrak{s}$ factors:[7]

$$\mathfrak{s}_\sigma(k)\equiv\mathfrak{s}_\sigma^{\{F\}}(k)+\mathfrak{s}_\sigma^{\{I\}}(k). \tag{56}$$

However, there are also nonleading IR singularities. Suppressing inessential spin indices, the whole real-IR structure is revealed in the following decomposition [8]:

[7]In the nonresonant case we may set $X=p_a+p_b$, for example.

$$\mathfrak{M}_n^{(\infty)}(k_1,k_2,k_3,\ldots,k_n)=\hat{\beta}_0\prod_{s=1}^{n}\mathfrak{s}(k_s)+\sum_{j=1}^{n}\hat{\beta}_1(k_j)\prod_{s\neq j}\mathfrak{s}(k_s)+\sum_{j_1>j_2}\hat{\beta}_2(k_{j_1},k_{j_2})\prod_{s\neq j_1,j_2}\mathfrak{s}(k_s)$$
$$+\sum_{j_1>j_2>j_3}\hat{\beta}_2(k_{j_1},k_{j_2},k_{j_3})\prod_{s\neq j_1,j_2,j_3}\mathfrak{s}(k_s)+\cdots+\sum_{j=1}^{n}\hat{\beta}_{n-1}(k_1,\ldots k_{j-1},k_{j+1},\ldots,k_n)\mathfrak{s}(k_j)$$
$$+\hat{\beta}_n(k_1,k_2,k_3,\ldots,k_n) \tag{57}$$

where the functions $\hat{\beta}_i$ are IR free and include finite-loop corrections to infinite order. Let us stress that these functions $\hat{\beta}_i$ are *genuinely new objects*. They were not used and even not considered in Ref. [8].

3. Finite-order $\hat{\beta}$'s

The decomposition of Eq. (57) also has its order-by-order representation, which at $\mathcal{O}(\alpha^r)$, $r=n+l$, reads as follows:

$$\mathfrak{M}_n^{(n+l)}(k_1,k_2,k_3,\ldots,k_n)=\hat{\beta}_0^{(l)}\prod_{s=1}^{n}\mathfrak{s}(k_s)+\sum_{j=1}^{n}\hat{\beta}_1^{(1+l)}(k_j)\prod_{s\neq j}\mathfrak{s}(k_s)+\sum_{j_1<j_2}\hat{\beta}_2^{(2+l)}(k_{j_1},k_{j_2})\prod_{s\neq j_1,j_2}\mathfrak{s}(k_s)$$
$$+\sum_{j_1<j_2<j_3}\hat{\beta}_2^{(3+l)}(k_{j_1},k_{j_2},k_{j_3})\prod_{s\neq j_1,j_2,j_3}\mathfrak{s}(k_s)+\cdots$$
$$+\sum_{j=1}^{n}\hat{\beta}_{n-1}^{(n-1+l)}(k_1,\ldots k_{j-1},k_{j+1},\ldots,k_n)\mathfrak{s}(k_j)+\hat{\beta}_n^{(n+l)}(k_1,k_2,k_3,\ldots,k_n) \tag{58}$$

$$=\prod_{s=1}^{n}\mathfrak{s}(k_s)\left\{\hat{\beta}_0^{(l)}+\sum_{j=1}^{n}\frac{\hat{\beta}_1^{(1+l)}(k_j)}{\mathfrak{s}(k_j)}+\sum_{j_1<j_2}\frac{\hat{\beta}_2^{(2+l)}(k_{j_1},k_{j_2})}{\mathfrak{s}(k_{j_1})\mathfrak{s}(k_{j_2})}+\sum_{j_1<j_2<j_3}\frac{\hat{\beta}_2^{(3+l)}(k_{j_1},k_{j_2},k_{j_3})}{\mathfrak{s}(k_{j_1})\mathfrak{s}(k_{j_2})\mathfrak{s}(k_{j_3})}\right.$$
$$\left.+\sum_{j=1}^{n}\frac{\hat{\beta}_{n-1}^{(n-1+l)}(k_1,\ldots k_{j-1},k_{j+1},\ldots,k_n)}{\prod_{s\neq j}\mathfrak{s}(k_s)}+\frac{\hat{\beta}_n^{(n+l)}(k_1,k_2,k_3,\ldots,k_n)}{\prod_{s}\mathfrak{s}(k_s)}\right\}.$$

The new functions $\hat{\beta}_n^{(n+l)}(k_1,k_2,k_3,\ldots,k_n)$ contain up to l-loop corrections, and are not only completely IR finite, but are also universal: for instance the $\hat{\beta}_1^{(2)}(k)$, which appears for the first time in the decomposition of $\mathfrak{M}_1^{(2)}(k)$, is functionally the same when decomposing $\mathfrak{M}_2^{(3)}(k_1,k_2)$ or any higher-order $\mathfrak{M}_n^{(n+l)}$. This feature is essential for reversing the relations of Eq. (58), that is for the practical order-by-order calculations of the $\hat{\beta}_n^{(n+l)}$ from $\mathfrak{M}_n^{(r)}$, obtained directly from the Feynman rules:

$$\hat{\beta}_0^{(l)}=\mathfrak{M}_0^{(l)}, \tag{59}$$

$$\hat{\beta}_1^{(1+l)}(k_1)=\mathfrak{M}_1^{(1+l)}(k_1)-\hat{\beta}_0^{(l)}\mathfrak{s}(k_1),$$

$$\hat{\beta}_2^{(2+l)}(k_1,k_2)=\mathfrak{M}_2^{(2+l)}(k_1,k_2)-\hat{\beta}_1^{(1+l)}(k_1)\mathfrak{s}(k_2)-\hat{\beta}_1^{(1+l)}(k_2)\mathfrak{s}(k_1)-\hat{\beta}_0^{(l)}\mathfrak{s}(k_1)\mathfrak{s}(k_2),$$

$$\hat{\beta}_3^{(3+l)}(k_1,k_2,k_3)=\mathfrak{M}_3^{(3+l)}(k_1,k_2,k_3)-\hat{\beta}_2^{(2+l)}(k_1,k_2)\mathfrak{s}(k_3)-\hat{\beta}_2^{(2+l)}(k_1,k_3)\mathfrak{s}(k_2)-\hat{\beta}_2^{(2+l)}(k_2,k_3)\mathfrak{s}(k_1)$$
$$-\hat{\beta}_1^{(1+l)}(k_1)\mathfrak{s}(k_2)\mathfrak{s}(k_3)-\hat{\beta}_1^{(1+l)}(k_2)\mathfrak{s}(k_1)\mathfrak{s}(k_3)-\hat{\beta}_1^{(1+l)}(k_3)\mathfrak{s}(k_1)\mathfrak{s}(k_2)-\hat{\beta}_0^{(l)}\mathfrak{s}(k_1)\mathfrak{s}(k_2)\mathfrak{s}(k_3),\ldots,$$

$$\hat\beta_n^{(n+l)}(k_1,\ldots,k_n)=\mathfrak{M}_n^{(n+l)}(k_1,\ldots,k_n)-\sum_{j=1}^{n}\hat\beta_{n-1}^{(n-1+l)}(k_1,\ldots k_{j-1},k_{j+1},\ldots,k_n)\mathfrak{s}(k_j)$$
$$-\sum_{j_1<j_2}\hat\beta_{n-2}^{(2-2+l)}(k_1,\ldots k_{j_1-1},k_{j_1+1},\ldots k_{j_2-1},k_{j_2+1},\ldots,k_n)\mathfrak{s}(k_{j_1})\mathfrak{s}(k_{j_2})\cdots$$
$$-\sum_{j_1<j_2}\hat\beta_2^{(2+l)}(k_{j_1},k_{j_2})\prod_{s\neq j_1,j_2}\mathfrak{s}(k_s)-\sum_{j=1}^{n}\hat\beta_1^{(1+l)}(k_j)\prod_{s\neq j}\mathfrak{s}(k_s)-\hat\beta_0^{(l)}\prod_{s=1}^{n}\mathfrak{s}(k_s).$$

The above set of equations is a recursive rule, i.e., the higher-order $\hat\beta$'s are constructed in terms of the lower-order ones. In practical calculations we do not go to infinite order but we stop at some $\mathcal{O}(\alpha^r)$ and the above set of equations is truncated for $\hat\beta_n^{(n+l)}$ by the requirement $n+l\leqslant r$. The above truncation is harmless from the point of view of IR cancellations, because we omit higher-order $\hat\beta$'s, which are IR finite. As a consequence of the above fixed-order truncation, Eq. (57) takes the following form:

$$\mathfrak{M}_n^{(r)}(k_1,k_2,k_3,\ldots,k_n)$$
$$=\prod_{s=1}^{n}\mathfrak{s}(k_s)\left\{\hat\beta_0^{(r)}+\sum_{j=1}^{n}\frac{\hat\beta_1^{(r)}(k_j)}{\mathfrak{s}(k_j)}+\sum_{j_1<j_2}\frac{\hat\beta_2^{(r)}(k_{j_1},k_{j_2})}{\mathfrak{s}(k_{j_1})\mathfrak{s}(k_{j_2})}\right.$$
$$+\sum_{j_1<j_2<j_3}\frac{\hat\beta_3^{(r)}(k_{j_1},k_{j_2},k_{j_3})}{\mathfrak{s}(k_{j_1})\mathfrak{s}(k_{j_2}\mathfrak{s}(k_{j_3})}$$
$$\left.+\sum_{j_1<j_2<\cdots<j_r}\frac{\hat\beta_r^{(r)}(k_{j_1},k_{j_2},\ldots,k_{j_r})}{\mathfrak{s}(k_{j_1})\mathfrak{s}(k_{j_2})\ldots\mathfrak{s}(k_{j_r})}\right\},\qquad(60)$$

where, contrary to Eq. (58), we now allow only for $r<n$; in such a case the sum has $r+1$ terms instead of n.

The above formula represents the general finite-order $\mathcal{O}(\alpha^r)_{exp}$ case, while for $r=0$ only the first term survives, and in our $\mathcal{O}(\alpha^2)$ case there are three terms. The CEEX spin amplitudes in our master formula [Eq. (31)] represent the cases of $r=0,1,2$.

Just to give an explicit example, in the recursive calculation of $\hat\beta$'s in $\mathcal{O}(\alpha^3)$, we would need to calculate $\hat\beta_0^{(l)}$, $l=0,1,2,3$; $\hat\beta_1^{(1+l)}$, $l=0,1,2$; $\hat\beta_2^{(2+l)}$, $l=0,1$; and $\hat\beta_3^{(3)}$. In the present work, at $\mathcal{O}(\alpha^r)$, $r=0,1,2$, we shall employ the following set of recursive definitions, based on Eqs. (59):

$$\hat\beta_0^{(l)}\left(\begin{matrix}p\\ \lambda\end{matrix}\right)=\mathfrak{M}_0^{(l)}\left(\begin{matrix}p\\ \lambda\end{matrix}\right),\quad l=0,1,2,\qquad(61)$$

$$\hat\beta_1^{(1+l)}\left(\begin{matrix}pk_1\\ \lambda\sigma_1\end{matrix}\right)=\mathfrak{M}_1^{(1+l)}\left(\begin{matrix}pk_1\\ \lambda\sigma_1\end{matrix}\right)-\hat\beta_0^{(l)}\left(\begin{matrix}p\\ \lambda\end{matrix}\right)\mathfrak{s}_{\sigma_1}(k_1),\quad l=0,1,$$

$$\hat\beta_2^{(2)}\left(\begin{matrix}pk_1k_2\\ \lambda\sigma_1\sigma_2\end{matrix}\right)=\mathfrak{M}_2^{(2)}\left(\begin{matrix}pk_1k_2\\ \lambda\sigma_1\sigma_2\end{matrix}\right)-\hat\beta_1^{(1)}\left(\begin{matrix}pk_1\\ \lambda\sigma_1\end{matrix}\right)\mathfrak{s}_{\sigma_2}(k_2)$$
$$-\hat\beta_1^{(1)}\left(\begin{matrix}pk_2\\ \lambda\sigma_2\end{matrix}\right)\mathfrak{s}_{\sigma_1}(k_1)$$
$$-\hat\beta_0^{(0)}\left(\begin{matrix}p\\ \lambda\end{matrix}\right)\mathfrak{s}_{\sigma_1}(k_1)\mathfrak{s}_{\sigma_2}(k_2),$$

where the $\mathfrak{M}$ amplitude is given by Eq. (49). Here we restored the spin indices but we still specialize to the nonresonant case, and our $\hat\beta$'s do not have the partition-dependent $X_\wp$ argument as in the $\hat\beta$'s of Eqs. (31) to (35). We shall provide a definition for the $\hat\beta$'s in the resonant case in Sec. III C 4.

4. IR cancellations in CEEX

At fixed-order $\mathcal{O}(\alpha^r)_{\rm CEEX}$, and remembering that $|\exp(B_4)|^2=\exp(2\Re B_4)$, we have obtained

$$\sigma^{(r)}=\sum_{n=0}^{\infty}\frac{1}{n!}\int d\tau_n(p_1+p_2;p_3,p_4,k_1,\ldots,k_n)$$
$$\times\exp[2\alpha\Re B_4(p_a,\ldots,p_d)]$$
$$\times\frac{1}{4}\sum_{\rm spin}|\mathfrak{M}_n^{(r)}(k_1,k_2,\ldots k_n)|^2,\qquad(62)$$

where $\mathfrak{M}_n^{(r)}$ is defined in Eq. (60) and we factorize out the $\mathfrak{s}$ factors

$$\frac{1}{4}\sum_{\rm spin}|\mathfrak{M}_n^{(r)}(k_1,k_2,k_3,\ldots,k_n)|^2\qquad(63)$$
$$=d_n(k_1,k_2,k_3,\ldots,k_n)\prod_{s=1}^{n}|\mathfrak{s}(k_s)|^2,$$

$$d_n(k_1,k_2,k_3,\ldots,k_n)$$
$$=\left|\hat\beta_0^{(r)}+\sum_{j=1}^{n}\frac{\hat\beta_1^{(r)}(k_j)}{\mathfrak{s}(k_j)}+\sum_{j_1<j_2}\frac{\hat\beta_2^{(r)}(k_{j_1},k_{j_2})}{\mathfrak{s}(k_{j_1})\mathfrak{s}(k_{j_2})}\right.$$

$$+\sum_{j_1<j_2<j_3}\frac{\hat{\beta}_3^{(r)}(k_{j_1},k_{j_2},k_{j_3})}{\mathfrak{s}(k_{j_1})\mathfrak{s}(k_{j_2})\mathfrak{s}(k_{j_3})}$$

$$+\cdots+\sum_{j_1<j_2<\cdots<j_r}\frac{\hat{\beta}_r^{(r)}(k_{j_1},k_{j_2},\ldots,k_{j_r})}{\mathfrak{s}(k_{j_1})\mathfrak{s}(k_{j_2}),\ldots,\mathfrak{s}(k_{j_r})}\Bigg|^2.$$

In the above, the function $d_n(k_1,k_2,k_3,\ldots,k_n)$ is IR finite and we are allowed to set $m_\gamma\to 0$ in it. Apart from $2\alpha\Re B_4$ the IR regulator m_γ still remains in all $\mathfrak{s}(k_i)$ factors and in the lower phase-space boundary of all real photons in $\int d^3k/2k^0$.

The above total cross section is perfectly IR finite, as can be checked with a little bit of effort by *analytical* partial differentiation[8] with respect the photon mass

$$\frac{\partial}{\partial m_\gamma}\sigma^{(r)}=\sum_{n=0}^{\infty}\frac{1}{n!}\int d\tau_n(P;p_3,p_4,k_1,\ldots,k_n)$$
$$\times\exp(2\alpha\Re B_4)\frac{\partial}{\partial m_\gamma}\{2\alpha\Re B_4\}$$
$$\times\frac{1}{4}\sum_{\text{spin}}|\mathfrak{M}_n^{(r)}(k_1,k_2,\ldots,k_n)|^2+\sum_{n=1}^{\infty}\frac{1}{n!}\sum_{s=1}^{n}$$
$$\times\int d\tau_{n-1}(P;p_3,p_4,k_1,\ldots,k_{s-1},k_{s+1},\ldots,k_n)$$
$$\times\exp(2\alpha\Re B_4)\frac{\partial}{\partial m_\gamma}\left\{\int\frac{d^3k_s}{(2\pi)^3 2k_s^0}|\mathfrak{s}(k_s)|^2\right\}$$
$$\times\prod_{j\neq s}|\mathfrak{s}(k_j)|^2 d_n(k_1,k_2,\ldots,k_s,\ldots,k_n). \qquad (64)$$

It is now necessary to notice that

$$\frac{\partial}{\partial m_\gamma}\left\{\int\frac{d^3k_s}{2k_s^0}|\mathfrak{s}(k_s)|^2\right\}$$

is a δ-like measure concentrated at $k_s=0$ and we may therefore use the limit

$$d_n(k_1,\ldots,k_s,\ldots,k_n)$$
$$\to d_n(k_1,k_2,\ldots,k_{s-1},0,k_{s+1},\ldots,k_n)$$
$$\equiv d_{n-1}(k_1,k_2,\ldots,k_{s-1},k_{s+1},\ldots,k_n).$$

The above limit helps us to notice that all of the terms in the $\Sigma_{s=1}^n$ are identical and we may sum them up (after formally renaming the photon integration variables in the second integral) and rewrite Eq. (64) as follows:

$$\frac{\partial}{\partial m_\gamma}\sigma^{(r)}=\sum_{n=0}^{\infty}\frac{1}{n!}\int d\tau_n(P;p_3,p_4,k_1,\ldots,k_n)$$
$$\times\exp(2\alpha\Re B_4)\frac{1}{4}\sum_{\text{spin}}|\mathfrak{M}_n^{(r)}(k_1,k_2,\ldots k_n)|^2$$
$$\times\frac{\partial}{\partial m_\gamma}\left\{2\alpha\Re B_4+\int\frac{d^3k_s}{(2\pi)^3 2k_s^0}|\mathfrak{s}(k_s)|^2\right\}=0, \qquad (65)$$

where the independence on m_γ of the sum of the one-photon real and virtual integrals is due to the usual cancellation of the IR divergences in the YFS scheme, shown explicitly many times.

The integrals of Eqs. (46) and (62) are perfectly implementable in the Monte Carlo form, with the small m_γ being the IR regulator, using a method very similar to that in Ref. [7]. Traditionally, however, the lower boundary on the real soft photons is defined using the energy cut condition $k^0>\varepsilon\sqrt{s}/2$ in the laboratory frame. The practical advantage of such a cut is the lower photon multiplicity in the MC simulation, and consequently a faster computer program.[9] If the above energy cut on the photon energy is adopted, then the real soft-photon integral between the lower LIPS (Lorentz invariant phase space) boundary defined by m_γ and that defined by ε can be evaluated by hand and summed up rigorously (the only approximation is $m_\gamma/m_e\to 0$), as we show in the following.

5. Explicit IR boundary for real photons

A general notation for the IR domain Ω was already introduced, see Eq. (36). Let us now exclude the Ω domain from the real-photon phase-space (integrate out analytically). Splitting the real-photon integration phase-space, we rewrite Eq. (62) as follows:

$$\sigma^{(r)}=\sum_{n=0}^{\infty}\frac{1}{n!}\prod_{j=1}^{n}\left\{\int\frac{d^3k_j}{(2\pi)^3 2k_j^0}|\mathfrak{s}(k_j)|^2\Theta(\Omega,k_j)\right.$$
$$\left.+\int\frac{d^3k_j}{(2\pi)^3 2k_j^0}|\mathfrak{s}(k_j)|^2\bar{\Theta}(\Omega,k_j)\right\}$$
$$\times\int d\tau_0\left(P-\sum_{j=1}^{n}k_j;p_3,p_4\right)$$
$$\times\exp(2\alpha\Re B_4)d_n(k_1,k_2,\ldots,k_n). \qquad (66)$$

After expanding the binomial product into 2^n terms let us consider for instance the sum of all $\binom{n}{1}=n$ terms in which one photon is in Ω and the other ones are not:

[8]This method of validating the IR-finiteness was noted by G. Burgers [29]. The classical method of Ref. [8] relies on the techniques of the Fourier transform, which could also be used here.

[9]The disadvantage of the cut $k^0>\varepsilon\sqrt{s}/2$ is that in the MC simulation it has to be implemented in *different* reference frames for ISR and for FSR; this costs the additional delicate procedure of bringing these two boundaries together, see Ref. [1] and the discussion about the analogous *t*-channel case in Ref. [11].

$$
\begin{aligned}
&\frac{1}{n!}\sum_{s=1}^{n}\int\frac{d^3k_s}{(2\pi)^3 2k_s^0}|\mathfrak{s}(k_s)|^2\Theta(\Omega,k_s)\\
&\quad\times\prod_{j\neq s}^{n}\int\frac{d^3k_j}{(2\pi)^3 2k_j^0}|\mathfrak{s}(k_j)|^2\overline{\Theta}(\Omega,k_j)\\
&\quad\times\int d\tau_0\left(P-\sum_{j=1}^{n}k_j;p_3,p_4\right)\\
&\quad\times\exp(2\alpha\Re B_4)d_n(k_1,k_2,\ldots,k_{s-1},0,k_{s+1},\ldots,k_n)\\
&=\frac{1}{n!}\binom{n}{1}\int\frac{d^3k}{(2\pi)^3 2k^0}|\mathfrak{s}(k)|^2\Theta(\Omega,k)\\
&\quad\times\int d\tau_{n-1}(P;p_3,p_4,k_1,k_2,\ldots,k_{n-1})\\
&\quad\times\prod_{j=1}^{n-1}\overline{\Theta}(\Omega,k_j)|\mathfrak{s}(k_j)|^2 d_{n-1}(k_1,k_2,\ldots,k_{n-1}). \qquad (67)
\end{aligned}
$$

A similar summation is performed for the $\binom{n}{s}$ terms where s photons are in Ω, giving rise to

$$
\begin{aligned}
\sigma^{(r)}&=\sum_{n=0}^{\infty}\frac{1}{n!}\sum_{s=0}^{n}\binom{n}{s}\left(\int\frac{d^3k}{(2\pi)^3 2k^0}|\mathfrak{s}(k)|^2\Theta(\Omega,k)\right)^s\\
&\quad\times\int d\tau_{n-s}(P;p_3,p_4,k_1,k_2,\ldots,k_{n-s})\\
&\quad\times\prod_{j=1}^{n-s}\{|\mathfrak{s}(k_j)|^2\overline{\Theta}(\Omega,k_j)\}\\
&\quad\times\exp(2\alpha\Re B_4)d_{n-s}(k_1,k_2,\ldots,k_{n-s})\\
&=\sum_{n=0}^{\infty}\frac{1}{n!}\int d\tau_n(P;p_3,p_4,k_1,k_2,\ldots,k_n)\\
&\quad\times\exp\left(\int\frac{d^3k_j}{(2\pi)^3 2k_j^0}|\mathfrak{s}(k_j)|^2\Theta(\Omega,k_j)\right)\\
&\quad\times\exp[2\alpha\Re B_4(p_1,\ldots,p_4)]\\
&\quad\times\prod_{j=1}^{n}\{|\mathfrak{s}(k_j)|^2\overline{\Theta}(\Omega,k_j)\}d_n(k_1,k_2,\ldots,k_n). \qquad (68)
\end{aligned}
$$

The additional overall exponential factor contains the well-known function

$$
\begin{aligned}
2\alpha\tilde{B}_4(p_1,\ldots,p_4)&=\int\frac{d^3k_j}{(2\pi)^3 2k_j^0}|\mathfrak{s}(k_j)|^2\Theta(\Omega,k_j)\\
&=2\alpha[Q_e^2\tilde{B}_2(p_1,p_2)+Q_f^2\tilde{B}_2(p_3,p_4)\\
&\quad+Q_eQ_f\tilde{B}_2(p_1,p_3)+Q_eQ_f\tilde{B}_2(p_2,p_4)\\
&\quad-Q_eQ_f\tilde{B}_2(p_1,p_4)-Q_eQ_f\tilde{B}_2(p_2,p_3)], \qquad (69)
\end{aligned}
$$

$$
\begin{aligned}
\tilde{B}_2(p,q)&\equiv-\int\frac{d^3k}{(2\pi)^2 2k^0}\Theta(\Omega,k)[j_p(k)-j_q(k)]^2\\
&\equiv\int\frac{d^3k}{k^0}\Theta(\Omega,k)\frac{(-1)}{8\pi^2}\left(\frac{p}{kp}-\frac{q}{kq}\right)^2,
\end{aligned}
$$

which forms together with $2\alpha\Re B_4(p_1,\ldots,p_4)$ the conventional YFS form factor

$$
\begin{aligned}
Y(\Omega;p_1,\ldots,p_4)&=2\alpha\tilde{B}_4(p_1,\ldots,p_4)\\
&\quad+2\alpha\Re B_4(p_1,\ldots,p_4) \qquad (70)
\end{aligned}
$$

in our master Eqs. (31) and (32). The dependence on m_γ in Y cancels out. The photon mass gets effectively replaced by the size of Ω in its role as the IR regulator. The YFS form-factor Y can be decomposed into six dipole components, see Eq. (37), and can be calculated analytically in terms of logs and Spence functions, see Refs. [30–32], keeping exactly all fermion masses.

As already indicated, in the MC with the YFS exponentiation, it would be possible to do without Ω (declaring it as empty) and to rely uniquely on the IR regularization with a small photon mass m_γ only [3]. In such a case the formulas (38) for the YFS form factor would include only the second virtual-photon integral part.

For the sake of the completeness of the discussion, it is necessary to examine once again the IR cancellations in the total cross section, with Ω as the new IR regulator:

$$
\begin{aligned}
\sigma^{(r)}&=\sum_{n=0}^{\infty}\frac{1}{n!}\int d\tau_n(P;p_3,p_4,k_1,k_2,\ldots,k_n)\\
&\quad\times\prod_{j=1}^{n}\{|\mathfrak{s}(k_j)|^2\overline{\Theta}(\Omega,k_j)\}\exp[\tilde{B}_4(\Omega;p_1,\ldots,p_4)\\
&\quad+2\alpha\Re B_4(p_1,\ldots,p_4)]d_n(k_1,k_2,\ldots,k_n). \qquad (71)
\end{aligned}
$$

IR finiteness of the total cross section now simply translates into its independence of the Ω domain (assuming, as usual, that the size of Ω is very small)

$$
\frac{\delta}{\delta\Omega}\sigma^{(r)}=0. \qquad (72)
$$

The proof can be given along the same lines as the previous one for the photon mass. Let us assume that we want to vary $\Omega\to\Omega'=\Omega+\delta\Omega$, that is $\overline{\Omega}'=\overline{\Omega}-\delta\Omega$. Note that Ω' can be much larger or smaller than Ω, the only requirement is that both be very small.[10] We proceed as follows:

[10] $\delta\Omega$ does not need to be infinitesimal with respect to Ω. Its size should be much smaller than $\sqrt{s}$.

$$
\begin{aligned}
\sigma^{(r)} &= \sum_{n=0}^{\infty} \frac{1}{n!} \prod_{j=1}^{n} \left\{ \int \frac{d^3k_j}{(2\pi)^3 2k_j^0} |\mathfrak{s}(k_j)|^2 \overline{\Theta}(\Omega', k_j) + \int \frac{d^3k_j}{(2\pi)^3 2k_j^0} |\mathfrak{s}(k_j)|^2 \Theta(\delta\Omega, k_j) \right\} \\
&\quad \times \int d\tau_0 \left(P - \sum k_j ; p_3, p_4 \right) \exp[2\alpha \tilde{B}_4(\Omega; p_1, \ldots, p_4) + 2\alpha \Re B_4(p_1, \ldots, p_4)] d_n(k_1, k_2, \ldots, k_n) \\
&= \sum_{n=0}^{\infty} \frac{1}{n!} \sum_{s=0}^{n} \binom{n}{s} \left\{ \int \frac{d^3k}{(2\pi)^3 2k^0} |\mathfrak{s}(k)|^2 \Theta(\delta\Omega, k) \right\}^s \int d\tau_{n-s}(P; p_3, p_4, k_1, \ldots, k_{n-s}) \\
&\quad \times \prod_{j=1}^{n-s} \{ |\mathfrak{s}(k_j)|^2 \overline{\Theta}(\Omega', k_j) \} \exp[2\alpha \tilde{B}_4(\Omega; p_1, \ldots, p_4) + 2\alpha \Re B_4(p_1, \ldots, p_4)] d_{n-s}(k_1, k_2, \ldots, k_{n-s}) \qquad (73) \\
&= \sum_{n=0}^{\infty} \frac{1}{n!} \int d\tau_n(P; p_3, p_4, k_1, \ldots, k_n) \exp\left[\int \frac{d^3k}{(2\pi)^3 2k^0} |\mathfrak{s}(k)|^2 \Theta(\delta\Omega, k) + 2\alpha \tilde{B}_4(\Omega; p_1, \ldots, p_4) + 2\alpha \Re B_4(p_1, \ldots, p_4) \right] \\
&\quad \times \prod_{j=1}^{n} \{ |\mathfrak{s}(k_j)|^2 \overline{\Theta}(\Omega', k_j) \} d_n(k_1, k_2, \ldots, k_n),
\end{aligned}
$$

recovering the same expression as Eq. (71), but with Ω' instead of Ω.

C. Narrow neutral resonance in CEEX

The main new feature of CEEX with respect to EEX is that the separation of the IR real singularities is done at the spin amplitude level; after squaring and spin-summing them (numerically) the higher order terms are retained, while in EEX they are truncated. For a more detailed discussion, see Sec. IV C, where we explicitly show the relations between the $\hat{\beta}$'s of CEEX and $\overline{\beta}$'s of EEX. Keeping the above in mind, we still have at least three possible versions of CEEX. In the following we shall describe them, concentrating mostly on the third one, which is designed for the neutral s-channel resonances[11] and which is the principal version implemented in the $\mathcal{KK}$ Monte Carlo. Let us stress immediately that the resonance may be arbitrarily narrow. However, our approach works without any modification for any value of the resonance width.

1. General discussion

We believe that CEEX is the only workable technique for the treatment of narrow resonances in the exclusive MC. To understand the essential difference between the three possible formulations of CEEX, it is sufficient to limit the discussion to the simplest case of the $\mathcal{O}(\alpha^0)$. The three possible options are the following.

(A) The version for the nonresonant Born without partitions:

$$
\mathfrak{M}_n^{(0)} \left(\begin{matrix} p k_1 k_2 \cdots k_n \\ \lambda \sigma_1 \sigma_2 \cdots \sigma_n \end{matrix} \right) = \prod_{i=1}^{n} [\mathfrak{s}_{\sigma_i}^{I}(k_i) + \mathfrak{s}_{\sigma_i}^{F}(k_i)] \mathfrak{B}_{[ba][cd]} . \qquad (74)
$$

(B) The version for the nonresonant Born with partitions:

$$
\mathfrak{M}_n^{(0)} \left(\begin{matrix} p k_1 k_2 \cdots k_n \\ \lambda \sigma_1 \sigma_2 \cdots \sigma_n \end{matrix} \right) = \sum_{\wp \in \{I,F\}^n} \prod_{i=1}^{n} \mathfrak{s}_{\sigma_i}^{\{\wp_i\}}(k_i) \mathfrak{B}_{[ba][cd]}(X_\wp). \qquad (75)
$$

(C) The version for the resonant Born:

$$
\begin{aligned}
&\mathfrak{M}_n^{(0)} \left(\begin{matrix} p k_1 k_2 \cdots k_n \\ \lambda \sigma_1 \sigma_2 \cdots \sigma_n \end{matrix} \right) \\
&\quad = \sum_{\wp \in \{I,F\}^n} \prod_{i=1}^{n} \mathfrak{s}_{\sigma_i}^{\{\wp_i\}}(k_i) \frac{X_\wp^2}{(p_3 + p_4)^2} \\
&\qquad \times \sum_{R=\gamma,Z} \mathfrak{B}_{[ba][cd]}^{B}(X_\wp) \exp[\alpha \Delta B_4^R(X_\wp)]. \qquad (76)
\end{aligned}
$$

Let us immediately define the additional form factor for the Z resonance [case (C)]:

$$
\begin{aligned}
\alpha \Delta B_4^Z(X) &= \int \frac{d^4k}{k^2 - m_\gamma^2 + i\epsilon} \frac{i}{(2\pi)^3} J_{I\mu}(k) \\
&\quad \times [J_F^\mu(k)]^* \left(\frac{(X)^2 - \overline{M}^2}{(X-k)^2 - \overline{M}^2} - 1 \right), \qquad (77)
\end{aligned}
$$

where $\overline{M}^2 = M_Z^2 - i M_Z \Gamma_Z$, the currents J^μ are defined in Eq. (50), while for the nonresonant part we have $\Delta B_4^\gamma(X) = 0$. The $\Delta B_4^Z(X)$ form factor sums up to infinite order the virtual $\alpha \ln(\Gamma_Z / M_Z)$ contributions; we postpone the discussion of its origin and importance to the latter part of this section.

[11] The simultaneous application of our CEEX methods to the production and decay processes of pair-produced charged resonances such as the $W^\pm$ resonances and of pair-produced charged unstable fermions such as $\tau^\pm$, $c\overline{c}$, $b\overline{b}$, and $t\overline{t}$ in e^+e^- annihilation is not yet covered in the literature.

Coming back to the more elementary level, we see that case (B) becomes case (A) if we can neglect the partition dependence of the four momentum in the Born amplitude: $\mathfrak{B}_{[ba][cd]}(X_\wp)\to\mathfrak{B}_{[ba][cd]}(P)$, where $P=p_a+p_b$ or $P=p_c+p_d$ or any other choice that does not depend on the momenta of the individual photons. This is thanks to the identity:

$$\prod_{i=1}^{n}[\mathfrak{s}_{\sigma_i}^{\{F\}}(k_i)+\mathfrak{s}_{\sigma_i}^{\{I\}}(k_i)]\equiv\sum_{\wp\in\{I,F\}}\prod_{i=1}^{n}\mathfrak{s}_{\sigma_i}^{\{\wp_i\}}(k_i). \tag{78}$$

Only case (C) is efficient for the resonant process, so obviously (A) and (B) are limited to nonresonant processes. The immediate question is the following: Which of them is better? If (A) does not sum the higher orders much better than (B), then it has the clear advantage of being simpler—the summation over partitions makes the computer code more complicated and adds heavily to the consumption of CPU time.[12] The answer is that, although we did not investigate quantitatively the differences between (A) and (B), we think that (B) sums up the LL higher orders more efficiently than (A) and is therefore better, even if there is no resonance. In our case, since we want to cover the resonant process anyway, it is a natural choice to use (B) for the nonresonant background component of the spin amplitudes (off-shell γ exchange), even if it is not vital. Once the summation over partitions is in place, it is the easiest to use it for the nonresonant background as well. The additional bonus of better higher-order convergence provides an extra justification. *Summarizing, if* (C) *is implemented, then* (B) *comes for free*.

Having discussed the differences between the three options, let us now concentrate on the option (C) for the resonant process, remembering that for the nonresonant background component it becomes automatically (B). First of all, for the narrow neutral resonance (the Z boson in our case), the photons emitted during the production and decay processes are separated by a long time interval; they are therefore completely independent and uncorrelated. In the perturbative QED this simple physical fact is reflected in a certain specific class of cancellations between the ISR and FSR photons on the one hand and the virtual and real corrections on the other. For inclusive observables such as the total cross section or charge asymmetry, the effects of the ISR-FSR interference in the nonresonant case are of order α/π, typically up to 1%, as can be seen from many examples of explicit $\mathcal{O}(\alpha^1)$ calculations. The IFI effect will be of order $(\alpha/\pi)(E_{\max}/E_{beam})$, when the experimental cut on the photon energy is $E_{\max}$. Note that the IFI effect is not directly enhanced by such big mass logarithms as $\ln s/m_e^2\sim 20$. For the resonant process the IFI effects in the inclusive observables are of order $(\alpha/\pi)(\Gamma/M)$ and are therefore often negligible on the scale of the experimental error. It must be remembered, however, that the additional suppression factor Γ/M disappears if the experimental cut on photon energy is of the order of the resonance width, $E_{\max}/E_{beam}\sim\Gamma/M$, and for an even stronger cut $E_{\max}<\Gamma$ the IFI effect becomes of order $(\alpha/\pi)(E_{\max}/\Gamma)$.

If Γ/M is extremely small, as for the τ lepton, the IFI cancellation can be taken for granted and the photon emission interference between production and decay can altogether be neglected. In the case of the Z boson close to the Z resonance (LEP1) the IFI effect is detectable experimentally, but it is small enough that it can be omitted in the Monte Carlo programs used for correcting for the detector acceptance only. In this case KORALZ/YFS3 [10] with the EEX matrix element was the acceptable solution.

The most convenient solution is the universal Monte Carlo program in which the IFI is included, which can evaluate the IFI effects near the resonance, far from the resonance, for inclusive quantities, and for strong energy cuts $E_{\max}\sim\Gamma$. This is exactly what our CEEX offers.

2. Derivation of the resonance form factor

As we have already pointed out (following Refs. [22,23]), in the presence of narrow resonances it is not sufficient to sum up the real emissions coherently, taking properly into account the energy shift in the resonance propagator (only due to the ISR photons). It is also necessary to do the same for the virtual emission, and also to sum them up to infinite order—this is why the resonance form factor $\exp(B_4^Z)$ has to be included, see Eqs. (76) and (77). In the following we shall derive Eq. (77) for B_4^Z and show analytically that the IFI cancellations do really work, as expected, to infinite order.

Let us write again the formula for the standard YFS function in Eq. (50) in a slightly modified notation

$$\begin{aligned}\alpha B_4(p_a,\ldots,p_d)&=\int\frac{d^4k}{k^2-m_\gamma^2+i\epsilon}\frac{i}{(2\pi)^3}S(k),\\ S(k)&=S_I(k)+S_F(k)+S_{Int}(k),\\ S_I(k)&=|J_I(k)|^2,\quad S_F(k)=|J_F(k)|^2,\\ S_{Int}(k)&=-2\Re[J_I(k)\cdot J_F^*(k)].\end{aligned} \tag{79}$$

In the presence of the narrow resonance, the YFS factorization of the virtual IR contributions has to take into account the dependence of the scalar part of the resonance propagator on photon energies of order Γ (the numerator is treated in the soft-photon approximation, as usual). The relevant integrals with n virtual photons look as follows:

$$\begin{aligned}I=&(P^2-\overline{M}^2)\sum_{n=0}^{\infty}\frac{1}{n!}\\ &\times\sum_{\wp\in\mathcal{P}_n}\prod_{i=0}^{n}\int\frac{i}{(2\pi)^3}\frac{d^4k_i}{k_i^2-m_\gamma^2}S_{\wp_i}(k_i)\frac{1}{P_\wp^2-\overline{M}^2},\end{aligned} \tag{80}$$

[12]We note that (A) is implemented in the $\mathcal{KK}$ MC and is a factor of $\sim$10 faster in evaluation than (B); it can be economical for cases without resonances, like the small-angle Bhabha scattering or for $\sqrt{(s)}<M_Z$, where (B) is an overkill.

where $\bar{M}^2=M^2-iM\Gamma$, and $\mathcal{P}_n$ is a set of all 3^n partitions $(\wp_1,\wp_2,\ldots,\wp_n)$ with $\wp_i=I,F,Int$, and $P_\wp\equiv P-\Sigma_{\wp_i=Int}k_i$ includes only the momenta of the photons in S_{Int} and not the momenta of photons in S_I or S_F. The $(P^2-\bar{M}^2)$ factor is conventional, to make the integral dimensionless. We shall show that the above integral factorizes into the conventional YFS form factor (dependent on the photon mass m_γ) and the additional non-IR factor due to the resonance $R=Z$:

$$I=\exp[\alpha B_4^R(m_\gamma,s,\bar{M})]=\exp[\alpha B_4(m_\gamma,s)+\alpha\Delta B_4^R(s,\bar{M})]. \tag{81}$$

Our aim is to find the analytical form of the additional function ΔB_4^R. In the current calculation, we use the following approximate formula, also used by Greco *et al.* [22,23],

$$\begin{aligned}\alpha\Delta B_4^R(s')&=-2Q_eQ_f\frac{\alpha}{\pi}\ln\left(\frac{t}{u}\right)\ln\left(\frac{\bar{M}^2-s}{\bar{M}^2}\right)\\&=-\frac{1}{2}\gamma_{Int}\ln\left(\frac{\bar{M}^2-s}{\bar{M}^2}\right).\end{aligned} \tag{82}$$

In the following, we shall derive the above approximate result and show explicitly that the above approximate virtual interference part of the form factor cancels exactly with the corresponding real interference contributions.

Since the soft virtual photons entering into S_I and S_F in Eq. (80) do not enter the resonance propagator, we may therefore factorize and sum up the contributions with S_I and S_F:

$$\begin{aligned}I=&\sum_{n_1=0}^{\infty}\frac{1}{n_1!}\prod_{i_1=0}^{n_1}\int\frac{i}{(2\pi)^3}\frac{d^4k_{i_1}}{k_{i_1}^2-m_\gamma^2}S_I(k_{i_1})\sum_{n_2=0}^{\infty}\frac{1}{n_2!}\\&\times\prod_{i_2=0}^{n_2}\int\frac{i}{(2\pi)^3}\frac{d^4k_{i_2}}{k_{i_2}^2-m_\gamma^2}S_F(k_{i_2})\\&\times\sum_{n_3=0}^{\infty}\frac{1}{n_3!}\prod_{i_3=0}^{n_3}\int\frac{i}{(2\pi)^3}\frac{d^4k_{i_3}}{k_{i_3}^2-m_\gamma^2}S_{Int}(k_{i_3})\\&\times\frac{1}{\left(P-\sum_{j=1}^{n_3}k_j\right)^2-\bar{M}^2}\\\equiv&\exp(\alpha B_I+\alpha B_F)\sum_{n=0}^{\infty}\frac{1}{n!}\prod_{i=0}^{n}\int\frac{i}{(2\pi)^3}\frac{d^4k_i}{k_i^2-m_\gamma^2}\\&\times S_{Iin}(k_i)\frac{1}{\left(P-\sum_{j=1}^{n}k_j\right)^2-\bar{M}^2}.\end{aligned} \tag{83}$$

Now we neglect the quadratic terms in the photon energies $\mathcal{O}(k_ik_j)$

$$\begin{aligned}\frac{1}{\left(P-\sum_{j=1}^{n}k_j\right)^2-\bar{M}^2}&\simeq\frac{1}{P^2-2P\sum_{j=1}^{n}k_j-\bar{M}^2}\\&=\frac{1}{P^2-\bar{M}^2}\frac{1}{1-\sum_{j=1}^{n}\frac{2Pk_j}{P^2-\bar{M}^2}}\\&\simeq\frac{1}{P^2-\bar{M}^2}\prod_{j=1}^{n}\frac{1}{1-\frac{2Pk_j}{P^2-\bar{M}^2}}\\&\simeq\frac{1}{P^2-\bar{M}^2}\prod_{j=1}^{n}\frac{P^2-\bar{M}^2}{(P-k_j)^2-\bar{M}^2},\end{aligned} \tag{84}$$

and this leads to

$$\begin{aligned}I=&\exp(\alpha B_I+\alpha B_F)\\&\times\exp\left(\int\frac{i}{(2\pi)^3}\frac{d^4k}{k_i^2-m_\gamma^2+i\epsilon}S_{Iin}(k)\frac{P^2-\bar{M}^2}{(P-k)^2-\bar{M}^2}\right)\\=&\exp[\alpha B_4(m_\gamma)+\alpha\Delta B_4^R(\Gamma)],\end{aligned} \tag{85}$$

$$\alpha\Delta B_4^R(\Gamma)=\int\frac{i}{(2\pi)^3}\frac{d^4k}{k^2}S_{Iin}(k)\left(\frac{P^2-\bar{M}^2}{(P-k)^2-\bar{M}^2}-1\right).$$

How solid is the above ''derivation''? Strictly speaking it is justified in the limit where we follow Yennie, Frautschi, and Suura in Ref. [8] and express the $k\to0$ emission amplitude as

$$\mathcal{M}\to\frac{1}{k}\left(\varepsilon_1+\mathcal{O}(k/\bar{M})+\frac{k}{\Gamma_Z}[\varepsilon_2+\mathcal{O}(k/\bar{M})]\right),$$

where $\varepsilon_{1,2}$ are constants independent of k, so that

$$|2Pk_j/(P^2-\bar{M}^2)|\ll1,$$

that is, if photon energy is below the resonance width. This restriction is thus entirely analogous to the usual YFS expansion into an IR-singular part and the rest. We note that Greco *et al.* in Refs. [22,23] have also pointed out that the result for $\Delta B_4^R(\Gamma)$ in Eq. (85) follows from the YFS expansion; we show here how this happens in detail.

The best situation would be to have a more precise evaluation of the integral of Eq. (80) (the integral is probably calculable analytically). For the moment, however, following Refs. [22,23], we choose an easier ''pragmatic'' approach based on the fact that the virtual and real contributions from the IFI for photons with $E_\gamma>\Gamma$ *do cancel*, as a consequence of the time separation between the production and decay, and we shall check that the above cancellation really works. In this way we trade the analytical evaluation of the more difficult multiphoton virtual integral for an easier evaluation of the multiphoton real integral.

3. Cancellation of the virtual form factor with the real emissions

Let us therefore examine analytically the real multiphoton emission contribution from the IFI.[13] The starting point is the integral in which the *total* photon energy $K=\Sigma_{j=1}^{n}k_j$ is kept below $E_{\max}=v_{\max}\sqrt{s}$, where $\Gamma<E_{\max}\ll\sqrt{s}$:

$$\begin{aligned}
\sigma=&\sum_{n=0}^{\infty}\frac{1}{n!}\int\prod_{i=1}^{n}\frac{d^3k_i}{(2\pi)^3 2k_i^0}\sum_{\sigma_1\cdots\sigma_n}\left|\sum_{\wp\in\{I,F\}^n}\prod_{j=1}^{n}\mathfrak{s}_{[j]}^{\{\wp_j\}}\frac{1}{X_\wp^2-\bar{M}^2}\exp[\alpha B_4^R(X_\wp)]\right|^2\Theta\left(E_{\max}-\sum_{j=1}^{n}k_j\right)\\
=&\sum_{n=0}^{\infty}\frac{1}{n!}\int_{K^0<v\sqrt{s}}\prod_{i=1}^{n}\frac{d^3k_i}{(2\pi)^3 2k_i^0}\sum_{\sigma_1\cdots\sigma_n}\sum_{\wp,\wp'\in\{I,F\}^n}\prod_{j=1}^{n}\mathfrak{s}_{[j]}^{\{\wp_j\}}\mathfrak{s}_{[j]}^{*\{\wp_j'\}}\frac{\exp[\alpha B_4^R(X_\wp)]}{X_\wp^2-\bar{M}^2}\left(\frac{\exp[\alpha B_4^R(X_{\wp'})]}{X_{\wp'}^2-\bar{M}^2}\right)^*\\
=&\sum_{n=0}^{\infty}\frac{1}{n!}\int_{K^0<v\sqrt{s}}\prod_{i=1}^{n}\frac{d^3k_i}{2k_i^0}\sum_{\wp,\in\{I^2,F^2,IF,FI\}^n}\prod_{\wp_j=I^2}2\tilde{S}_I(k_j)\prod_{\wp_j=F^2}2\tilde{S}_F(k_j)\prod_{\wp_j=IF}2\tilde{S}_{Int}(k_j)\prod_{\wp_j=FI}2\tilde{S}_{Int}(k_j)\\
&\times\frac{\exp[\alpha B_4^R(P-K_I-K_{IF})]}{(P-K_I-K_{IF})^2-\bar{M}^2}\left(\frac{\exp[\alpha B_4^R(P-K_I-K_{FI})]}{(P-K_I-K_{FI})^2-\bar{M}^2}\right)^*,
\end{aligned}\tag{86}$$

where we have simplified the Born amplitude to the level of the scalar part of the resonance propagator and we write

$$2(2\pi)^3\tilde{S}_I(k_j)=\sum_{\sigma_j}|\mathfrak{s}_{[j]}^{\{I\}}|^2,\quad 2(2\pi)^3\tilde{S}_F(k_j)=\sum_{\sigma_j}|\mathfrak{s}_{[j]}^{\{F\}}|^2,$$

$$2(2\pi)^3\tilde{S}_{Int}(k_j)=\sum_{\sigma_j}\mathfrak{s}_{[j]}^{\{I\}}(\mathfrak{s}_{[j]}^{\{F\}})^*=\sum_{\sigma_j}\mathfrak{s}_{[j]}^{\{F\}}(\mathfrak{s}_{[j]}^{\{I\}})^*,$$

$$K_{I^2}=\sum_{\wp_j=I^2}k_j,\quad K_{F^2}=\sum_{\wp_j=F^2}k_j,\tag{87}$$

$$K_{IF}=\sum_{\wp_j=IF}k_j,\quad K_{FI}=\sum_{\wp_j=FI}k_j,$$

$$K=K_{I^2}+K_{F^2}+K_{IF}+K_{FI}.$$

As we see, the product of two sums, each over 2^n partitions $\wp,\wp'\in\{I,F\}^n$, is now replaced by the single sum over 4^n partitions $\wp\in\{I^2,F^2,IF,FI\}^n$, where the IF,FI represent the interference terms.

Keeping track of the dependence of the propagators on K_{I^2}, K_{IF}, and K_{FI}, the summation over the number of photons can be reorganized, leading us back to the following factorized formula:

$$\begin{aligned}
\sigma(v_{\max})=&\sum_{n_1=0}^{\infty}\frac{1}{n_1!}\int\prod_{i_1=1}^{n_1}\frac{d^3k_{i_1}}{2k_{i_1}^0}2\tilde{S}_I(k_{i_1})\sum_{n_2=0}^{\infty}\frac{1}{n_2!}\int\prod_{i_2=1}^{n_2}\frac{d^3k_{i_2}}{2k_{i_2}^0}2\tilde{S}_F(k_{i_2})\sum_{n_3=0}^{\infty}\frac{1}{n_3!}\int\prod_{i_3=1}^{n_3}\frac{d^3k_{i_2}}{2k_{i_3}^0}2\tilde{S}_{Int}(k_{i_3})\\
&\times\frac{\exp[\alpha B_4^R(P-K_{I^2}-K_{IF})]}{(P-K_{I^2}-K_{IF})^2-\bar{M}^2}\sum_{n_4=0}^{\infty}\frac{1}{n_4!}\int\prod_{i_4=1}^{n_4}\frac{d^3k_{i_4}}{2k_{i_4}^0}2\tilde{S}_{Int}(k_{i_4})\\
&\times\left(\frac{\exp[\alpha B_4^R(P-K_{I^2}-K_{FI})]}{(P-K_{I^2}-K_{FI})^2-\bar{M}^2}\right)^*\Theta(E_{\max}-K_{I^2}^0-K_{F^2}^0-K_{IF}^0-K_{FI}^0),
\end{aligned}\tag{88}$$

where $K_{I^2}=\Sigma_{i_1}k_{i_1}$, $K_{F^2}=\Sigma_{i_2}k_{i_2}$, $K_{IF}=\Sigma_{i_3}k_{i_3}$, and $K_{FI}=\Sigma_{i_4}k_{i_4}$. The sums over the pure initial- and final-state contributions, and over the interference contributions, are now well factorized and can be performed analytically. As a first step, we integrate and sum up contributions from the very soft photons below $\varepsilon\sqrt{s}$, similarly to what was shown in Ref. [7]:

[13]In the practical CEEX calculation, the contribution from the IFI is evaluated numerically, inside the MC program.

$$\sigma(v_{\max})=\int_0^{E_{\max}}dE'\int_0^{E_{\max}}\delta(E'-E_I-E_F-E_{Int})dE_I dE_F dE_{IF}dE_{FI}\sum_{n_1=0}^{\infty}\frac{1}{n_1!}\prod_{i_1=1}^{n_1}\int_{k_{i_1}^0>\varepsilon E}\frac{d^3k_{i_1}}{2k_{i_1}^0}2\tilde{S}_I(k_{i_1})$$

$$\times\exp[2\alpha\tilde{B}_I(\varepsilon E)+2\alpha\Re B_I]\delta\left(E_I-\sum_{i_1}k_{i_1}^0\right)\sum_{n_2=0}^{\infty}\frac{1}{n_2!}\prod_{i_2=1}^{n_2}\int_{k_{i_2}^0>\varepsilon E}\frac{d^3k_{i_2}}{2k_{i_2}^0}2\tilde{S}_F(k_{i_2})$$

$$\times\exp[2\alpha\tilde{B}_F(\varepsilon E)+2\alpha\Re B_F]\delta\left(E_F-\sum_{i_2}k_{i_2}^0\right)\sum_{n_3=0}^{\infty}\frac{1}{n_3!}\prod_{i_3=1}^{n_3}\int_{k_{i_3}^0>\varepsilon E}\frac{d^3k_{i_3}}{2k_{i_3}^0}2\tilde{S}_{Int}(k_{i_3})\frac{\exp[\alpha\Delta B_4^R(P-K_{I^2}-K_{IF})]}{(P-K_{I^2}-K_{IF})^2-\bar{M}^2}$$

$$\times\exp[\alpha\tilde{B}_{Int}(\varepsilon E)+\alpha\Re B_{Int}]\delta\left(E_{IF}-\sum_{i_3}k_{i_3}^0\right)\sum_{n_4=0}^{\infty}\frac{1}{n_4!}\prod_{i_4=1}^{n_4}\int_{k_{i_4}^0>\varepsilon E}\frac{d^3k_{i_4}}{2k_{i_4}^0}2\tilde{S}_{Int}(k_{i_4})\left(\frac{\exp[\alpha\Delta B_4^R(P-K_{I^2}-K_{FI})]}{(P-K_{I^2}-K_{FI})^2-\bar{M}^2}\right)^*$$

$$\times\exp[\alpha\tilde{B}_{Int}(\varepsilon E)+\alpha\Re B_{Int}]\exp(2\alpha\Re\Delta B_4^R)\delta\left(E_{FI}-\sum_{i_4}k_{i_4}^0\right), \tag{89}$$

where $E=\sqrt{s}/2$. The integration over the photon momenta can be performed without any approximation, leading to the following result (here, $\gamma_{Int}=\gamma_{IF}=\gamma_{FI}$):

$$\sigma(v_{\max})=\int_0^{v_{\max}}dv\,\delta(v-v_I-v_F-v_{IF}-v_{FI})\int dv_I F(\gamma_I)\gamma_I v_I^{\gamma_I-1}\exp[2\alpha\tilde{B}_I(E)+2\alpha\Re B_I]$$

$$\times\int dv_F F(\gamma_F)\gamma_F v_F^{\gamma_F-1}\exp[2\alpha\tilde{B}_F(E)+2\alpha\Re B_F]$$

$$\times\int dv_{IF}F\left(\frac{\gamma_{Int}}{2}\right)\frac{1}{2}\gamma_{Int}v_{IF}^{(1/2)\gamma_{IF}-1}\left(\frac{\exp\{\alpha\Delta B_4^R[s(1-v_I)(1-v_{IF})]\}}{s(1-v_I)(1-v_{IF})-\bar{M}^2}\right)\exp[\alpha\tilde{B}_{Int}(E)+\alpha\Re B_{Int}]$$

$$\times\int dv_{FI}F\left(\frac{\gamma_{Int}}{2}\right)\frac{1}{2}\gamma_{Int}v_{FI}^{(1/2)\gamma_{FI}-1}\left(\frac{\exp\{\alpha\Delta B_4^R[s(1-v_I)(1-v_{FI})]\}}{s(1-v_I)(1-v_{FI})-\bar{M}^2}\right)^*\exp[\alpha\tilde{B}_{Int}(E)+\alpha\Re B_{Int}], \tag{90}$$

which is explicitly free of any IR divergences.

The essential question is whether we have perfect cancellations of the $\ln(\Gamma/M_Z)$ terms in the interference subintegral

$$I_{Int}=\Re\int_0^{v_{\max}-v_I-v_F-v_{FI}}dv_{IF}F\left(\frac{\gamma_{IF}}{2}\right)$$

$$\times\frac{1}{2}\gamma_{IF}v_{IF}^{(1/2)\gamma_{Int}-1}\frac{\exp\{\alpha\Delta B_4^R[s'(1-v_{IF})]\}}{s'(1-v_{IF})-\bar{M}^2}. \tag{91}$$

We omit from consideration the constant IR-finite factor $\exp[\alpha\tilde{B}_{Int}(E)+\alpha\Re B_{Int}]$, because it does not depend on the resonance parameters. The bulk of the integral comes from the neighborhood of $v_{IF}=0$ and the integrand is $\sim 1/v^2$ at large v, due to the resonance; we can therefore extend the integration limit to $\int_0^{\infty}dv_{Int}$, at the expense of an error of $\mathcal{O}(\Gamma/M_Z)$. One possible evaluation method is to use the standard techniques of the complex functions. First, we reformulate the integral as an integral over the discontinuity C_1 along the real axis[14]

$$I_{Int}=F\left(\frac{\gamma_{IF}}{2}\right)\exp[\alpha\Delta B_4^R(s')]\frac{1}{i\sin(\pi\frac{1}{2}\gamma_{Int})}$$

$$\times\int_{C_1}dz\frac{1}{2}\gamma_{Int}(-z)^{(1/2)\gamma_{Int}-1}\frac{1}{s'-\bar{M}^2-s'z}. \tag{92}$$

[14]We have also pulled out of the integral the $\exp(\alpha\Delta B_4^R)$ factor, because most of the integral comes from the neighborhood of the singularity at $v_{IF}=0$.

Since the contour can be closed in a standard way with the big circle, the integral is given by the value of the residue at $z=1-\bar{M}^2/s'$:

$$
\begin{aligned}
I_{Int} &= F\left(\frac{\gamma_{IF}}{2}\right)\exp[\alpha\Delta B_4^R(s')]\frac{\pi^{\frac{1}{2}}\gamma_{Int}}{\sin(\pi^{\frac{1}{2}}\gamma_{Int})} \\
&\quad\times\left(\frac{\bar{M}^2-s'}{s'}\right)^{\gamma_{Int}-1}\frac{1}{s'} \\
&= \frac{1}{\bar{M}^2-s'}F\left(\frac{\gamma_{Int}}{2}\right)\frac{\pi^{\frac{1}{2}}\gamma_{Int}}{\sin(\pi^{\frac{1}{2}}\gamma_{Int})}\exp[\alpha\Delta B_4^R(s')] \\
&\quad\times\left(\frac{\bar{M}^2-s'}{s'}\right)^{(1/2)\gamma_{Int}} \\
&= \frac{1}{\bar{M}^2-s'}[1+\mathcal{O}(\gamma_{Int})]. \qquad (93)
\end{aligned}
$$

The above is true because

$$
\begin{aligned}
\alpha\Delta B_4^R(s') &= -2Q_eQ_f\frac{\alpha}{\pi}\ln\left(\frac{t}{u}\right)\ln\left(\frac{\bar{M}^2-s'}{\bar{M}^2}\right) \\
&= -\frac{1}{2}\gamma_{Int}\ln\left(\frac{\bar{M}^2-s'}{\bar{M}^2}\right). \qquad (94)
\end{aligned}
$$

We have therefore proved the full cancellation of the dependence on the resonance parameters for the integrated cross section.

4. Definitions of $\hat{\beta}$'s with partitions

The $\mathcal{O}(\alpha^r)$, $r=0,1,2$, $\hat{\beta}$-functions for the variant of the CEEX with the summation over the partitions, as in Eqs. (31)–(35), are derived with the recursive relations of Eqs. (59) [similar to those of Eqs. (61)]. The only additional complication is that we must keep track of the indices, which say whether an external real photon is of the ISR or FSR type, and of the total photon momentum after emission of the ISR photons (the one that enters the resonance propagator, if such a resonance is present):

$$
\hat{\beta}_0^{(l)}\left(\begin{matrix}p\\ \lambda\end{matrix};P\right)=\mathfrak{M}_0^{(l)}\left(\begin{matrix}p\\ \lambda\end{matrix};P\right),\quad l=0,1,2, \qquad (95)
$$

$$
\begin{aligned}
\hat{\beta}_{1\{I\}}^{(1+l)}\left(\begin{matrix}pk_1\\ \lambda\sigma_1\end{matrix};P-k_1\right) &= \mathfrak{M}_{1\{I\}}^{(1+l)}\left(\begin{matrix}pk_1\\ \lambda\sigma_1\end{matrix};P-k_1\right) \\
&\quad-\hat{\beta}_0^{(l)}\left(\begin{matrix}p\\ \lambda\end{matrix};P-k_1\right)\mathfrak{s}_{\sigma_1}^{\{I\}}(k_1),
\end{aligned}
$$

$$
l=0,1,
$$

$$
\hat{\beta}_{1\{F\}}^{(1+l)}\left(\begin{matrix}pk_1\\ \lambda\sigma_1\end{matrix};P\right)=\mathfrak{M}_{1\{F\}}^{(1+l)}\left(\begin{matrix}pk_1\\ \lambda\sigma_1\end{matrix};P\right)-\hat{\beta}_0^{(l)}\left(\begin{matrix}p\\ \lambda\end{matrix};P\right)\mathfrak{s}_{\sigma_1}^{\{F\}}(k_1),
$$

$$
l=0,1,
$$

$$
\begin{aligned}
\hat{\beta}_{2\{\omega_1,\omega_2\}}^{(2)}\left(\begin{matrix}pk_1k_2\\ \lambda\sigma_1\sigma_2\end{matrix};X_\omega\right) &= \mathfrak{M}_{2\{\omega_1,\omega_2\}}^{(2)}\left(\begin{matrix}pk_1k_2\\ \lambda\sigma_1\sigma_2\end{matrix};X_\omega\right) \\
&\quad-\hat{\beta}_{1\{\omega_1\}}^{(1)}\left(\begin{matrix}pk_1\\ \lambda\sigma_1\end{matrix};X_\omega\right)\mathfrak{s}_{\sigma_2}^{\{\omega_2\}}(k_2) \\
&\quad-\hat{\beta}_{1\{\omega_2\}}^{(1)}\left(\begin{matrix}pk_2\\ \lambda\sigma_2\end{matrix};X_\omega\right)\mathfrak{s}_{\sigma_1}^{\{\omega_1\}}(k_1) \\
&\quad-\hat{\beta}_0^{(0)}\left(\begin{matrix}p\\ \lambda\end{matrix};X_\omega\right)\mathfrak{s}_{\sigma_1}^{\{\omega_1\}}(k_1)\mathfrak{s}_{\sigma_2}^{\{\omega_2\}}(k_2),
\end{aligned}
$$

where $X_\omega=P-\Sigma_{\omega_i=l}k_i$, $P=p_a+p_b$. Introduction of the partition index ω_i defining whether a photon belongs to the ISR or the FSR is in a sense not such a deep and great complication—it is now just another (third) attribute of the photon similar to its helicity.

Let us look closer into the structure of terms like $\hat{\beta}_{1\{\omega_1\}}^{(1)}(\begin{smallmatrix}pk_1\\ \lambda\sigma_1\end{smallmatrix};X_\omega)\mathfrak{s}_{\sigma_2}^{\{\omega_2\}}(k_2)$. For example, if $\omega_1=F$ and $\omega_2=I$, it reads $\hat{\beta}_{1\{F\}}^{(1)}(\begin{smallmatrix}pk_1\\ \lambda\sigma_1\end{smallmatrix};P-k_2)\mathfrak{s}_{\sigma_2}^{\{I\}}(k_2)$, that is, the total shift in X in $\hat{\beta}^{(1)}$ depends not only on the type ω_1 of ''its own photon,'' but also on the type ω_2 of the photon in the $\mathfrak{s}^{\{\omega_2\}}$ factor that multiplies it.

The $\mathfrak{M}$ amplitude in Eq. (95) is given essentially by Eq. (49), with the form factor including the resonance part (if present):

$$
\begin{aligned}
&\mathfrak{M}_{n\{\omega\}}^{(r)R}\left(\begin{matrix}pk_1\cdots k_n\\ \lambda\sigma_1\cdots\sigma_n\end{matrix};X_\omega\right) \\
&\quad=\Big\{\exp[-\alpha B_4-\alpha\Delta B_4^R(X_\omega)] \\
&\qquad\times\mathcal{M}_{n\{\omega\}}^{(r)R}\left(\begin{matrix}pk_1\cdots k_n\\ \lambda\sigma_1\cdots\sigma_n\end{matrix};X_\omega\right)\Big\}\Big|_{\mathcal{O}(\alpha^r)}. \qquad (96)
\end{aligned}
$$

As we see the type $R=\gamma,Z$ of the ''resonance'' form factor B_4^R has to be adjusted to the type of the component in $\mathcal{M}^{(r)R}$ (we have temporarily introduced an explicit index R into $\mathcal{M}$ and $\mathfrak{M}$, and γ is essentially a ''resonance'' of zero width).

D. Virtual corrections, no real photons

We now start to accumulate the actual formulas for the $\hat{\beta}$ functions entering the CEEX amplitudes of in Eqs. (31)–(35) with the case of no real photons and up to two virtual photons. The ''raw materials'' are the $\mathcal{M}$ amplitudes from the Feynman diagrams, which are turned into the $\hat{\beta}$ functions using the recursive relations of Eqs. (95).

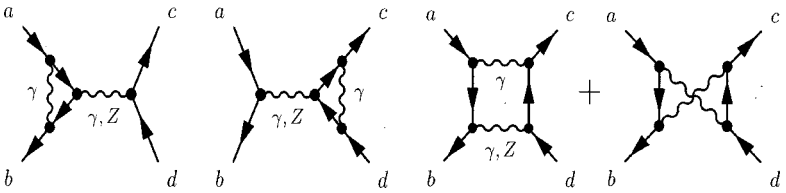

FIG. 3. First-order diagrams.

1. Photonic corrections

Let us start with the simple case of the $\mathcal{O}(\alpha^1)$ spin amplitudes with one virtual and zero real photons coming directly from the Feynman diagrams, which will be used to obtain the first order $\hat{\beta}_0^{(1)}$. The relevant spin amplitudes are

$$\mathcal{M}_0^{(1)}\left(\begin{matrix} p \\ \lambda \end{matrix};X\right)=\mathfrak{B}\left(\begin{matrix} p \\ \lambda \end{matrix};X\right)[1+Q_e^2F_1(s,m_e,m_\gamma)][1+Q_f^2F_1(s,m_f,m_\gamma)]+\mathcal{M}_{\rm box}^{(1)}\left(\begin{matrix} p \\ \lambda \end{matrix};X\right), \tag{97}$$

where F_1 is the standard electric form factor regularized with a photon mass, see Fig. 3. We omit, for the moment, the magnetic form factor F_2; this is justified for light final fermions. It will be restored in the future. In F_1 we keep the exact final fermion mass. If not stated otherwise, the four-momentum conservation $p_a+p_b=p_c+p_d$ holds.

In the present work we use the spin amplitudes for γ-γ and γ-Z boxes in the small mass approximation $m_e^2/s\to 0$, $m_f^2/s\to 0$, see Fig. 3, following Refs. [33,34]:

$$\mathcal{M}_{\rm Box}^{(1)}\left(\begin{matrix} p \\ \lambda \end{matrix};X\right)=2ie^2\sum_{B=\gamma,Z}\frac{g_{\lambda_a}^{B,e}g_{-\lambda_a}^{B,f}T_{\lambda_c\lambda_a}T'_{\lambda_b\lambda_d}+g_{\lambda_a}^{B,e}g_{\lambda_a}^{B,f}U'_{\lambda_c\lambda_b}U_{\lambda_a\lambda_d}}{X^2-M_B^2+i\Gamma_BX^2/M_B}$$

$$\times\delta_{\lambda_a,-\lambda_b}\delta_{\lambda_c,-\lambda_d}\frac{\alpha}{\pi}Q_eQ_f[\,\delta_{\lambda_a,\lambda_c}f_{\rm BDP}(\bar{M}_B^2,m_\gamma,s,t,u)-\delta_{\lambda_a,-\lambda_c}f_{\rm BDP}(\bar{M}_B^2,m_\gamma,s,u,t)], \tag{98}$$

where (here, BDP refers to Brown, Decker, and Paschos in Ref. [34])

$$f_{\rm BDP}(\bar{M}_B^2,m_\gamma,s,u,t)=\ln\left(\frac{t}{u}\right)\ln\left(\frac{m_\gamma^2}{(tu)^{1/2}}\right)-2\ln\left(\frac{t}{u}\right)\ln\left(\frac{\bar{M}_B^2-s}{\bar{M}_B^2}\right)+{\rm Li}_2\left(\frac{\bar{M}_B^2+u}{\bar{M}_B^2}\right)-{\rm Li}_2\left(\frac{\bar{M}_B^2+t}{\bar{M}_B^2}\right)$$

$$+\frac{(\bar{M}_B^2-s)(u-t-\bar{M}_B^2)}{u^2}\left\{\ln\left(\frac{-t}{s}\right)\ln\left(\frac{\bar{M}_B^2-s}{\bar{M}_B^2}\right)+{\rm Li}_2\left(\frac{\bar{M}_B^2+t}{\bar{M}_B^2}\right)-{\rm Li}_2\left(\frac{\bar{M}_B^2-s}{\bar{M}_B^2}\right)\right\}$$

$$+\frac{(\bar{M}_B^2-s)(\bar{M}_B^2-s)}{us}\ln\left(\frac{\bar{M}_B^2-s}{\bar{M}_B^2}\right)+\frac{\bar{M}_B^2-s}{u}\ln\left(\frac{-t}{\bar{M}_B^2}\right), \tag{99}$$

$\bar{M}_Z^2=M_Z^2-iM_Z\Gamma_Z$, $\bar{M}_\gamma^2=m_\gamma^2$, and the function $f_{\rm BDP}$ is that of Eq. (11) of Ref. [34]. The standard Mandelstam variables s, t, and u are defined as usual: $s=(p_a+p_b)^2$, $t=(p_a-p_c)^2$, $u=(p_a-p_d)^2$. Since in the rest of our calculation we do not use $m_f^2/s\to 0$, we intend to replace the above box spin amplitudes with the finite-mass results[15] that were given in Ref. [35].

Now using Eq. (96) we determine

$$\hat{\beta}_0^{(1)}\left(\begin{matrix} p \\ \lambda \end{matrix};X\right)=\mathfrak{B}\left(\begin{matrix} p \\ \lambda \end{matrix};X\right)[1+\delta_{Virt}^{(1)e}(s)][1+\delta_{Virt}^{(1)f}(s)]$$

$$+\mathcal{R}_{\rm Box}^{(1)}\left(\begin{matrix} p \\ \lambda \end{matrix};X\right), \tag{100}$$

where

$$\delta_{Virt}^{(1)e}(s)=Q_e^2F_1(s,m_e,m_\gamma)-Q_e^2\alpha B_2(p_a,p_b,m_\gamma)$$

$$=Q_e^2\frac{\alpha}{\pi}\frac{1}{2}\overline{L}_e, \tag{101}$$

[15]For the γ-γ box we can use the spin amplitudes with the exact final fermion mass. It seems, however, that the γ-Z box for the heavy fermion is missing in the literature.

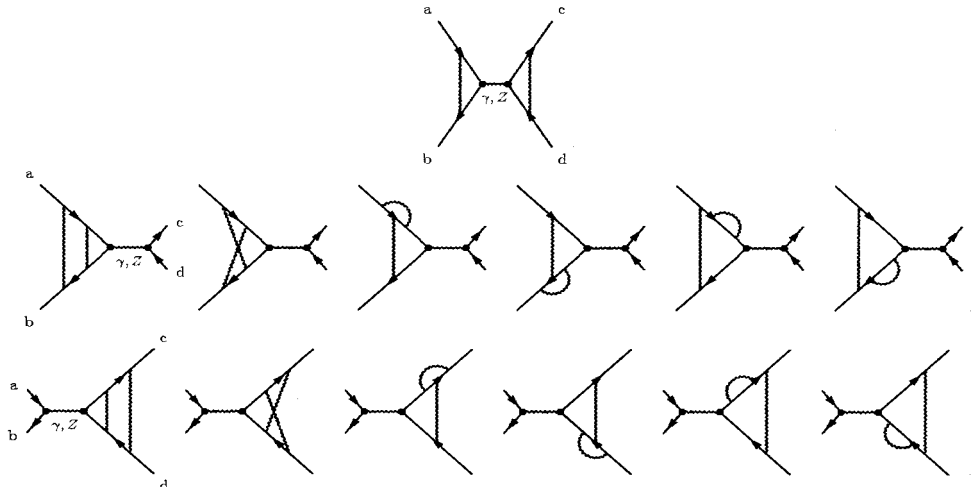

FIG. 4. Second-order vertex diagrams.

$$\delta^{(1)f}_{Virt}(s)=Q_f^2F_1(s,m_f,m_\gamma)-Q_f^2\alpha B_2(p_c,p_d,m_\gamma)$$
$$=Q_f^2\frac{\alpha}{\pi}\frac{1}{2}\overline{L}_f,$$

$$\overline{L}_e=\ln\left(\frac{s}{m_e^2}\right)+i\pi-1,\quad \overline{L}_f=\ln\left(\frac{s}{m_f^2}\right)+i\pi-1.$$

Note that we departed in Eq. (100) from the strict $\mathcal{O}(\alpha^1)$ by retaining the $\delta^{(1)e}_{Virt}(s)\delta^{(1)f}_{Virt}(s)$ term, i.e., by replacing the ''additive'' form $1+\delta^{(1)e}_{Virt}(s)+\delta^{(1)f}_{Virt}(s)$ with the ''factorized'' form $[1+\delta^{(1)e}_{Virt}(s)][1+\delta^{(1)f}_{Virt}(s)]$. The above does not need really much justification—it is obviously closer to the reality of the higher-orders, so the ''factorized'' form is preferable. The only question is whether the above method does not disturb the IR cancellations. It does not, as is seen from the definitions of $\delta^{(1)e}_{Virt}(s)$ and $\delta^{(1)f}_{Virt}(s)$.

The IR subtraction in $\mathcal{M}^{(1)}_{\rm Box}$ using Eq. (96) at $\mathcal{O}(\alpha^1)$ leads to the IR-finite $\mathcal{R}_{\rm Box}$. The above subtraction is equivalent to the following substitution:

$$f_{\rm BDP}(\overline{M}_B^2,m_\gamma,s,t,u)\to f_{\rm BDP}(\overline{M}_B^2,m_\gamma,s,t,u)-f_{\rm IR}(m_\gamma,t,u), \tag{102}$$

where

$$f_{\rm IR}(m_\gamma,t,u)=\frac{2}{\pi}B_2(p_a,p_c,m_\gamma)-\frac{2}{\pi}B_2(p_a,p_d,m_\gamma)$$
$$=\ln\left(\frac{t}{u}\right)\ln\left(\frac{m_\gamma^2}{\sqrt{tu}}\right)+\frac{1}{2}\ln\left(\frac{t}{u}\right), \tag{103}$$

and the additional resonance factor $\exp[-\alpha\Delta B_4^Z(s)]$ in Eq. (96) induces the additional subtraction in the γ-Z box part:

$$f_{\rm BDP}(s,t,u)\to f_{\rm BDP}(s,t,u)-\alpha\Delta B_4^Z(s); \tag{104}$$

see Eq. (82) for the definition of $\alpha\Delta B_4^Z$.

Our $\mathcal{O}(\alpha^2)$ expressions for $\hat{\beta}_0^{(2)}$ are still incomplete. We base them on the graphs depicted in Fig. 4 in which we omitted some trivial transpositions of the diagrams. Following again Eq. (96), we obtain

$$\hat{\beta}_0^{(2)}\left(\begin{matrix}p\\ \lambda\end{matrix};X\right)=\mathfrak{B}\left(\begin{matrix}p\\ \lambda\end{matrix};X\right)[1+\delta^{(2)e}_{Virt}(s,m_e)][1+\delta^{(2)f}_{Virt}(s,m_f)]$$
$$+\mathcal{R}^{(2)}_{\rm Box}\left(\begin{matrix}p\\ \lambda\end{matrix};X\right). \tag{105}$$

In the present calculation we neglect the two-loop double-box contributions in $\mathcal{R}^{(2)}_{\rm Box}$, depicted in the first row in Fig. 5 and the vertex-box type of diagrams, see the examples of diagrams in the second row of Fig. 5.[16] In fact we keep only the first-order box contribution $\mathcal{R}^{(1)}_{\rm Box}$ in our incomplete $\mathcal{O}(\alpha^2)$-type matrix element.

Two remarks: in spite of the temporary lack of the above contribution, we are not stuck because what we neglect is IR finite. This statement is not as trivial as it may look because, in the calculation without exponentiation, neglecting such contributions would violate IR cancellations, and correcting for such a violation would be rather complicated and physically dangerous. Secondly, what we neglect is expected to be numerically small, of $\mathcal{O}(\alpha^2L^1)$, and therefore it does not do much harm to our overall physical precision.

Coming back to the $\mathcal{O}(\alpha^2)$ corrections to the electric form factor from the diagrams in Fig. 4, they are well known since they were calculated in Refs. [18,37–39] and they contribute as follows:

$$\delta^{(2)e}_{Virt}(s,m_e)=\delta^{(1)e}_{Virt}(s)+\left(\frac{\alpha}{\pi}\right)^2\left[\frac{\overline{L}_e^2}{8}+\overline{L}_e\left(\frac{3}{32}-\frac{3}{4}\zeta_2+\frac{3}{2}\zeta_3\right)\right],$$

[16] In fact the two-loop double-box contribution became known recently [36], so there is a chance of including it in the future.

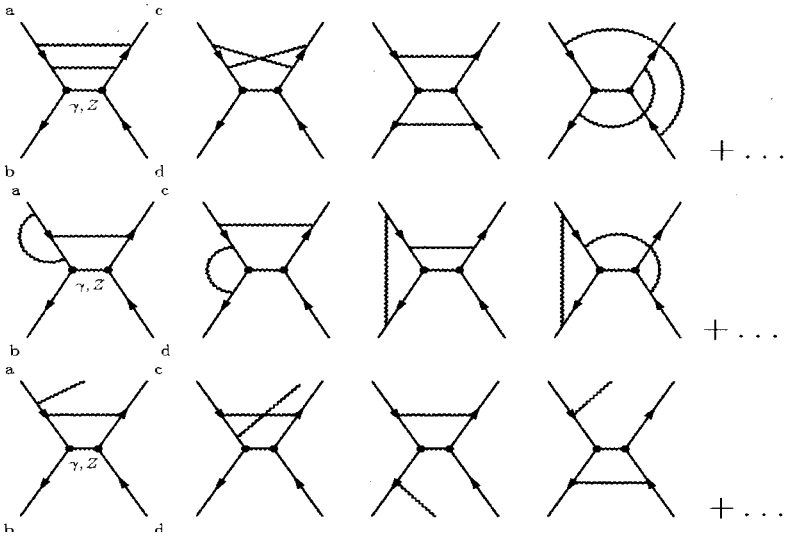

FIG. 5. Missing second-order diagrams.

$$\delta^{(2)f}_{Virt}(s,m_f)=\delta^{(1)f}_{Virt}(s)+\left(\frac{\alpha}{\pi}\right)^2\left[\frac{\overline{L}_f^2}{8}+\overline{L}_f\left(\frac{3}{32}-\frac{3}{4}\zeta_2+\frac{3}{2}\zeta_3\right)\right]. \tag{106}$$

In the above we kept terms of $\mathcal{O}(\alpha^2L^2)$ and $\mathcal{O}(\alpha^2L^1)$, and neglected the known [39,40] negligible terms of $\mathcal{O}(\alpha^2L^0)$.

2. Electroweak corrections

In the not-so-interesting case of the absence of the electroweak (EW) corrections, the couplings of the two neutral bosons γ and Z are defined in a conventional way:

$$G^{Z,f}_\lambda=g^{Z,f}_V-\lambda g^{Z,f}_A,\quad G^{\gamma,f}_\lambda=g^{Z,f}_V,\quad \lambda=+,-=R,L,$$

$$g^{\gamma,e}_V=Q_e=-1,\quad g^{\gamma}_{V,f}=Q_f,\quad g^{\gamma,e}_A=0,\quad g^{\gamma}_{A,f}=0,$$

$$g^{Z,e}_V=\frac{2T^3_e-4Q_e\sin^2\theta_W}{16\sin^2\theta_W\cos^2\theta_W},\quad g^{Z,f}_V=\frac{2T^3_f-4Q_f\sin^2\theta_W}{16\sin^2\theta_W\cos^2\theta_W},$$

$$g^{Z,e}_A=\frac{2T^3_e}{16\sin^2\theta_W\cos^2\theta_W},\quad g^{Z,f}_A=\frac{2T^3_f}{16\sin^2\theta_W\cos^2\theta_W}, \tag{107}$$

where T^3_f is the isospin of the left-handed component of the fermion f ($T^3_d=-1/2, T^3_e=-1/2$).

The actual implementation of EW corrections is practically the same as in KORALZ [10]. It goes as follows: the γ and Z propagators are multiplied by the corresponding hook-functions (scalar form factors) due to the vacuum polarization:

$$H_\gamma\to H_\gamma\times\frac{1}{2-\Pi_\gamma},$$

$$H_Z\to H_Z\times 16\sin^2\theta_W\cos^2\theta_W\frac{G_\mu M_Z^2}{\alpha_{\rm QED}8\pi\sqrt{2}}\rho_{\rm EW}. \tag{108}$$

In addition the vector couplings of the Z get multiplied by the respective extra form factors. First of all we replace

$$g^{Z,e}_V=\frac{2T^3_e-4Q_e\sin^2\theta_W}{16\sin^2\theta_W\cos^2\theta_W}\to\frac{2T^3_e-4Q_e\sin^2\theta_WF^e_{EW}(s)}{16\sin^2\theta_W\cos^2\theta_W},$$

$$g^{Z,f}_V=\frac{2T^3_f-4Q_f\sin^2\theta_W}{16\sin^2\theta_W\cos^2\theta_W}\to\frac{2T^3_f-4Q_f\sin^2\theta_WF^f_{EW}(s)}{16\sin^2\theta_W\cos^2\theta_W}, \tag{109}$$

where $F^e_{EW}(s)$ and $F^f_{EW}(s)$ are the electroweak form factors provided by the DIZET package [14], which is a part of the ZFITTER semianalytical code [5] and corresponds to the electroweak vertex corrections.

The electroweak box diagrams require a more complicated treatment. In the Born spin amplitudes we have essentially two products of the coupling constants

$$g^{Z,e}_\lambda g^{Z,f}_{-\lambda}=(g^{Z,e}_V-\lambda g^{Z,e}_A)(g^{Z,f}_V+\lambda g^{Z,f}_A)=g^{Z,e}_Vg^{Z,f}_V-\lambda g^{Z,e}_Ag^{Z,f}_V+\lambda g^{Z,e}_Vg^{Z,f}_A-g^{Z,e}_Ag^{Z,f}_A,$$

$$g^{Z,e}_\lambda g^{Z,f}_{\lambda}=(g^{Z,e}_V-\lambda g^{Z,e}_A)(g^{Z,f}_V-\lambda g^{Z,f}_A)=g^{Z,e}_Vg^{Z,f}_V-\lambda g^{Z,e}_Ag^{Z,f}_V-\lambda g^{Z,e}_Vg^{Z,f}_A+g^{Z,e}_Ag^{Z,f}_A. \tag{110}$$

In the above the following modification is done for the doubly-vector component:

$$g^{Z,e}_Vg^{Z,f}_V=>\frac{4T^3_eT^3_f-8T^3_eQ_fF^f_{EW}(s)-8T^3_fQ_eF^e_{EW}(s)+16Q_fQ_fF^{ef}_{EW}(s,t)}{(16\sin^2\theta_W\cos^2\theta_W)^2}, \tag{111}$$

where the new form factor $F_{EW}^{ef}(s,t)$ corresponds to electroweak boxes and is angle-dependent. The Born spin amplitudes modified in the above way are also used in the case when a single and multiple real photons are present, see the next sections.

E. One real photon

We start the discussion of the $\hat{\beta}_1$ tensors corresponding to the emission of a single real photon with the tree-level case (zero virtual photons). The starting point is the well-known $\mathcal{O}(\alpha^1)$ split amplitude for the single bremsstrahlung, which we shall reconsider separately first in the case of the emission from the initial-state beams and later for emission from the final-state fermions. This will be the ''raw material'' for obtaining $\hat{\beta}_1^{(0)}$ using Eqs. (95).

The first-order, one-photon, ISR matrix element from the Feynman diagrams depicted in Fig. 6 reads

$$\begin{aligned}\mathcal{M}_{1\{I\}}&\left(\begin{matrix}pk_1\\ \lambda\sigma_1\end{matrix}\right)\\ &=eQ_e\overline{v}(p_b,\lambda_b)\mathbf{M}_{\{I\}}\frac{\not p_a+m-\not k_1}{-2k_1p_a}\not\epsilon^*_{\sigma_1}(k_1)u(p_a,\lambda_a)\\ &\quad+eQ_e\overline{v}(p_b,\lambda_b)\not\epsilon^*_{\sigma_1}(k_1)\frac{-\not p_b+m+\not k_1}{-2k_1p_b}\mathbf{M}_{\{I\}}u(p_a,\lambda_a),\end{aligned} \tag{112}$$

where

$$\mathbf{M}_{\{I\}}=ie^2\sum_{B=\gamma,Z}\Pi_B^{\mu\nu}(X)G^B_{e,\mu}(G^B_{f,\nu})_{[cd]} \tag{113}$$

is the annihilation scattering spinor matrix, including the final-state spinors. We split the above expression into the soft IR parts[17] proportional to $(\not p\pm m)$ and the non-IR parts proportional to $\not k_1$. Employing the completeness relations of Eq. (A14) in the Appendix to those parts we obtain:

$$\begin{aligned}\mathcal{M}_{1\{I\}}\left(\begin{matrix}pk_1\\ \lambda\sigma_1\end{matrix}\right)=&-\frac{eQ_e}{2k_1p_a}\sum_\rho\ \mathfrak{B}\left[\begin{matrix}p_bp_a\\ \lambda_b\rho_a\end{matrix}\right]_{[cd]}U\left[\begin{matrix}p_ak_1p_a\\ \rho_a\sigma_1\lambda_a\end{matrix}\right]\\ &+\frac{eQ_e}{2k_1p_b}\sum_\rho\ V\left[\begin{matrix}p_bk_1p_b\\ \lambda_b\sigma_1\rho_b\end{matrix}\right]\mathfrak{B}\left[\begin{matrix}p_bp_a\\ \rho_b\lambda_a\end{matrix}\right]_{[cd]}\\ &+\frac{eQ_e}{2k_1p_a}\sum_\rho\ \mathfrak{B}\left[\begin{matrix}p_bk_1\\ \lambda_b\rho\end{matrix}\right]_{[cd]}U\left[\begin{matrix}k_1k_1p_a\\ \rho\sigma_1\lambda_a\end{matrix}\right]\\ &-\frac{eQ_e}{2k_1p_b}\sum_\rho\ V\left[\begin{matrix}p_bk_1k_1\\ \lambda_b\sigma_1\rho\end{matrix}\right]\mathfrak{B}\left[\begin{matrix}k_1p_a\\ \rho\lambda_a\end{matrix}\right]_{[cd]}.\end{aligned} \tag{114}$$

[17]This kind of separation was already exploited in Ref. [21]. We thank E. Richter-Wąs for attracting our attention to this method.

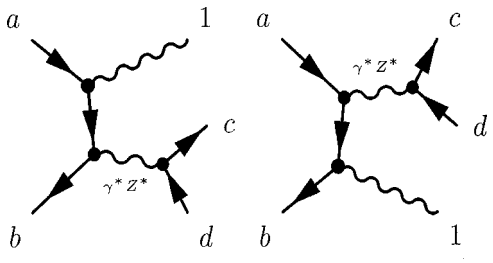

FIG. 6. ISR diagrams.

The summation in the first two terms gets eliminated by the diagonality property of U and V, see Eq. (A21) in the Appendix, and leads to

$$\begin{aligned}\mathcal{M}_{1\{I\}}&\left(\begin{matrix}pk_1\\ \lambda\sigma_1\end{matrix}\right)=\mathfrak{s}^{\{I\}}_{\sigma_1}(k_1)\mathfrak{B}\left[\begin{matrix}p\\ \lambda\end{matrix}\right]+r_{\{I\}}\left(\begin{matrix}pk_1\\ \lambda\sigma_1\end{matrix}\right),\\ r_{\{I\}}&\left(\begin{matrix}pk_1\\ \lambda\sigma_1\end{matrix}\right)=+\frac{eQ_e}{2k_1p_a}\sum_\rho\ \mathfrak{B}\left[\begin{matrix}p_bk_1\\ \lambda_b\rho\end{matrix}\right]_{[cd]}U\left[\begin{matrix}k_1k_1p_a\\ \rho\sigma_1\lambda_a\end{matrix}\right]\\ &\quad-\frac{eQ_e}{2k_1p_b}\sum_\rho\ V\left[\begin{matrix}p_bk_1k_1\\ \lambda_b\sigma_1\rho\end{matrix}\right]\mathfrak{B}\left[\begin{matrix}k_1p_a\\ \rho\lambda_a\end{matrix}\right]_{[cd]},\\ \mathfrak{s}^{\{I\}}_{\sigma_1}(k_1)&=-eQ_e\frac{b_{\sigma_1}(k_1,p_a)}{2k_1p_a}+eQ_e\frac{b_{\sigma_1}(k_1,p_b)}{2k_1p_b}.\end{aligned} \tag{115}$$

The soft part is now clearly separated and the remaining non-IR part, necessary for the CEEX, is obtained.

The case of final-state, one-real-photon emission, see Fig. 7, can be analyzed in a similar way. The first-order FSR, one-photon, matrix element is

$$\begin{aligned}\mathcal{M}_{1\{F\}}\left(\begin{matrix}pk_1\\ \lambda\sigma_1\end{matrix}\right)=&eQ_f\overline{u}(p_c,\lambda_c)\not\epsilon^*_{\sigma_1}(k_1)\\ &\times\frac{\not p_c+m+\not k_1}{2k_1p_c}\mathbf{M}_{\{F\}}v(p_d,\lambda_d)\\ &+eQ_f\overline{u}(p_c,\lambda_c)\mathbf{M}_{\{F\}}\frac{-\not p_d+m-\not k_1}{2k_1p_d}\\ &\times\not\epsilon^*_{\sigma_1}(k_1)v(p_d,\lambda_d),\end{aligned} \tag{116}$$

where

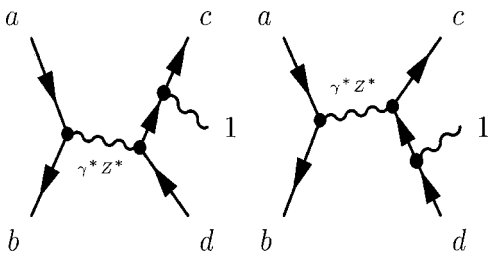

FIG. 7. FSR diagrams.

$$\mathbf{M}_{\{F\}} = ie^2 \sum_{B=\gamma,Z} \Pi_B^{\mu\nu}(X)(G^B_{e,\mu})_{[ba]} G^B_{f,\nu} \tag{117}$$

is the spinor matrix for annihilation scattering, including the initial spinors. Similarly, the expansion into soft and non-IR parts for the FSR spin amplitudes is done in a way completely analogous to the ISR case:

$$\mathcal{M}_{1\{F\}}\begin{pmatrix} pk_1 \\ \lambda\sigma_1 \end{pmatrix} = \mathfrak{s}^{\{F\}}_{\sigma_1}(k_1)\mathfrak{B}\begin{pmatrix} p \\ \lambda \end{pmatrix} + r_{\{F\}}\begin{pmatrix} pk_1 \\ \lambda\sigma_1 \end{pmatrix},$$

$$r_{\{F\}}\begin{pmatrix} pk_1 \\ \lambda\sigma_1 \end{pmatrix} = \frac{eQ_f}{2k_1p_c}\sum_\rho U\begin{bmatrix} p_ck_1k_1 \\ \lambda_c\sigma_1\rho \end{bmatrix}\mathfrak{B}_{[ba]}\begin{bmatrix} k_1p_d \\ \rho\lambda_d \end{bmatrix} - \frac{eQ_f}{2k_1p_d}\sum_\rho \mathfrak{B}_{[ba]}\begin{bmatrix} p_ck_1 \\ \lambda_c\rho \end{bmatrix} V\begin{bmatrix} k_1k_1p_d \\ \rho\sigma_1\lambda_d \end{bmatrix},$$

$$\mathfrak{s}^{\{F\}}_{\sigma_1}(k_1) = eQ_f\frac{b_{\sigma_1}(k_1,p_c)}{2k_1p_c} - eQ_f\frac{b_{\sigma_1}(k_1,p_d)}{2k_1p_d}. \tag{118}$$

For the purpose of the following discussion of the remaining non-IR terms, it is useful to introduce an even more compact tensor notation:

$$U\begin{bmatrix} p_fk_ik_j \\ \lambda_f\sigma_i\sigma_j \end{bmatrix} \equiv U_{[f,i,j]}, \quad \mathfrak{B}\begin{bmatrix} p_bp_a \\ \lambda_b\lambda_a \end{bmatrix}\begin{bmatrix} p_cp_d \\ \lambda_c\lambda_d \end{bmatrix} \equiv \mathfrak{B}_{[ba][cd]}, \tag{119}$$

etc. For the ''primed'' indices we understand contractions, for instance

$$U_{[a,i,j']}V_{[j',j,b]} \equiv \sum_{\sigma'_j=\pm} U\begin{bmatrix} p_ak_ik_j \\ \lambda_a\sigma_i\sigma'_j \end{bmatrix} V\begin{bmatrix} k_jk_jp_b \\ \sigma'_j\sigma_j\lambda_b \end{bmatrix}. \tag{120}$$

Using the above notation, the complete $\mathcal{O}(\alpha^1)$ spin amplitude for the one-photon ISR+FSR, coming directly from the Feynman diagrams, with the explicit split into IR and non-IR parts, and ISR and FSR parts, reads

$$\begin{aligned}\mathfrak{M}^{(1)}_1\begin{pmatrix} pk_1 \\ \lambda\sigma_1 \end{pmatrix} &= \mathfrak{M}^{(1)}_{1\{I\}}\begin{pmatrix} pk_1 \\ \lambda\sigma_1 \end{pmatrix}(P-k_1) + \mathfrak{M}^{(1)}_{1\{F\}}\begin{pmatrix} pk_1 \\ \lambda\sigma_1 \end{pmatrix}(P) \\ &= \mathfrak{s}^{\{I\}}_{[1]}\mathfrak{B}\begin{pmatrix} p \\ \lambda \end{pmatrix};P-k_1\Big) + r_{\{I\}}\begin{pmatrix} pk_1 \\ \lambda\sigma_1 \end{pmatrix};P-k_1\Big) \\ &\quad + \mathfrak{s}^{\{F\}}_{[1]}\mathfrak{B}\begin{pmatrix} p \\ \lambda \end{pmatrix};P\Big) + r_{\{F\}}\begin{pmatrix} pk_1 \\ \lambda\sigma_1 \end{pmatrix};P\Big),\end{aligned} \tag{121}$$

$$r_{\{I\}}\begin{pmatrix} pk_1 \\ \lambda\sigma_1 \end{pmatrix};X\Big) = \frac{eQ_e}{2kp_a}\mathfrak{B}_{[b1'cd]}(X)U_{[1'1a]} - \frac{eQ_e}{2kp_b}V_{[b11']}\mathfrak{B}_{[1'acd]}(X)$$

$$r_{\{F\}}\begin{pmatrix} pk_1 \\ \lambda\sigma_1 \end{pmatrix};X\Big) = \frac{eQ_f}{2kp_c}U_{[c11']}\mathfrak{B}_{[ba1'd]}(X) - \frac{eQ_f}{2kp_d}\mathfrak{B}_{[bac1']}(X)V_{[1'1d]}.$$

In the lowest order, the Born spin amplitudes $\mathfrak{B}$ are defined in Eq. (44), and we show explicitly as an argument the four-momentum X that enters the propagator of the s-channel exchange. Note that the formulas here differ by an overall sign from those of Ref. [3].

First- and second-order $\hat{\boldsymbol{\beta}}_1$

Now we employ the tree-level, $\mathcal{O}(\alpha^1)$ variant of Eqs. (95) obtaining the following results:

$$\hat{\beta}^{(1)}_{1\{I\}}\begin{pmatrix} pk_1 \\ \lambda\sigma_1 \end{pmatrix};P-k_1\Big) \equiv r_{\{I\}}\begin{pmatrix} pk_1 \\ \lambda\sigma_1 \end{pmatrix};P-k_1\Big)$$

$$\hat{\beta}^{(1)}_{1\{F\}}\begin{pmatrix} pk_1 \\ \lambda\sigma_1 \end{pmatrix};P\Big) \equiv r_{\{F\}}\begin{pmatrix} pk_1 \\ \lambda\sigma_1 \end{pmatrix};P\Big) + \left(\frac{(p_c+p_d+k_1)^2}{(p_c+p_d)^2}-1\right)\mathfrak{B}\begin{pmatrix} p \\ \lambda \end{pmatrix};X\Big). \tag{122}$$

The ''context-dependent'' reduced total momentum X (the total four-momentum in the resonance propagator, if present) is in the above definition uniquely defined as $X=P-k_1$ in the case of the ISR, and $X=P$ in the case of the FSR. In the general context of the CEEX amplitude of Eqs. (31)–(35), that is in the presence of the additional ''spectator'' ISR photons in a given term, X is also defined quite unambiguously: $X_\wp$ includes not only k_1 but also all additional ISR momenta in the process. For the pseudoflux factor there is some ambiguity, however. In the presence of the additional ''spectator'' ISR photons it can be defined either as $(p_a+p_b-k_1)^2/(p_a+p_b)^2$ or $(p_c+p_d+k_1)^2/(p_c+p_d)^2$. We are free to choose either of them and we opted for the second choice (it seems to lead to more stable MC weights).

The one-loop level, $\mathcal{O}(\alpha^2)$ case of $\hat{\beta}^{(2)}_1$ is quite interesting, because this is the first time that we deal with the nontrivial case of the simultaneous emission of virtual and real photons. It is therefore instructive to write the formal definitions of $\hat{\beta}^{(2)}_1$ following Eqs. (96) and (95) in this particular case:

$$\mathfrak{M}^{(2)}_{1\{\omega\}}\begin{pmatrix} pk_1 \\ \lambda\sigma_1 \end{pmatrix};X_\omega\Big) = \Big\{\exp[-\alpha B_4 - \alpha\Delta B^R_4(X_\omega)]\mathcal{M}^{(2)}_{1\{\omega\}}\begin{pmatrix} pk_1 \\ \lambda\sigma_1 \end{pmatrix};X_\omega\Big)\Big\}\Big|_{\mathcal{O}(\alpha^2)}, \quad \omega = I,F, \quad R=\gamma,Z, \tag{123}$$

$$\hat{\beta}^{(2)}_{1\{I\}}\left(\begin{matrix} pk_1 \\ \lambda\sigma_1 \end{matrix};P-k_1\right)=\mathfrak{M}^{(2)}_{1\{I\}}\left(\begin{matrix} pk_1 \\ \lambda\sigma_1 \end{matrix};P-k_1\right) - \mathfrak{s}^{\{I\}}_{\sigma_1}(k_1)\hat{\beta}^{(1)}_0\left(\begin{matrix} p \\ \lambda \end{matrix};P-k_1\right) \quad (124)$$

$$\hat{\beta}^{(2)}_{1\{F\}}\left(\begin{matrix} pk_1 \\ \lambda\sigma_1 \end{matrix};P\right)=\mathfrak{M}^{(2)}_{1\{F\}}\left(\begin{matrix} pk_1 \\ \lambda\sigma_1 \end{matrix};P\right)-\mathfrak{s}^{\{F\}}_{\sigma}(k_1)\hat{\beta}^{(1)}_0\left(\begin{matrix} p \\ \lambda \end{matrix};P\right).$$

What is at present available from the Feynman diagrams? For the moment we have at our disposal the amplitudes corresponding to vertexlike diagrams in Fig. 8, and we miss diagrams of the ''5-box'' type shown in the third (bottom) row in Fig. 5. More precisely, after applying the IR virtual subtraction of Eq. (123) we expand in the number of loops, keeping track of the initial- and final-state attachment of the *virtual* photon:

$$\begin{aligned}\mathfrak{M}^{(2)}_{1\{\omega\}}\left(\begin{matrix} pk_1 \\ \lambda\sigma_1 \end{matrix};X\right)=&\mathfrak{M}^{(1)}_{1\{\omega\}}\left(\begin{matrix} pk_1 \\ \lambda\sigma_1 \end{matrix};X\right)+\alpha Q_e^2\mathfrak{M}^{[1]}_{1\{\omega\},I^2}\left(\begin{matrix} pk_1 \\ \lambda\sigma_1 \end{matrix};X\right)\\ &+\alpha Q_f^2\mathfrak{M}^{[1]}_{1\{\omega\},F^2}\left(\begin{matrix} pk_1 \\ \lambda\sigma_1 \end{matrix};X\right)\\ &+\alpha Q_eQ_f\mathfrak{M}^{[1]}_{1\{\omega\},Box5}\left(\begin{matrix} pk_1 \\ \lambda\sigma_1 \end{matrix};X\right). \qquad (125)\end{aligned}$$

In the above expression the first term describes the already discussed tree-level single bremsstrahlung, the next two correspond to the vertexlike diagrams in Fig. 8, and the last one represents the ''5-box''-type diagrams in the third row of Fig. 5. In the present version we temporarily omit from the calculation the contribution to $\hat{\beta}^{(2)}_1$ from the last, ''5-box'' term, which looks as follows:

$$\begin{aligned}\hat{\beta}^{(2)}_{1\{\omega\},Box5}\left(\begin{matrix} pk_1 \\ \lambda\sigma_1 \end{matrix};X\right)=&\alpha Q_eQ_f\mathfrak{M}^{[1]}_{1\{\omega\},Box5}\left(\begin{matrix} pk_1 \\ \lambda\sigma_1 \end{matrix};X\right)\\ &-\mathfrak{s}^{\{I\}}_{[1]}\mathcal{R}^{(1)}_{\rm Box}\left(\begin{matrix} p \\ \lambda \end{matrix};X\right)-\mathfrak{s}^{\{F\}}_{[1]}\mathcal{R}^{(1)}_{\rm Box}\left(\begin{matrix} p \\ \lambda \end{matrix};X\right).\end{aligned} \qquad (126)$$

As we see, the trivial IR part, which we remove, is proportional to the ordinary box contributions discussed before. We expect the above to contribute in the integrated cross section at most of $\mathcal{O}(\alpha^2L^1)$, and in the resonance scattering it will be suppressed by an additional Γ/M factor.

Limiting ourselves to the pure ''vertexlike'' diagrams of Fig. 8, for one real ISR ($\omega=I$) photon we obtain from the Feynman rules the following $\mathcal{O}(Q_e^2\alpha^2)$ result:

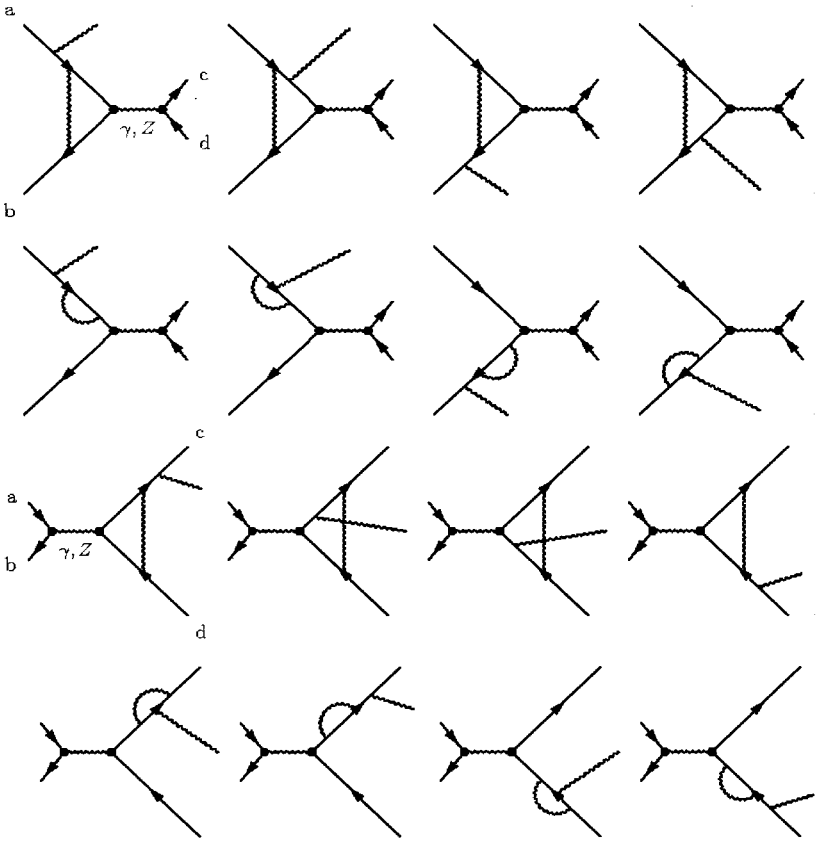

FIG. 8. One-loop corrections to single bremsstrahlung.

$$\hat{\beta}^{(2)}_{1\{I\}}\left(\begin{matrix} pk_1 \\ \lambda\sigma_1 \end{matrix};X\right) \equiv r_{\{I\}}\left(\begin{matrix} pk_1 \\ \lambda\sigma_1 \end{matrix};X\right)[1+\delta^{(1)e}_{Virt}(s) + \rho^{(2)e}_{Virt}(s,\tilde{\alpha}_1,\tilde{\beta}_1)][1+\delta^{(1)f}_{Virt}(s)] + \mathfrak{B}\left(\begin{matrix} p \\ \lambda \end{matrix};X\right)\mathfrak{s}^{\{I\}}_{\sigma_1}(k_1)\rho^{(2)e}_{Virt}(s,\tilde{\alpha},\tilde{\beta}) \tag{127}$$

where

$$\rho^{(2)e}_{Virt}(s,\tilde{\alpha},\tilde{\beta}) = \frac{\alpha}{\pi}Q_e^2\frac{1}{2}[V(s,\tilde{\alpha},\tilde{\beta})+V(s,\tilde{\beta},\tilde{\alpha})],$$

$$V(s,\tilde{\alpha},\tilde{\beta}) = \ln(\tilde{\alpha})\ln(1-\tilde{\beta}) + \mathrm{Li}_2(\tilde{\alpha}) - \frac{1}{2}\ln^2(1-\tilde{\alpha}) + \frac{3}{2}\ln(1-\tilde{\alpha}) + \frac{1}{2}\frac{\tilde{\alpha}(1-\tilde{\alpha})}{[1+(1-\tilde{\alpha})^2]} \tag{128}$$

and we use the Sudakov variables

$$\tilde{\alpha}_i = \frac{2k_ip_b}{2p_ap_b}, \quad \tilde{\beta}_i = \frac{2k_ip_a}{2p_ap_b}. \tag{129}$$

Let us make a number of observations concerning Eq. (127):

The terms of $\mathcal{O}(\alpha^4)$ like $|\mathfrak{s}^{\{I\}}_{\sigma}\rho^{(2)e}_{Virt}|^2$ in the cross section, although beyond $\mathcal{O}(\alpha^2)$, are not rejected, as would be the case in an ordinary $\mathcal{O}(\alpha^2)$ calculation without exponentiation. They are included in the process of numerical evaluation of the differential cross sections out of spin amplitudes. (It is essential that they be IR finite.)

The term $r_{\{I\}}\delta^{(1)e}_{Virt}$ contributes to $\mathcal{O}(\alpha^2L^2)$ to the integrated cross section: one L^1 is explicit (from the virtual photon) and another L^1 is from the integration over the angle of the real photon.

The term $\sim\ln(\tilde{\alpha})\ln(1-\tilde{\beta})$ contributes a correction of $\mathcal{O}(\alpha^2L^2)$ to the integrated cross section, with the double logarithm L^2 resulting directly from the integration over the angle of the real photon:

$$\int \frac{dk^3}{k^0}\Re[\rho^{(2)e}_{Virt}(k)\{\hat{\beta}_0\mathfrak{s}^{\{I\}}_{\sigma}(k)\}^*] \sim Q_e^2\alpha^2\int_{m_e^2/s}\frac{d\tilde{\alpha}}{\tilde{\alpha}}\ln(\tilde{\alpha}) \sim Q_e^2\alpha^2\ln^2\frac{s}{m_e^2}.$$

The other terms in $\hat{\beta}^{(2)}_{1\{I\}}$ contribute at most $\mathcal{O}(\alpha^2L^1)$.

The FSR virtual corrections are included multiplicatively through the factor $[1+\delta^{(1)f}_{Virt}(s)]$ and are not included additively like $[1+\delta^{(1)e}_{Virt}(s)+\delta^{(1)f}_{Virt}(s)]$. This is our deliberate choice.

The subleading term $\tilde{\alpha}(1-\tilde{\alpha})/[1+(1-\tilde{\alpha})^2]$ has in fact a more complicated spin structure than that of the Born amplitude (it should be restored in the future). The unpolarized integrated cross section is however correct in $\mathcal{O}(\alpha^2L^1)$.

The analogous $\mathcal{O}(Q_f^2\alpha^2)$ contribution for one real FSR ($\omega=0$) photon is

$$\hat{\beta}^{(2)}_{1\{F\}}\left(\begin{matrix} pk \\ \lambda\sigma \end{matrix};X\right) \equiv r_{\{F\}}\left(\begin{matrix} pk \\ \lambda\sigma \end{matrix};X\right)[1+\delta^{(1)e}_{Virt}(s)][1+\delta^{(1)f}_{Virt}(s) + \rho^{(2)f}_{Virt}(s,\tilde{\alpha}',\tilde{\beta}')] + \mathfrak{B}\left(\begin{matrix} p \\ \lambda \end{matrix};X\right)\mathfrak{s}^{\{F\}}_{\sigma}(k)\rho^{(2)f}_{Virt}(s,\tilde{\alpha}',\tilde{\beta}') + \mathfrak{B}\left(\begin{matrix} p \\ \lambda \end{matrix};X\right)\mathfrak{s}^{\{F\}}_{\sigma}(k)[1+\delta^{(1)e}_{Virt}(s)] \times[1+\delta^{(1)f}_{Virt}(s)]\left(1-\frac{(p_c+p_d+k)^2}{(p_c+p_d)^2}\right) \tag{130}$$

where

$$\rho^{(2)f}_{Virt}(s,\tilde{\alpha}',\tilde{\beta}') = \frac{\alpha}{\pi}Q_f^2\frac{1}{4}\overline{L}_f[\ln(1-\tilde{\alpha}'')+\ln(1-\tilde{\beta}'')],$$

$$\tilde{\alpha}' = \frac{2kp_d}{2p_cp_d}, \quad \tilde{\beta}' = \frac{2kp_c}{2p_cp_d}, \quad \tilde{\alpha}'' = \frac{\tilde{\alpha}'}{1+\tilde{\alpha}'+\tilde{\beta}'}, \quad \tilde{\beta}'' = \frac{\tilde{\beta}'}{1+\tilde{\alpha}'+\tilde{\beta}'}. \tag{131}$$

In the above FSR amplitudes we keep only the LL part, averaged over the photon angles, much as in EEX. This corresponds to the present status of our CEEX amplitudes implemented in the $\mathcal{KK}$ MC version 4.13, and we expect this to be improved in the future.

F. Two real photons

In the $\mathcal{O}(\alpha^2)$, the contributions from two real photons are completely at the tree level, without virtual corrections [in the future $\mathcal{O}(\alpha^3)$ version we shall include the virtual corrections to the double bremsstrahlung in the LL approximation]. The double bremsstrahlung is considered in three separate cases: two ISR photons, two FSR photons, and one ISR plus one FSR photon. The corresponding spin amplitudes will be given without any approximation, in particular we do not use

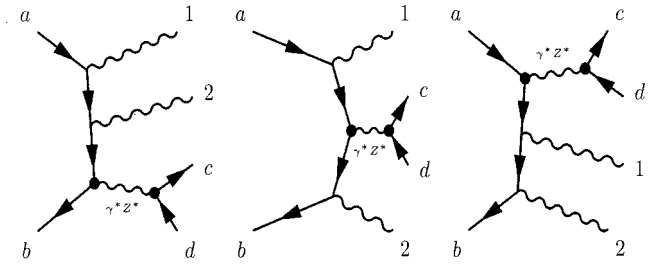

FIG. 9. Feynman diagrams of the ISR double bremsstrahlung.

the small-mass approximation $m_f/\sqrt{s}\ll 1$. The main problems to be solved will be (a) to write all spin amplitudes in a form that will be easy for numerical evaluation, that is in terms of the U and V matrices, (b) to extract the $\hat{\beta}_2$ functions by removing IR-singular parts.

1. Two real ISR photons

The second-order, two-photon, ISR matrix element from the Feynman rules, see Fig. 9, reads as follows:

$$\begin{aligned}\mathcal{M}^{(2)}_{2\{II\}}\left(\begin{matrix}p_a p_b k_1 k_2\\ \lambda_a\lambda_b\sigma_1\sigma_2\end{matrix};P-k_1-k_2\right)=ie^2\sum_{B=\gamma,Z}\Pi^{\mu\nu}_B(P-k_1-k_2)(G^B_{f,\nu})_{[cd]}(eQ_e)^2\overline{v}(p_b,\lambda_b)\\ \times\Bigg\{G^B_{e,\mu}\frac{(\not p_a+m)-\not k_1-\not k_2}{-2k_1p_a-2k_2p_a+2k_1k_2}\not\epsilon^*_{\sigma_1}(k_1)\frac{(\not p_a+m)-\not k_2}{-2k_2p_a}\not\epsilon^*_{\sigma_2}(k_2)\\ +\not\epsilon^*_{\sigma_1}(k_1)\frac{(-\not p_b+m)+\not k_1}{-2k_1p_b}\not\epsilon^*_{\sigma_2}(k_2)\frac{(-\not p_b+m)+\not k_1+\not k_2}{-2k_1p_b-2k_2p_b+2k_1k_2}G^B_{e,\mu}\\ +\not\epsilon^*_{\sigma_1}(k_1)\frac{(-\not p_b+m)+\not k_1}{-2k_1p_b}G^B_{e,\mu}\frac{(\not p_a+m)-\not k_2}{-2k_2p_a}\not\epsilon^*_{\sigma_2}(k_2)+(1\leftrightarrow 2)\Bigg\}u(p_a,\lambda_a).\end{aligned}\tag{132}$$

We shall use Eq. (95), which in this case reads

$$\begin{aligned}\hat{\beta}^{(2)}_{2\{II\}}\left(\begin{matrix}pk_1k_2\\ \lambda\sigma_1\sigma_2\end{matrix};P-k_1-k_2\right)=\mathfrak{M}^{(2)}_{2\{II\}}\left(\begin{matrix}pk_1k_2\\ \lambda\sigma_1\sigma_2\end{matrix};P-k_1-k_2\right)-\hat{\beta}^{(1)}_{1\{I\}}\left(\begin{matrix}pk_1\\ \lambda\sigma_1\end{matrix};P-k_1-k_2\right)\mathfrak{s}^{\{I\}}_{\sigma_2}(k_2)\\ -\hat{\beta}^{(1)}_{1\{I\}}\left(\begin{matrix}pk_2\\ \lambda\sigma_2\end{matrix};P-k_1-k_2\right)\mathfrak{s}^{\{I\}}_{\sigma_1}(k_1)-\hat{\beta}^{(0)}_{0}\left(\begin{matrix}p\\ \lambda\end{matrix};P-k_1-k_2\right)\mathfrak{s}^{\{I\}}_{\sigma_1}(k_1)\mathfrak{s}^{\{I\}}_{\sigma_2}(k_2).\end{aligned}\tag{133}$$

We shall proceed similarly to the way we used in the one-photon case, isolating from the above expression the group of terms containing two factors of $(\not p+m)$, then the group containing a single factor of $(\not p+m)$, and finally the rest. Such a split represents almost exactly the split in Eq. (60) into a contribution with two $\mathfrak{s}$ factors (the double IR singularity), with a single $\mathfrak{s}$ factor (the single IR singularity), and the IR-finite remnant $\hat{\beta}^{(2)}_2$, which is our primary goal. In other words, we decompose $\mathfrak{M}^{(2)}_{2\{II\}}$ into several terms or parts, as described above, and we apply the IR subtraction of Eq. (133) term by term.

Let us first discuss the doubly IR-singular part proportional to two factors of $(\not p+m)$. To simplify maximally the discussion, let us neglect for the moment $2k_1k_2$ in the propagator. Using the completeness relations of Eq. (A14) and the diagonality property of Eq. (A21) in the Appendix, we can factorize the soft factors exactly and completely:

$$\begin{aligned}&(eQ_e)^2\overline{v}(p_b,\lambda_b)\Bigg\{G^B_{e,\mu}\frac{(\not p_a+m)}{2k_1p_a+2k_2p_a}\not\epsilon^*_{\sigma_1}(k_1)\frac{(\not p_a+m)}{2k_2p_a}\not\epsilon^*_{\sigma_2}(k_2)+\not\epsilon^*_{\sigma_1}(k_1)\frac{(-\not p_b+m)}{2k_1p_b}\not\epsilon^*_{\sigma_2}(k_2)\frac{(-\not p_b+m)}{2k_1p_b+2k_2p_b}G^B_{e,\mu}\\ &\quad+\not\epsilon^*_{\sigma_1}(k_1)\frac{(-\not p_b+m)}{2k_1p_b}G^B_{e,\mu}\frac{(\not p_a+m)}{2k_2p_a}\not\epsilon^*_{\sigma_2}(k_2)+(1\leftrightarrow 2)\Bigg\}u(p_a,\lambda_a)\\ &=(G^B_{e,\mu})_{[ba]}(eQ_e)^2\Bigg\{\frac{b_{\sigma_1}(k_1,p_a)}{2k_1p_a+2k_2p_a}\frac{b_{\sigma_2}(k_2,p_a)}{2k_2p_a}+\frac{b_{\sigma_1}(k_1,p_b)}{2k_1p_b}\frac{b_{\sigma_2}(k_2,p_b)}{2k_1p_b+2k_2p_b}-\frac{b_{\sigma_1}(k_1,p_b)}{2k_1p_b}\frac{b_{\sigma_2}(k_2,p_a)}{2k_2p_a}+(1\leftrightarrow 2)\Bigg\}\\ &=(G^B_{e,\mu})_{[ba]}\mathfrak{s}^{\{I\}}_{\sigma_1}(k_1)\mathfrak{s}^{\{I\}}_{\sigma_2}(k_2),\end{aligned}\tag{134}$$

where the identity

$$\frac{1}{2k_1p_a+2k_2p_a}\frac{1}{2k_1p_a}+\frac{1}{2k_1p_a+2k_2p_a}\frac{1}{2k_2p_a}=\frac{1}{2k_1p_a}\frac{1}{2k_2p_a}\tag{135}$$

was instrumental.

If we restore the terms $2k_1k_2$ in the propagator, the corresponding analog of Eq. (134), $\mathcal{M}^{\text{Double IR}}_{2\{II\}}$, leads to

$$\hat{\beta}^{(2)\text{Double}}_{2\{II\}}\begin{bmatrix} p k_1 k_2 \\ \lambda \sigma_1 \sigma_2 \end{bmatrix} = \mathcal{M}^{\text{Double IR}}_{2\{II\}}\begin{bmatrix} p k_1 k_2 \\ \lambda \sigma_1 \sigma_2 \end{bmatrix} - \mathfrak{s}^{\{I\}}_{\sigma_1}(k_1)\mathfrak{s}^{\{I\}}_{\sigma_2}(k_2)\mathfrak{B}\begin{bmatrix} p \\ \lambda \end{bmatrix} = (\mathfrak{s}^{(a)}_{[1]}\mathfrak{s}^{(a)}_{[2]}\Delta_a + \mathfrak{s}^{(b)}_{[1]}\mathfrak{s}^{(b)}_{[2]}\Delta_b)\mathfrak{B}\begin{bmatrix} p \\ \lambda \end{bmatrix}, \tag{136}$$

$$\mathfrak{s}^{(a)}_{\sigma_i}(k_i) \equiv \mathfrak{s}^{(a)}_{[i]} = -eQ_e \frac{b_{\sigma_1}(k_i, p_a)}{2k_i p_a},$$

$$\mathfrak{s}^{(b)}_{\sigma_i}(k_i) \equiv \mathfrak{s}^{(b)}_{[i]} = +eQ_e \frac{b_{\sigma_1}(k_i, p_b)}{2k_i p_b},$$

$$\mathfrak{s}^{\{I\}}_{\sigma_i}(k_i) \equiv \mathfrak{s}^{(a)}_{[i]} + \mathfrak{s}^{(b)}_{[i]} \equiv \mathfrak{s}^{(a)}_{\sigma_i}(k_i) + \mathfrak{s}^{(b)}_{\sigma_i}(k_i),$$

$$\Delta_f = \frac{2k_1 p_f + 2k_2 p_f}{2k_1 p_f + 2k_2 p_f \mp 2k_1 k_2} - 1 = \frac{\pm 2k_1 k_2}{2k_1 p_f + 2k_2 p_f \mp 2k_1 k_2},$$

$$f = a, b, c, d,$$

and the upper sign should be taken for $f = a, b$. Obviously, $\hat{\beta}^{(2)\text{Double}}$ is IR finite because of the Δ_f factor. In the above we have introduced a more compact notation for the $\mathfrak{s}$ factors. In addition, from now on we shall use the following shorthand notation

$$r_{if} = 2k_i \cdot p_f, \quad r_{ij} = 2k_i \cdot k_j, \quad f = a, b, c, d, \quad i, j, = 1, 2, \ldots, n. \tag{137}$$

The next class of terms that we are going to consider carefully is the one in which we sum terms with a single $(\not{p} + m)$; more precisely, let us include terms that may lead to a single IR singularity (if $k_1 \ll k_2$ or $k_2 \ll k_1$), that is, with $(\not{p} + m)$ next to a spinor, at the end of the fermion line:

$$\mathcal{M}^{\text{Single IR}}_{2\{II\}}\begin{bmatrix} p k_1 k_2 \\ \lambda \sigma_1 \sigma_2 \end{bmatrix} = ie^2 \sum_{B=\gamma,Z} \Pi^{\mu\nu}_B(X)(G^B_{f,\nu})_{[cd]}(eQ_e)^2 \overline{v}(p_b, \lambda_b)\Bigg\{ G^B_{e,\mu} \frac{-\not{k}_1 - \not{k}_2}{-r_{1a} - r_{2a} + r_{12}} \not{\epsilon}^*_{\sigma_1}(k_1) \frac{(\not{p}_a + m)}{-r_{2a}} \not{\epsilon}^*_{\sigma_2}(k_2)$$
$$+ \not{\epsilon}^*_{\sigma_1}(k_1) \frac{(-\not{p}_b + m)}{-r_{1b}} \not{\epsilon}^*_{\sigma_2}(k_2) \frac{\not{k}_1 + \not{k}_2}{-r_{1b} - r_{2b} + r_{12}} G^B_{e,\mu} + \not{\epsilon}^*_{\sigma_1}(k_1) \frac{(-\not{p}_b + m)}{-r_{1b}} G^B_{e,\mu} \frac{-\not{k}_2}{-r_{2a}} \not{\epsilon}^*_{\sigma_2}(k_2)$$
$$+ \not{\epsilon}^*_{\sigma_1}(k_1) \frac{\not{k}_1}{-r_{1b}} G^B_{e,\mu} \frac{(\not{p}_a + m)}{-r_{2a}} \not{\epsilon}^*_{\sigma_2}(k_2) + (1 \leftrightarrow 2)\Bigg\} u(p_a, \lambda_a). \tag{138}$$

Using the compact notation, already introduced when (re)calculating the single bremsstrahlung, we express $\mathcal{M}^{\text{Single IR}}_{2\{II\}}$ in a form that will make numerical evaluation easy, that is in terms of U and V matrices:

$$\mathcal{M}^{\text{Single IR}}_{2\{II\}}\begin{pmatrix} p k_1 k_2 \\ \lambda \sigma_1 \sigma_2 \end{pmatrix} = eQ_e \frac{-\mathfrak{B}_{[b1'][cd]}U_{[1'1a]} - \mathfrak{B}_{[b2'][cd]}U_{[2'1a]}}{-r_{1a} - r_{2a} + r_{12}} \mathfrak{s}^{(a)}_{[2]} + eQ_e \mathfrak{s}^{(b)}_{[1]} \frac{V_{[b22']}\mathfrak{B}_{[2'a][cd]} + V_{[b21']}\mathfrak{B}_{[1'a][cd]}}{-r_{1a} - r_{2a} + r_{12}}$$
$$- eQ_e \mathfrak{s}^{(b)}_{[1]}\mathfrak{B}_{[b2'][cd]} \frac{U_{[2'2a]}}{-r_{2a}} + eQ_e \frac{V_{[b11']}}{-r_{1b}}\mathfrak{B}_{[1'a][cd]}\mathfrak{s}^{(a)}_{[2]} + (1 \leftrightarrow 2). \tag{139}$$

On the other hand, the single-IR part to be eliminated is

$$\hat{\beta}^{(1)}_{1(1)[1]}\mathfrak{s}^{\{I\}}_{[2]} + \hat{\beta}^{(1)}_{1(1)[2]}\mathfrak{s}^{\{I\}}_{[1]} = r^{\{I\}}_{[1]}\mathfrak{s}^{\{I\}}_{[2]} + r^{\{I\}}_{[2]}\mathfrak{s}^{\{I\}}_{[1]} = \left(eQ_e \mathfrak{B}_{[b1'][cd]} \frac{U_{[1'1a]}}{r_{1a}} - eQ_e \frac{V_{[b11']}}{r_{1a}} \mathfrak{B}_{[1'a][cd]} \right) \mathfrak{s}^{\{I\}}_{[2]} + (1 \leftrightarrow 2). \tag{140}$$

Altogether we get

$$\hat{\beta}^{\rm Single}_{2\{II\}}\left(\begin{matrix} pk_1k_2 \\ \lambda\sigma_1\sigma_2\end{matrix}\right)=\mathcal{M}^{\rm Single\ IR}_{2\{II\}}\left(\begin{matrix} pk_1k_2 \\ \lambda\sigma_1\sigma_2\end{matrix}\right)-\hat{\beta}^{(1)}_{1(1)[1]}\mathfrak{s}^{\{I\}}_{[2]}-\hat{\beta}^{(1)}_{1(1)[2]}\mathfrak{s}^{\{I\}}_{[1]}$$

$$=-eQ_e\mathfrak{B}_{[b2']cd]}\frac{U_{[2'1a]}}{-r_{1a}-r_{2a}+r_{12}}\mathfrak{s}^{(a)}_{[2]}+eQ_e\mathfrak{s}^{(b)}_{[1]}\frac{V_{[b21']}}{-r_{1a}-r_{2a}+r_{12}}\mathfrak{B}_{[1'a][cd]}$$

$$-eQ_e\mathfrak{B}_{[b1']cd]}\left(\frac{U_{[1'1a]}}{-r_{1a}-r_{2a}+r_{12}}-\frac{U_{[1'1a]}}{-r_{1a}}\right)\mathfrak{s}^{(a)}_{[2]}$$

$$+eQ_e\mathfrak{s}^{(b)}_{[1]}\left(\frac{V_{[b22']}}{-r_{1a}-r_{2a}+r_{12}}-\frac{V_{[b22']}}{-r_{2b}}\right)\mathfrak{B}_{[2'a][cd]}+(1\leftrightarrow 2). \tag{141}$$

It is rather straightforward to see that the above is IR finite.

Finally, we have to include all of the remaining terms from Eq. (134), which have not yet been included in $\hat{\beta}_{2\{II\}}$. They are IR finite (in the case of only soft-photon energy) and they read

$$\hat{\beta}^{\rm Rest}_{2\{II\}}\left(\begin{matrix} pk_1k_2 \\ \lambda\sigma_1\sigma_2\end{matrix}\right)=ie^2\sum_{B=\gamma,Z}\Pi^{\mu\nu}_B(X)(G^B_{f,\nu})_{[cd]}(eQ_e)^2\overline{v}(p_b,\lambda_b)\Big\{G^B_{e,\mu}\frac{(\not p_a+m)-\not k_1-\not k_2}{-r_{1a}-r_{2a}+r_{12}}\not\epsilon^*_{\sigma_1}(k_1)\frac{-\not k_2}{-r_{2a}}\not\epsilon^*_{\sigma_2}(k_2)$$

$$+\not\epsilon^*_{\sigma_1}(k_1)\frac{\not k_1}{-r_{1b}}\not\epsilon^*_{\sigma_2}(k_2)\frac{(-\not p_b+m)+\not k_1+\not k_2}{-r_{1b}-r_{2b}+r_{12}}G^B_{e,\mu}$$

$$+\not\epsilon^*_{\sigma_1}(k_1)\frac{\not k_1}{-r_{1b}}G^B_{e,\mu}\frac{-\not k_2}{-r_{2a}}\not\epsilon^*_{\sigma_2}(k_2)+(1\leftrightarrow 2)\Big\}u(p_a,\lambda_a). \tag{142}$$

Using tensor notation in the fermion helicity indices, the above can be expressed in terms of the U and V matrices as follows:

$$\hat{\beta}^{\rm Rest}_{2\{II\}}\left(\begin{matrix} pk_1k_2 \\ \lambda\sigma_1\sigma_2\end{matrix}\right)=(eQ_e)^2\frac{\mathfrak{B}_{[ba'][cd]}U_{[a'12'']}-\mathfrak{B}_{[b1']cd]}U_{[1'12'']}-\mathfrak{B}_{[b2']cd]}U_{[2'12'']}}{-r_{1a}-r_{2a}+r_{12}}\frac{-U_{[2''2a]}}{-r_{2a}}$$

$$+(eQ_e)^2\frac{V_{[b11'']}}{-r_{1b}}\frac{-V_{[1''2b']}\mathfrak{B}_{[b'a][cd]}+V_{[1''21']}\mathfrak{B}_{[1'a][cd]}+V_{[1''22']}\mathfrak{B}_{[2'a][cd]}}{-r_{1b}-r_{2b}+r_{12}}$$

$$+(eQ_e)^2\frac{V_{[b11']}}{-r_{1b}}\mathfrak{B}_{[1'2'][cd]}\frac{-U_{[2'2a]}}{-r_{2a}}+(1\leftrightarrow 2). \tag{143}$$

The total ISR $\hat{\beta}_{2\{II\}}$ is the sum of the three,

$$\hat{\beta}_{2\{II\}}\left(\begin{matrix} pk_1k_2 \\ \lambda\sigma_1\sigma_2\end{matrix}\right)=\hat{\beta}^{\rm Double}_{2\{II\}}\left(\begin{matrix} pk_1k_2 \\ \lambda\sigma_1\sigma_2\end{matrix}\right)+\hat{\beta}^{\rm Single}_{2\{II\}}\left(\begin{matrix} pk_1k_2 \\ \lambda\sigma_1\sigma_2\end{matrix}\right)+\hat{\beta}^{\rm Rest}_{2\{II\}}\left(\begin{matrix} pk_1k_2 \\ \lambda\sigma_1\sigma_2\end{matrix}\right). \tag{144}$$

2. Two-real FSR photons

The case of final-state double real photon emission can be analyzed in a similar way. The second-order FSR, two-photon, matrix element is

$$\mathcal{M}^{(2)}_{2\{FF\}}\left(\begin{matrix} pk_1k_2 \\ \lambda\sigma_1\sigma_2\end{matrix};P\right)=ie^2\sum_{B=\gamma,Z}\Pi^{\mu\nu}_B(P)(G^B_{e,\mu})_{[ba]}(eQ_f)^2\overline{u}(p_c,\lambda_c)\Big\{\not\epsilon^*_{[1]}\frac{(\not p_c+m)+\not k_1}{2k_1p_c}\not\epsilon^*_{[2]}\frac{(\not p_c+m)+\not k_1+\not k_2}{2k_1p_c+2k_2p_c+2k_1k_2}G^B_{f,\nu}$$

$$+G^B_{f,\nu}\frac{(-\not p_d+m)-\not k_1-\not k_2}{2k_1p_d+2k_2p_d+2k_1k_2}\not\epsilon^*_{[1]}\frac{(-\not p_d+m)-\not k_2}{2k_2p_d}\not\epsilon^*_{[2]}$$

$$+\not\epsilon^*_{[1]}\frac{(\not p_c+m)+\not k_1}{2k_1p_c}G^B_{f,\nu}\frac{(-\not p_d+m)-\not k_2}{2k_2p_d}\not\epsilon^*_{[2]}+(1\leftrightarrow 2)\Big\}v(p_d,\lambda_d). \tag{145}$$

Similarly, the expansion into soft and non-IR parts for the FSR spin amplitudes is done in a way completely analogous to the ISR case. The subtraction formula is now

$$\hat{\beta}^{(2)}_{2\{FF\}}\left(\begin{matrix} pk_1k_2 \\ \lambda\sigma_1\sigma_2 \end{matrix};P\right)=\mathfrak{M}^{(2)}_{2\{FF\}}\left(\begin{matrix} pk_1k_2 \\ \lambda\sigma_1\sigma_2 \end{matrix};P\right)-\hat{\beta}^{(1)}_{1\{F\}}\left(\begin{matrix} pk_1 \\ \lambda\sigma_1 \end{matrix};P\right)\mathfrak{s}^{\{F\}}_{\sigma_2}(k_2)-\hat{\beta}^{(1)}_{1\{F\}}\left(\begin{matrix} pk_2 \\ \lambda\sigma_2 \end{matrix};P\right)\mathfrak{s}^{\{F\}}_{\sigma_1}(k_1)-\hat{\beta}^{(0)}_{0}\left(\begin{matrix} p \\ \lambda \end{matrix};P\right)\mathfrak{s}^{\{F\}}_{\sigma_1}(k_1)\mathfrak{s}^{\{F\}}_{\sigma_2}(k_2). \tag{146}$$

First we obtain the contribution from terms with two $(\not{p}-m)$ factors:

$$\hat{\beta}^{(2)\text{Double}}_{2\{FF\}}\left[\begin{matrix} pk_1k_2 \\ \lambda\sigma_1\sigma_2 \end{matrix}\right]=\mathcal{M}^{\text{Double IR}}_{2\{FF\}}\left[\begin{matrix} pk_1k_2 \\ \lambda\sigma_1\sigma_2 \end{matrix}\right]-\mathfrak{s}^{\{F\}}_{[1]}\mathfrak{s}^{\{F\}}_{[2]}\mathfrak{B}_{[ba][cd]}\frac{(p_c+p_d+k_1+k_2)^2}{(p_c+p_d)^2}$$

$$=(\Delta_c\mathfrak{s}^{(c)}_{[1]}\mathfrak{s}^{(c)}_{[2]}+\Delta_d\mathfrak{s}^{(d)}_{[1]}\mathfrak{s}^{(d)}_{[2]})\mathfrak{B}_{[ba][cd]}-\mathfrak{s}^{\{F\}}_{[1]}\mathfrak{s}^{\{F\}}_{[2]}\mathfrak{B}_{\text{F}}\left[\begin{matrix} p_bp_a \\ \lambda_b\lambda_a \end{matrix}\right]\left(\frac{(p_c+p_d+k_1+k_2)^2}{(p_c+p_d)^2}-1\right); \tag{147}$$

$$\mathfrak{s}^{(c)}_{\sigma_i}(k_i)\equiv\mathfrak{s}^{(c)}_{[i]}=+eQ_f\frac{b_{\sigma_i}(k_i,p_c)}{r_{ic}},$$

$$\mathfrak{s}^{(d)}_{\sigma_i}(k_i)\equiv\mathfrak{s}^{(d)}_{[i]}=-eQ_f\frac{b_{\sigma_i}(k_i,p_d)}{r_{id}},$$

$$\mathfrak{s}^{\{F\}}_{\sigma_i}(k_i)\equiv\mathfrak{s}^{(c)}_{\sigma_i}(k_i)+\mathfrak{s}^{(d)}_{\sigma_i}(k_i)\equiv\mathfrak{s}^{(c)}_{[i]}+\mathfrak{s}^{(d)}_{[i]},$$

which is explicitly IR finite. The second group of terms with only one $(\not{p}-m)$ factor at the end of the fermion line is

$$\mathcal{M}^{\text{Single IR}}_{2\{FF\}}\left(\begin{matrix} pk_1k_2 \\ \lambda\sigma_1\sigma_2 \end{matrix}\right)=ie^2\sum_{B=\gamma,Z}\Pi^{\mu\nu}_B(X)(G^B_{e,\mu})_{[ba]}(eQ_f)^2\overline{u}(p_c,\lambda_c)\Big\{\not{\epsilon}^*_{[1]}\frac{(\not{p}_c+m)}{r_{1c}}\not{\epsilon}^*_{[2]}\frac{\not{k}_1+\not{k}_2}{r_{1c}+r_{2c}+r_{12}}G^B_{f,\nu}$$

$$+G^B_{f,\nu}\frac{-\not{k}_1-\not{k}_2}{r_{1d}+r_{2d}+r_{12}}\not{\epsilon}^*_{[1]}\frac{(-\not{p}_d+m)}{r_{2d}}\not{\epsilon}^*_{[2]}+\not{\epsilon}^*_{[1]}\frac{(\not{p}_c+m)}{r_{1c}}G^B_{f,\nu}\frac{-\not{k}_2}{r_{2d}}\not{\epsilon}^*_{[2]}$$

$$+\not{\epsilon}^*_{[1]}\frac{\not{k}_1}{r_{1c}}G^B_{f,\nu}\frac{(-\not{p}_d+m)}{r_{2d}}\not{\epsilon}^*_{[2]}+(1\leftrightarrow2)\Big\}v(p_d,\lambda_d), \tag{148}$$

and it translates, in the matrix notation (in the fermion spin indices), into

$$\mathcal{M}^{\text{Single IR}}_{2\{FF\}}\left(\begin{matrix} pk_1k_2 \\ \lambda\sigma_1\sigma_2 \end{matrix}\right)=eQ_f\mathfrak{s}^{(c)}_{[1]}\frac{U_{[c21']}}{r_{1c}+r_{2c}+r_{12}}\mathfrak{B}_{[ba][1'd]}+eQ_f\mathfrak{s}^{(c)}_{[1]}\frac{U_{[c22']}}{r_{1c}+r_{2c}+r_{12}}\mathfrak{B}_{[ba][2'd]}+eQ_f\mathfrak{B}_{[ba][c1']}\frac{-V_{[1'1d]}}{r_{1d}+r_{2d}+r_{12}}\mathfrak{s}^{(d)}_{[2]}$$

$$+eQ_f\mathfrak{B}_{[ba][c2']}\frac{-V_{[2'1d]}}{r_{1d}+r_{2d}+r_{12}}\mathfrak{s}^{(d)}_{[2]}+eQ_f\mathfrak{s}^{(c)}_{[1]}\mathfrak{B}_{[ba][c2']}\frac{-V_{[2'2d]}}{r_{2d}}+eQ_f\frac{U_{[c11']}}{r_{1c}}\mathfrak{B}_{[ba][1'd]}\mathfrak{s}^{(d)}_{[2]}+(1\leftrightarrow2). \tag{149}$$

On the other hand, the single-IR part to be eliminated is

$$\hat{\beta}^{(1)}_{1(0)[1]}\mathfrak{s}^{\{F\}}_{[2]}+\hat{\beta}^{(1)}_{1(0)[2]}\mathfrak{s}^{\{F\}}_{[1]}=r^{\{F\}}_{[1]}\mathfrak{s}^{\{F\}}_{[2]}+r^{\{F\}}_{[2]}\mathfrak{s}^{\{F\}}_{[1]}$$

$$=\left(+eQ_e\mathfrak{B}_{[ba][1'd]}\frac{U_{[c11']}}{r_{1c}}-eQ_e\frac{V_{[1'1d]}}{r_{1d}}\mathfrak{B}_{[ba][c1']}\right)\mathfrak{s}^{\{F\}}_{[2]}$$

$$+(1\leftrightarrow2)-\mathfrak{B}_{[ba][cd]}\left(\frac{(p_c+p_d+k_1)^2}{(p_c+p_d)^2}-1\right)\mathfrak{s}^{\{F\}}_{[1]}\mathfrak{s}^{\{F\}}_{[2]}+(1\leftrightarrow2). \tag{150}$$

Altogether we get

$$\hat{\beta}^{\rm Single}_{2\{FF\}}\left(\begin{matrix} pk_1k_2 \\ \lambda\sigma_1\sigma_2\end{matrix}\right)=\mathcal{M}^{\rm Single\ IR}_{2\{FF\}}\left(\begin{matrix} pk_1k_2 \\ \lambda\sigma_1\sigma_2\end{matrix}\right)-\hat{\beta}^{(1)}_{1(0)}\left(\begin{matrix} pk_1 \\ \lambda\sigma_1\end{matrix}\right)\mathfrak{s}^{\{F\}}\left[\begin{matrix} k_2 \\ \sigma_2\end{matrix}\right]-\hat{\beta}^{(1)}_{1(0)}\left(\begin{matrix} pk_2 \\ \lambda\sigma_2\end{matrix}\right)\mathfrak{s}^{\{F\}}\left[\begin{matrix} k_1 \\ \sigma_1\end{matrix}\right]$$

$$\begin{aligned}
&=eQ_f\mathfrak{s}^{(c)}_{[1]}\left\{\left(\frac{U_{[c22']}}{r_{2c}+r_{1c}+r_{12}}-\frac{U_{[c22']}}{r_{2c}}\right)\mathfrak{B}_{[ba][2'd]}+\frac{U_{[c21']}}{r_{2c}+r_{1c}+r_{12}}\mathfrak{B}_{[ba][1'd]}\right\}\\
&\quad+eQ_f\left\{\mathfrak{B}_{[ba][c1']}\left(\frac{-V_{[1'1d]}}{r_{1d}+r_{2d}+r_{12}}-\frac{-V_{[1'1d]}}{r_{1d}}\right)+\frac{-V_{[2'1d]}}{r_{1d}+r_{2d}+r_{12}}\mathfrak{B}_{[ba][c2']}\right\}\mathfrak{s}^{(d)}_{[2]}\\
&\quad+\mathfrak{B}_{[ba][cd]}\left(\frac{(p_c+p_d+k_1)^2}{(p_c+p_d)^2}-1\right)\mathfrak{s}^{\{F\}}_{[1]}\mathfrak{s}^{\{F\}}_{[2]}+(1\leftrightarrow 2).
\end{aligned}\tag{151}$$

Finally we include the remaining terms in Eq. (145),

$$\begin{aligned}
\mathcal{M}^{\rm Rest}_{2\{FF\}}\left(\begin{matrix} pk_1k_2 \\ \lambda\sigma_1\sigma_2\end{matrix}\right)&=ie^2\sum_{B=\gamma,Z}\Pi^{\mu\nu}_B(X)(G^B_{e,\mu})_{[ba]}(eQ_f)^2\overline{u}(p_c,\lambda_c)\left\{\not\epsilon^*_{[1]}\frac{\not k_1}{r_{1c}}\not\epsilon^*_{[2]}\frac{(\not p_c+m)+\not k_1+\not k_2}{r_{1c}+r_{2c}+r_{12}}G^B_{f,\nu}\right.\\
&\left.+G^B_{f,\nu}\frac{(-\not p_d+m)-\not k_1-\not k_2}{r_{1d}+r_{2d}+r_{12}}\not\epsilon^*_{[1]}\frac{-\not k_2}{r_{2d}}\not\epsilon^*_{[2]}+\not\epsilon^*_{[1]}\frac{\not k_1}{r_{1c}}G^B_{f,\nu}\frac{-\not k_2}{r_{2d}}\not\epsilon^*_{[2]}+(1\leftrightarrow 2)\right\}v(p_d,\lambda_d),
\end{aligned}\tag{152}$$

which in the programmable matrix notation looks as follows:

$$\begin{aligned}
\hat{\beta}^{\rm Rest}_{2\{FF\}}\left(\begin{matrix} pk_1k_2 \\ \lambda\sigma_1\sigma_2\end{matrix}\right)&=\mathcal{M}^{\rm Rest}_{2\{FF\}}\left(\begin{matrix} pk_1k_2 \\ \lambda\sigma_1\sigma_2\end{matrix}\right)\\
&=(eQ_f)^2\frac{U_{[c11'']}}{r_{1c}}\frac{U_{[1''2c']}\mathfrak{B}_{[ba][c'd]}+U_{[1''21']}\mathfrak{B}_{[ba][1'd]}+U_{[1''22']}\mathfrak{B}_{[ba][2'd]}}{r_{1c}+r_{2c}+r_{12}}\\
&\quad+(eQ_f)^2\frac{-\mathfrak{B}_{[ba][cd']}V_{[d'12'']}-\mathfrak{B}_{[ba][c1']}V_{[1'12'']}-\mathfrak{B}_{[ba][c2']}V_{[2'12'']}}{r_{1d}+r_{2d}+r_{12}}\frac{-V_{[2''2d]}}{r_{2d}}\\
&\quad+(eQ_f)^2\frac{U_{[c11']}}{r_{1c}}\mathfrak{B}_{[ba][1'2']}\frac{-V_{[2'2d]}}{r_{2d}}+(1\leftrightarrow 2).
\end{aligned}\tag{153}$$

The total contribution from the double FSR real photon emission is

$$\hat{\beta}_{2\{FF\}}\left(\begin{matrix} pk_1k_2 \\ \lambda\sigma_1\sigma_2\end{matrix}\right)=\hat{\beta}^{\rm Double}_{2\{FF\}}\left(\begin{matrix} pk_1k_2 \\ \lambda\sigma_1\sigma_2\end{matrix}\right)+\hat{\beta}^{\rm Single}_{2\{FF\}}\left(\begin{matrix} pk_1k_2 \\ \lambda\sigma_1\sigma_2\end{matrix}\right)+\hat{\beta}^{\rm Rest}_{2\{FF\}}\left(\begin{matrix} pk_1k_2 \\ \lambda\sigma_1\sigma_2\end{matrix}\right).\tag{154}$$

3. One-real ISR and one-real FSR photon

As we have seen in the previous cases of the double-real emission, most of the complications are due to the simultaneous emission from one fermion ''leg.'' The case of one-real ISR and one-real FSR photon is easier, because there is at most one photon on one leg:

$$\begin{aligned}
\mathcal{M}^{(2)}_{2\{IF\}}\left(\begin{matrix} p_ap_bp_cp_dk_1k_2 \\ \lambda_a\lambda_b\lambda_c\lambda_d\sigma_1\sigma_2\end{matrix};P-k_1\right)&=ie^2\sum_{B=\gamma,Z}\Pi^{\mu\nu}_B(P-k_1)eQ_e\overline{v}(p_b,\lambda_b)\\
&\times\left(G^B_{e,\mu}\frac{\not p_a+m-\not k_1}{-2k_1p_a}\not\epsilon^*_{[1]}+\not\epsilon^*_{[1]}\frac{-\not p_b+m+\not k_1}{-2k_1p_b}G^B_{e,\mu}\right)u(p_a,\lambda_a)eQ_f\overline{u}(p_c,\lambda_c)\\
&\times\left(G^B_{f,\nu}\frac{-\not p_d+m-\not k_2}{2k_2p_d}\not\epsilon^*_{[2]}+\not\epsilon^*_{[2]}\frac{\not p_c+m+\not k_2}{2k_2p_c}G^B_{f,\nu}\right)v(p_d,\lambda_d)
\end{aligned}\tag{155}$$

and the subtraction formula is now

$$\hat{\beta}^{(2)}_{2\{IF\}}\left(\begin{matrix} pk_1k_2 \\ \lambda\sigma_1\sigma_2 \end{matrix};P-k_1\right)=\mathfrak{M}^{(2)}_{2\{IF\}}\left(\begin{matrix} pk_1k_2 \\ \lambda\sigma_1\sigma_2 \end{matrix};P-k_1\right)-\hat{\beta}^{(1)}_{1\{I\}}\left(\begin{matrix} pk_1 \\ \lambda\sigma_1 \end{matrix};P-k_1\right)\mathfrak{s}^{\{F\}}_{\sigma_2}(k_2)$$
$$-\hat{\beta}^{(1)}_{1\{F\}}\left(\begin{matrix} pk_2 \\ \lambda\sigma_2 \end{matrix};P-k_1\right)\mathfrak{s}^{\{I\}}_{\sigma_1}(k_1)-\hat{\beta}^{(0)}_{0}\left(\begin{matrix} p \\ \lambda \end{matrix};P-k_1\right)\mathfrak{s}^{\{I\}}_{\sigma_1}(k_1)\mathfrak{s}^{\{F\}}_{\sigma_2}(k_2). \tag{156}$$

The simplicity of this contribution is manifest in the fact that $\hat{\beta}_{2\{IF\}}$ is obtained by the simple subtraction (omission) of all terms proportional to one or two $(\not{p}-m)$ factors

$$\hat{\beta}_{2\{IF\}}\left(\begin{matrix} pk_1k_2 \\ \lambda\sigma_1\sigma_2 \end{matrix};X\right)=ie^2\sum_{B=\gamma,Z}\Pi^{\mu\nu}_B(X)eQ_e\overline{v}(p_b,\lambda_b)\left(G^B_{e,\mu}\frac{-\not{k}_1}{-r_{1a}}\not{\epsilon}^*_{[1]}+\not{\epsilon}^*_{[1]}\frac{\not{k}_1}{-r_{1b}}G^B_{e,\mu}\right)$$
$$\times u(p_a,\lambda_a)eQ_f\overline{u}(p_c,\lambda_c)\left(G^B_{f,\nu}\frac{-\not{k}_2}{r_{2d}}\not{\epsilon}^*_{[2]}+\not{\epsilon}^*_{[2]}\frac{\not{k}_2}{r_{2c}}G^B_{f,\nu}\right)v(p_d,\lambda_d). \tag{157}$$

In the computation-friendly matrix notation it reads

$$\hat{\beta}_{2\{IF\}}\left(\begin{matrix} pk_1k_2 \\ \lambda\sigma_1\sigma_2 \end{matrix};X\right)=ie^2\sum_{B=\gamma,Z}\Pi^{\mu\nu}_B(X)eQ_eeQ_f\left((G^B_{e,\mu})_{[b1']}\frac{-U_{[1'1a]}}{-r_{1a}}+\frac{V_{[b11']}}{-r_{1b}}(G^B_{e,\mu})_{[1'a]}\right)$$
$$\times\left((G^B_{f,\nu})_{[c2']}\frac{-V_{[2'2d]}}{r_{2d}}+\frac{U_{[c22']}}{r_{2c}}(G^B_{f,\nu})_{[2'd]}\right)$$
$$=eQ_eeQ_f\left(\mathfrak{B}_{[b1'][c2']}(X)\frac{-U_{[1'1a]}}{-r_{1a}}\frac{-V_{[2'2d]}}{r_{2d}}\right.$$
$$\left.+\frac{U_{[c22']}}{r_{2c}}\mathfrak{B}_{[b1'][2'd]}(X)\frac{-U_{[1'1a]}}{-r_{1a}}+\frac{V_{[b11']}}{-r_{1b}}\mathfrak{B}_{[1'a][c2']}(X)\frac{-V_{[2'2d]}}{r_{2d}}+\frac{V_{[b11']}}{-r_{1b}}\frac{U_{[c22']}}{r_{2c}}\mathfrak{B}_{[1'a][2'd]}(X)\right). \tag{158}$$

IV. RELATIONS BETWEEN CEEX AND EEX

Having shown the CEEX and EEX schemes in detail, we would like to compare certain important and interesting features of both schemes in more detail. In particular we would like to show how the two examples of the EEX scheme can be obtained as a limiting case of the CEEX, and to show the exact relation between the $\overline{\beta}$'s of the EEX and the $\hat{\beta}$'s of the CEEX. From these considerations it will be clear that the CEEX scheme is more general than the EEX scheme.

A. Neglecting partition dependence

Let us first examine the interesting limit of the CEEX in which we drop the dependence on the partition index $X_\wp \to P$, where $P=p_a+p_b$, for example. Note that it is not in the EEX class. In this limit, in the simplest case of the $\mathcal{O}(\alpha^0)$ exponentiation, we have

$$\sum_{\wp\in\mathcal{P}}e^{\alpha B_4(X_\wp)}\frac{X^2_\wp}{s_{cd}}\mathfrak{B}\left(\begin{matrix} p \\ \lambda \end{matrix};X_\wp\right)\prod_{i=1}^{n}\mathfrak{s}^{\{\wp_i\}}_{[i]}$$
$$\Rightarrow e^{\alpha B_4}\mathfrak{B}\left(\begin{matrix} p \\ \lambda \end{matrix};P\right)\prod_{i=1}^{n}(\mathfrak{s}^{\{I\}}_{[i]}+\mathfrak{s}^{\{F\}}_{[i]}), \tag{159}$$

because of the identity (78). Note that in the above transition we keep the ISR⊗FSR interference contribution.

B. Neglecting IFI

The second important case we would like to discuss is the case of the very narrow resonances, when the ISR⊗FSR interference contribution to any physical observable is so small that it can be altogether neglected. This corresponds to a well-defined limit in the CEEX scheme. In this limit, in the simplest case of the $\mathcal{O}(\alpha^0)$ exponentiation we have

$$|\mathcal{M}^{(0)}_n|^2=\sum_{\wp\in\mathcal{P}}\sum_{\wp'\in\mathcal{P}}\exp[\alpha B_4(X_\wp)]$$
$$\times\exp[\alpha B_4(X_{\wp'})]^*\mathfrak{B}\left(\begin{matrix} p \\ \lambda \end{matrix};X_\wp\right)\mathfrak{B}\left(\begin{matrix} p \\ \lambda \end{matrix};X_{\wp'}\right)^*$$
$$\times\prod_{i=1}^{n}\mathfrak{s}^{\{\wp_i\}}_{[i]}\prod_{j=1}^{n}\mathfrak{s}^{\{\wp'_i\}}_{[j]*}$$
$$\Rightarrow\exp[2\alpha\Re B_2(p_a,p_b)]\exp[2\alpha\Re B_2(p_c,p_d)]$$
$$\times\sum_{\wp\in\mathcal{P}}\left|\mathfrak{B}\left(\begin{matrix} p \\ \lambda \end{matrix};X_\wp\right)\right|^2\prod_{i=1}^{n}|\mathfrak{s}^{\{\wp_i\}}_{[i]}|^2. \tag{160}$$

What we did in the above transition is to neglect the ISR⊗FSR interferences entirely, by dropping the nondiagonal terms $\wp\neq\wp'$ in the double sum over partitions, and to re-

place the resonance-type form factor by the sum of the traditional YFS form factors for the ISR and the FSR (no interference). In this way we have the $\mathcal{O}(\alpha^0)_{\rm EEX}$, which at this order is identical to $\mathcal{O}(\alpha^0)_{\rm CEEX}$. At $\mathcal{O}(\alpha^r)_{\rm CEEX}$, $r=1,2$, in order to get from $\mathcal{O}(\alpha^r)_{\rm CEEX}$ to $\mathcal{O}(\alpha^r)_{\rm EEX}$, we have in addition to truncate the $\hat{\beta}$'s down to $\overline{\beta}$'s, as will be shown in the next subsection.

The $\mathcal{O}(\alpha^r)_{\rm EEX}$, $r=1,2$, neglecting the ISR$\otimes$FSR interferences was used in the YFS2/3 [7,9] of KORALZ [10] and it is well justified close to the Z resonance position at LEP1; see also the relevant numerical results in the next section. At LEP2 the above approximation can no longer be justified.

C. Relation among $\overline{\beta}$'s for EEX and $\hat{\beta}$'s of CEEX

For the sake of completeness of the discussion, it is necessary to find out the relation between the $\hat{\beta}$'s defined at the amplitude level and the older EEX/YFS $\overline{\beta}$'s defined at the level of the differential distributions. Let us suppress all spin indices, understanding that for every term like $|\cdots|^2$ or $\Re[AB^*]$ the appropriate spin sum or average is done. The traditional $\overline{\beta}$'s of the YFS scheme at the $\mathcal{O}(\alpha^2)$ level are

$$\overline{\beta}_0^{(l)}=|\mathfrak{M}_0^{(l)}|^2_{(\alpha^l)},\quad l=0,1,2,$$

$$\overline{\beta}_1^{(l)}(k)=|\mathfrak{M}_1^{(l)}(k)|^2_{(\alpha^{l+1})}-\overline{\beta}_0^{(l)}|\mathfrak{s}(k)|^2,\quad l=0,1, \tag{161}$$

$$\begin{aligned}\overline{\beta}_2^{(2)}(k_1,k_2)=&|\mathfrak{M}_1^{(2)}(k_1,k_2)|^2-\overline{\beta}_1^{(1)}(k_1)|\mathfrak{s}(k_2)|^2\\&-\overline{\beta}_1^{(1)}(k_2)|\mathfrak{s}(k_1)|^2\\&-\overline{\beta}_0^{(0)}|\mathfrak{s}(k_1)|^2|\mathfrak{s}(k_2)|^2,\end{aligned}$$

where the subscript $|_{(\alpha^r)}$ means a truncation to $\mathcal{O}(\alpha^r)$. Now for each $\mathfrak{M}_n^{(n+l)}$ we substitute its expansion in terms of $\hat{\beta}$'s according to Eq. (58), getting the following relation:

$$\overline{\beta}_0^{(l)}=|\hat{\beta}_0^{(l)}|^2_{(\alpha^l)},\quad l=0,1,2,$$

$$\overline{\beta}_1^{(l)}(k)=|\hat{\beta}_1^{(l)}(k)|^2+2\Re[\hat{\beta}_0^{(l)}\{\hat{\beta}_1^{(l)}(k)\}^*]_{(\alpha^{l+1})},\quad l=0,1, \tag{162}$$

$$\begin{aligned}\overline{\beta}_2^{(2)}(k_1,k_2)=&|\hat{\beta}_2^{(2)}(k_1,k_2)|^2+2\Re[\hat{\beta}_1^{(1)}(k_1)\mathfrak{s}(k_2)\\&\times\{\hat{\beta}_1^{(1)}(k_2)\mathfrak{s}(k_1)\}^*]+2\Re[\hat{\beta}_2^{(2)}(k_1,k_2)\\&\times\{\hat{\beta}_1^{(1)}(k_1)\mathfrak{s}(k_2)\hat{\beta}_1^{(1)}(k_2)\mathfrak{s}(k_1)\\&+\hat{\beta}_1^{(0)}\mathfrak{s}(k_1)\mathfrak{s}(k_2)\}^*].\end{aligned}$$

As we see, the relation is not completely trivial; there are some extra terms on the rhs, which are all IR finite. From the above exercise it is obvious that $\overline{\beta}$'s are generally more complicated objects than the $\hat{\beta}$'s and that, for example, the inclusion of the spin density matrix formalism into the $\overline{\beta}$'s would be quite a nontrivial exercise—the great advantage of the CEEX scheme is that this is done numerically. It is also seen that in the $\overline{\beta}_0$ and $\overline{\beta}_1$ some higher-order virtual terms are *unnecessarily* truncated, which probably worsens the perturbative convergence of the EEX/YFS scheme in comparison with that of the CEEX. The above formula shows in a most clear and clean way the difference between the EEX and CEEX exponentiation schemes.

V. SEMIANALYTICAL APPROACH

This section is devoted to the so-called semianalytical calculations. Their role in this work is to reproduce and/or cross-check our Monte Carlo numerical results for the integrated cross sections and asymmetries. In the following introduction we characterize briefly the well-known features of semianalytical methods. In the main part of this section we derive unpublished semianalytical formulas mainly within $\mathcal{O}(\alpha^2)_{prag}$, and occasionally up to $\mathcal{O}(\alpha^3)_{prag}$. Numerical comparisons of these semianalytical results with the Monte Carlo results will be presented either immediately or in the following sections.

In the semianalytical approach an integration over the phase-space is done analytically, leaving the last one- or two-dimensional integrations for numerical treatment (usually non-Monte-Carlo). Well-known examples of semianalytical programs are ZFITTER and TOPAZ0 [5,41]. Semianalytical programs are generally faster in terms of computer CPU time than MC programs and are therefore better suited for fitting the standard model to experimental data.[18] Semianalytical calculations have also important disadvantages: (a) they are able to provide predictions only for quite primitive or absent experimental cutoffs, in practice they are always used in combination with the MC event generators; (b) they are rather complicated beyond the three-body final state, that is they are limited practically to $\mathcal{O}(\alpha^1)$ calculations (the single photon emission in the fermion pair production).

In the testing of the Monte Carlo programs semianalytical calculations can (a) check the technical/numerical correctness of the phase-space integration, (b) check the correctness of the implementation of the SM matrix element, and (c) give an estimate of some unaccounted higher orders. In the following we shall illustrate all possible examples of such tests. In particular, we shall see the test of the technical precision of the $\mathcal{KK}$ MC at the 2×10^{-4} level, based on the semianalytical formula obtained in this section.

The role of semianalytical calculations as a test of the Monte Carlo programs is seriously limited in the following sense: a numerical problem may show up not for the simple kinematical cuts accessible for the semianalytical code, but rather for a more realistic/complicated event selection. The *ultimate test* of the MC calculation is always the comparison of two independent MC programs, because it can be done for arbitrary cutoffs.[19] One may argue that the two-MC test costs

[18] It is definitely possible to fit SM parameters to experimental data with the help of the Monte Carlo event generators, as it is currently done in the measurements of the W-pair process in LEP2.

[19] This kind of test was for instance done for the first modern $\mathcal{O}(\alpha^1)$ Monte Carlo event generator MUSTRAAL of Refs. [16,17], with the very high precision at that time of 1%.

too much work to realize in practice. However, our past experience shows that at the subpermille precision level the amount of work required to obtain the semianalytical formulas and to test the corresponding code is probably the same as the amount of work necessary in the development of another Monte Carlo code. The above remark does not contradict the fact that the semianalytical calculations will always be very useful, especially when the precision requirement is not excessive and when the observables do not involve complicated experimental cuts.

A. Inclusive exponentiation: IEX

The meaning of ''exponentiation'' in the literature is strongly context dependent. Following the unpublished presentation of Ref. [4] we call an ''*ad hoc* exponentiation'' the exponentiation of the typical semianalytical approach. The essence of the *ad hoc* exponentiation is to take as a starting point an analytical result for a certain one- or two-dimensional *inclusive* distribution from a QED finite-order calculation, $\mathcal{O}(\alpha)$ or $\mathcal{O}(\alpha^2)$, and to ''improve'' this result in a rather *ad hoc* way, such that the soft limit (no hard photons) agrees with the result of the Yennie, Frautschi, and Suura [8].

The well-known examples of the *ad hoc* exponentiation are presented in Refs. [42,43] and later in Ref. [44] for the initial-state bremsstrahlung in e^+e^- annihilation; it was also practiced in many QED calculations for the deep inelastic and Bhabha scattering processes. With some effort, the *ad hoc* exponentiation procedure may be improved gradually by taking into account missing higher-order effects. For example, the $\mathcal{O}(\alpha)$ procedure of Ref. [42] was extended to $\mathcal{O}(\alpha^2)$ in Ref. [43] and later to $\mathcal{O}(\alpha^3)$ in Ref. [44]. However, the upgrade to higher orders is rather an art than a science, i.e., the *ad hoc* approach is not systematic—it has to be ''reinvented'' again and again for each perturbative order and for each inclusive observable.[20]

The important practical question is therefore the following: *Is there any better and more systematic way of reformulating the ad hoc exponentiation, such that it applies to any inclusive distribution at any perturbative order?* It would be also desirable to have a direct connection to the exclusive YFS exponentiation of the EEX or CEEX type, both of which are discussed and implemented in this work. The obvious hint as to which direction to go in is the following well-known fact: when all photons are soft, the following *exact* analytical formula for the multiphoton phase-space integral is available [8]:

$$f(\gamma,V)=\exp(\gamma\ln\varepsilon)\sum_{n=0}^{\infty}\frac{1}{n!}\prod_{i=1}^{n}\int_{k_0>2\varepsilon\sqrt{s}/2}\frac{d^3k_i}{k_i^0}\times\tilde{S}(p_1;p_2;k_i)\,\delta\left(V-\frac{1}{s}(p_1+p_2)\cdot\left(\sum_{i=1}^{n}k_i\right)\right)$$

$$=\frac{\exp(-C\gamma)}{\Gamma(1+\gamma)}\gamma V^{\gamma-1}=F(\gamma)\gamma V^{\gamma-1},$$

$$C=0.577\,215\,66\ldots.$$

We propose to include hard photons in the game, and from now on we define the ''YFS inclusive exponentiation'' (IEX) in a straightforward way as the result of the *analytical* phase-space integration of the distributions of the YFS exclusive exponentiation:

YFS inclusive exponentiation

$\equiv$*Analytical integration of YFS multiphoton integrals.*

We do not need any ''recipes'' for IEX at higher orders, and what we only need to know is how to integrate (analytically) the phase-space.

One may argue, however, that with the above definition of IEX we are replacing one difficult problem by another one that is even more difficult—the analytical integration over *n* real photon phase-space. We shall see in the present section that this approach can really work in practice. Our methods of the analytical evaluation of the phase-space integrals will follow the following general rule: in spite of the use of certain approximations, all of our approximate methods will be always *exact* in the soft-photon limit. The soft-photon part will be integrated exactly and only the remaining noninfrared (non-IR) contribution will be calculated using approximate methods, typically the leading-logarithmic collinear approximation. The LL approximations in non-IR parts may concern both the phase-space and the matrix element.[21]

In the following subsections we shall show explicitly the analytical integrations leading to the $\mathcal{O}(\alpha^2)_{prag}$ IEX results. We shall compare the Monte Carlo with the EEX matrix element and the IEX formulas, both in the $\mathcal{O}(\alpha^2)_{prag}$ class. Their difference will be then necessarily of $\mathcal{O}(\alpha^3)_{prag}$, i.e., up to a factor of 10 smaller than $\mathcal{O}(\alpha^2)_{prag}$—quite a strong test of both calculations. On one occasion, we shall go to a more difficult level of the $\mathcal{O}(\alpha^3)_{prag}$, in which case the difference between the MC and IEX is of order $\mathcal{O}(\alpha^4)_{prag}$.

Finally, let us note that the set of IEX formulas presented in this section was used over many years as a basic, albeit unpublished, test of the precisions of the YFS2 [7] and KORALZ/YFS3 [9,10] programs. Only very limited examples of the IEX results were already shown (without derivation) in Refs. [7] and [4]. Most of the IEX results for our *s*-channel process are presented here for the first time. In the mean time the analogous set of IEX results was obtained and published for the *t*-channel-dominated Bhabha process [13]. In fact Ref. [13] describes a case of the IEX at the $\mathcal{O}(\alpha^3)_{prag}$ that is even more sophisticated than the $\mathcal{O}(\alpha^2)_{prag}$ example presented here. With the experience of Ref. [13] it would definitely be possible to do an $\mathcal{O}(\alpha^3)_{prag}$ IEX calculation for our *s*-channel process, both for the ISR and the FSR.

[20]For instance it is still not known how to do inclusive exponentiation for the acollinearity distribution.

[21]Let us note that the LL evaluation of the phase-space integral was already employed to some extent in the original YFS work [8]. At that time, because of the lack of fast computers, it was the only accessible method.

B. Semianalytical formulas for ISR

We shall start the construction of IEX expressions with the ISR case, first showing the basic techniques in working out the example with the $\mathcal{O}(\alpha^0)$ EEX matrix element. In this case the multiphoton differential distribution is just the Born cross section times the real-soft factors. While for the other IEX formulas the phase-space will be integrated basically in the $\mathcal{O}(\alpha^2)_{prag}$, we shall make more effort in the case of the $\mathcal{O}(\alpha^0)_{\rm EEX}$ and do it in the $\mathcal{O}(\alpha^3)_{prag}$, as it is done in Ref. [13]. Let us call the attention of the reader to the fact that we have the matrix element in the $\mathcal{O}(\alpha^0)_{\rm EEX}$ and the phase-space integration is in the $\mathcal{O}(\alpha^2)_{prag}$ or the $\mathcal{O}(\alpha^3)_{prag}$. There is no contradiction in this, as we shall see in the following.

1. Baseline high-precision results for $\mathcal{O}(\alpha^{(0)})_{EEX}$

The complete $\mathcal{O}(\alpha^2)_{prag}$ calculation/exponentiation according to the rules laid down at the beginning of this section will be rather involved; let us therefore illustrate our calculational methods with the simplest possible example. Even this simple example features some non-trivial technical features and we shall therefore present two versions of the calculation.

The basic example discussed in the following is the $\mathcal{O}(\alpha^0)$ initial-state YFS inclusive exponentiation. In the master equation (4) we set the charge of the final fermion to zero, $Q_f=0$, and we replace the sum of $\overline{\beta}$'s with the $\mathcal{O}(\alpha^0)$ version of $\overline{\beta}_0$ that is proportional to the Born differential cross section:

$$\overline{\beta}_0^{(0)}(q_1,q_2)=\frac{2}{\beta_f}\frac{d\sigma^{\rm Born}}{d\Omega}((q_1+q_2)^2,\vartheta),$$
$$\beta_f=[1-4m_f^2/(q_1+q_2)^2]^{1/2}, \tag{163}$$

where the normalization is such that

$$\int \frac{d^3q_1}{q_1^0}\frac{d^3q_2}{q_2^0}\delta^{(4)}(X-q_1-q_2)\overline{\beta}_0^{(0)}(q_1,q_2) = \sigma^{\rm Born}((q_1+q_2)^2). \tag{164}$$

The initial-state $\mathcal{O}(\alpha^0)$ YFS formula reads

$$\sigma_0=\sum_{n=0}^{\infty}\frac{1}{n!}\int\frac{d^3q_1}{q_1^0}\frac{d^3q_2}{q_2^0}\prod_{i=1}^{n}\int\frac{d^3k_i}{k_i^0}\tilde{S}_I(k_i) \times\Theta\left(k_i^0-\frac{1}{2}\varepsilon\sqrt{s}\right)\delta^{(4)}\left(p_1+p_2-q_1-q_2-\sum_j k_j\right) \times\exp[Y_I(\varepsilon)]\overline{\beta}_0^{(0)}((q_1+q_2)^2,\vartheta_0). \tag{165}$$

Integration over the final-state fermion two-body phase-space is done trivially, leading to

$$\sigma_0=\int_0^1 dv\,\sigma^{\rm Born}[s(1-v)]\exp(\delta_{YFS})\rho_0(v), \tag{166}$$

where the essential multiphoton integral

$$\rho_0(v)=\exp(\gamma\ln\varepsilon)\sum_{n=0}^{\infty}\frac{1}{n!}\int\frac{d^3q_1}{q_1^0}\frac{d^3q_2}{q_2^0}\prod_{i=1}^{n}\int_{k_i^0>\varepsilon\sqrt{s}/2} \times\frac{d^3k_i}{k_i^0}\tilde{S}_I(k_i)\,\delta\left(1-v-\frac{1}{s}\left(p_1+p_2-\sum_j k_j\right)^2\right) \tag{167}$$

is the main object of our interest. Note that we have split $Y_I(\varepsilon)=\gamma\ln\varepsilon+\delta_{YFS}$.

In this simplified case, the QED matrix element is totally absent beyond the soft photon integral. The inclusive YFS exponentiation, as defined above, amounts to calculating analytically the multiphoton phase-space integral for $\rho_0(v)$. As explained above, we shall do it in the $\mathcal{O}(\alpha^2)_{prag}$, but we shall keep the proper soft limit undestroyed. Let us note first that in the soft limit $v\to 0$ the function $\rho_0(v)$ coincides with the soft integral of Eq. (163), i.e., $\rho(v)\to f(\gamma,v)$. Since the most singular part in this limit is known, we isolate it and we expect the $\mathcal{O}(\alpha^2)_{prag}$ result to be in the form

$$\rho_0(v)=f(\gamma,v)[1+v\,\gamma f_1(v)], \tag{168}$$

where $f_1(v)$ is nonsingular. How does one find the function $f_1(v)$? Let us inspect the difference

$$d_0(v)=\rho(v)-f(\gamma,v) =\frac{1}{2!}\int\frac{d^3k_1}{k_1^0}\tilde{S}_I(k_1)\int\frac{d^3k_2}{k_2^0}\tilde{S}_I(k_2) \times\left[\delta\left(1-v-\frac{1}{s}\left(p_1+p_2-\sum_j k_j\right)^2\right) -\delta\left(v-\frac{1}{s}(p_1+p_2)\cdot\left(\sum_{i=1}^{n}k_i\right)\right)\right]. \tag{169}$$

This new object has rather interesting properties. First of all, the $\mathcal{O}(\alpha^1)$ integrals cancel exactly and the first nontrivial integral is of $\mathcal{O}(\alpha^2)$. This second-order integral is not, however, IR divergent. According to our general rules we are therefore allowed, without any danger of spoiling the soft limit, to calculate it in the LL approximation.

Let us now present our first of two methods of calculating $\rho_0(v)$. In the LL approximation we replace the collinear singularities in the photon angle $\vartheta_\gamma=0,\pi$ by δ-like peaks

$$\int\frac{d^3k_i}{k_i^0}\tilde{S}_I(k_i) =\frac{\alpha}{2\pi^2}\int_0^1\frac{dx_i}{x_i}\int_{-1}^{1}dc_i\frac{s_i^2}{(1-\beta_e^2c_i^2)^2}\int_0^{2\pi}d\phi_i \to\int_0^1\frac{dx_i}{x_i}\int dc_i\left[\frac{1}{2}\gamma\delta(c_i-1)+\frac{1}{2}\gamma\delta(c_i+1)\right] \tag{170}$$

where

$$\beta_e=(1-4m_e^2/s)^{1/2},\quad c_i=\cos\theta_i,\quad s_i=\sin\theta_i,\quad i=1,2,$$

and using the above LL substitution we get

$$d_0(v)=\lim_{\varepsilon\to 0}\frac{\gamma^2}{4}\int_\varepsilon^1\frac{dx_1}{x_1}\int_\varepsilon^1\frac{dx_2}{x_2}[\,\delta(v-(1-x_1)(1-x_2))-\delta(v-x_1-x_2)]. \tag{171}$$

Two immediate remarks are in order: out of the four terms in the product $[\,\delta(c_1-1)+\delta(c_1+1)][\,\delta(c_2-1)\,\delta(c_2+1)]$ only two contribute, those with two anticollinear photons $c_1=1,c_2=-1$, and $c_1=-1,c_2=1$. The result of the integration depends critically on careful regularization and for this reason we explicitly keep the ε IR regulator. A quick careless calculation gives a zero value for the integral. A very similar phenomenon is present in the calculation of $f(\gamma,v)$, where a naive calculation up to second order gives the $v^{\gamma-1}$ factor only. The remaining $F(\gamma)=1-(\pi^2/12)\gamma^2+\cdots$ factor comes from careful consideration of the $k^0>\varepsilon\sqrt{s}/2$ condition for two photons. With our proper regularization we obtain

$$d_0(v)=-\frac{\gamma^2}{4}\frac{\ln(1-v)}{v}, \tag{172}$$

which is finite in the $v\to 0$ limit.

Now we present the second calculational method, which will often be employed in the following. In this variant we take into account the influence of additional soft photons (in addition to the two hard ones). They do not change the second-order result, but provide the proper IR regulation by replacing the former ε regulator. The LL treatment of the phase-space will be a little different. Starting from Eq. (163) we split (in the CMS frame) the photon integration into its forward and backward hemisphere parts:

$$\int\frac{d^3k}{k^0}=\int_{\theta>\pi/2}\frac{d^3k}{k^0}+\int_{\theta<\pi/2}\frac{d^3k}{k^0}$$

and after changing the summation order we get

$$f(\gamma,v)=\exp(\gamma\ln\varepsilon)\sum_n\sum_{n'}\frac{1}{n!}\frac{1}{n'!}\times\prod_{i=1}^n\int_{\theta_i>\pi/2}\frac{d^3k_i^+}{k_i^{+0}}\tilde S_I(k_i^+)\Theta\left(k_i^{+0}-\varepsilon\sqrt{\frac{s}{2}}\right)\prod_{j=1}^{n'}\int_{\theta_j<\pi/2}\frac{d^3k_j^-}{k_j^{-0}}\tilde S_I(k_j^-)\Theta\left(k_j^{-0}-\varepsilon\sqrt{\frac{s}{2}}\right)\delta\left(v-\frac{2}{s}P\cdot(K^++K^-)\right), \tag{173}$$

where

$$P=p_1+p_2,\quad K^+=\sum_{i=1}^n k_i^+,\quad K^-=\sum_{j=1}^{n'}k_j^-.$$

The above sum of integrals factorizes into two sums. Each of the sums can be evaluated exactly, leading to the following simple convolution

$$f(\gamma,v)=\int dv_+dv_-\,\delta(v-v_--v_+)f\left(\frac{\gamma}{2},v_+\right)f\left(\frac{\gamma}{2},v_-\right). \tag{174}$$

This identity holds for the integration result anyway, but we have also obtained it through the direct phase-space integration. So far all calculations were exact and we only reorganized the phase-space integration, which will be useful in the next step. Let us consider the $d_0(v)$ difference again

$$d_0(v)=\exp(\gamma\ln\varepsilon)\sum_n\sum_{n'}\frac{1}{n!}\frac{1}{n'!}\prod_{i=1}^n\int_{\theta_i>\pi/2}\frac{d^3k_i^+}{k_i^{+0}}\times\tilde S_I(k_i^+)\Theta\left(k_i^{+0}-\varepsilon\sqrt{\frac{s}{2}}\right)\times\prod_{j=1}^{n'}\int_{\theta_j<\pi/2}\frac{d^3k_j^-}{k_j^{-0}}\tilde S_I(k_j^-)\Theta\left(k_j^{-0}-\varepsilon\sqrt{\frac{s}{2}}\right)\times\left[\delta\left(v-1+\frac{1}{s}(P-K^+-K^-)^2\right)-\delta\left(v-\frac{2}{s}P\cdot(K^++K^-)\right)\right]. \tag{175}$$

As before, the whole integral is finite in the $v\to 0$ limit and it gets the first nonzero contribution in the second order. From the previous exercises we know that the essential second-order LL contribution comes from two anticollinear photons—this is why we divided the photon phase-space into two hemispheres. Now, the LL approximation is realized by substituting in the first δ

$$K^{\pm\mu}=(K^{\pm 0},0,0,\pm|K^{\pm 0}|).$$

Note that, contrary to the previous calculation, we did not modify the $\tilde S$ factors, we did not introduce collinear δ's in the photon angular distribution, and we kept an infinite number of photons. In spite of the apparent increase of the complication level, the integral reduces to a nice form

$$f(\gamma,v)=\int dv_+dv_-[\,\delta(v-v_--v_++v_+v_-)-\delta(v-v_--v_+)]f\left(\frac{\gamma}{2},v_+\right)f\left(\frac{\gamma}{2},v_-\right), \tag{176}$$

which is calculable analytically. Neglecting terms $\mathcal{O}(\gamma^3)$ we obtain

$$d_0(v)=-\frac{\exp(-C\gamma)}{\Gamma(1+\gamma)}\gamma v^{\gamma-1}\frac{1}{4}\gamma\ln(1-v). \quad (177)$$

Note that since in the present variant of the calculation we have treated the soft photons in a more friendly way, we recovered the proper soft factor $f(\gamma,v)$ as a factor in the solution.

Summarizing, the $\mathcal{O}(\alpha^2)_{prag}$ phase-space integration result is

$$\rho_0(v)=\frac{\exp(-C\gamma)}{\Gamma(1+\gamma)}\gamma v^{\gamma-1}\left(1-\frac{1}{4}\gamma\ln(1-v)\right), \quad (178)$$

and the corresponding cross section reads

$$\sigma_0(v_{\max})=\exp(\delta_{YFS})\frac{\exp(-C\gamma)}{\Gamma(1+\gamma)}\int_0^{v_{\max}}dv\,\sigma^{\rm Born}[s(1-v)]$$
$$\times\gamma v^{\gamma-1}\left(1-\frac{1}{4}\gamma\ln(1-v)\right). \quad (179)$$

The above integration methods provide us with the $\mathcal{O}(\alpha^2)_{prag}$ phase-space integration result for any of the $\overline{\beta}_0$ contributions as listed in Eq. (9). For example, the contribution from $\overline{\beta}_0^{(2)}$ reads

$$\sigma_0^{(2)}=\int_0^1 dv\,\sigma^{\rm Born}[s(1-v)]\rho_0^{(2)},$$

$$\rho_0^{(2)}=F(\gamma)\exp(\delta_{YFS})\gamma v^{\gamma-1}(1+\delta_I^{(2)})$$
$$\times\left(1-\frac{1}{4}\gamma\ln(1-v)\right). \quad (180)$$

From now on, we shall not restrict ourselves to the $\mathcal{O}(\alpha^0)_{prag}$ EEX matrix elements, but rather consider the complete EEX class $\mathcal{O}(\alpha^2)_{prag}$ matrix elements as defined in Sec. II. The practical significance of the IEX formula of Eq. (180) is rather important. The biggest terms neglected in it are of $\mathcal{O}(\gamma^3)$ and $\mathcal{O}(\alpha\gamma)$, and we expect them to stay below 0.1%. (This will be true provided there are no extra enhancement factors, see the discussion below.) In other words we expect, for the $\overline{\beta}_0^{(2)}$ contribution in the EEX matrix element in Sec. II, that the result of the Monte Carlo phase-space integration will agree with the formula (180) to within about 0.1% for an arbitrary cut $v_{\max}$.

Let us check the above conjecture with a numerical exercise. In the numerical test we shall already include at this moment not only the ISR $\overline{\beta}_0^{(2)}$ contribution of Eq. (180), see also Table I, but also the analogous FSR $\overline{\beta}_0^{(2)}$ contribution, which will be calculated[22] in the next subsection, see Eq. (204) and Table II. We consider the total cross section with the cut on the total photon energy defined by $v_{\max}$ as follows:

$$\sigma^{(2)}_{\overline{\beta}_0^{(2)}\otimes\overline{\beta}_0^{(2)}}=\int_0^{v_{\max}}dv\int_0^{v/(1-u_{\max})}du\,\sigma^f_{\rm Born}$$
$$\times[s(1-u)(1-v)]\rho^{(2)}_{I\overline{\beta}_0^{(2)}}(v)\rho^{(2)}_{F\overline{\beta}_0^{(2)}}(u). \quad (181)$$

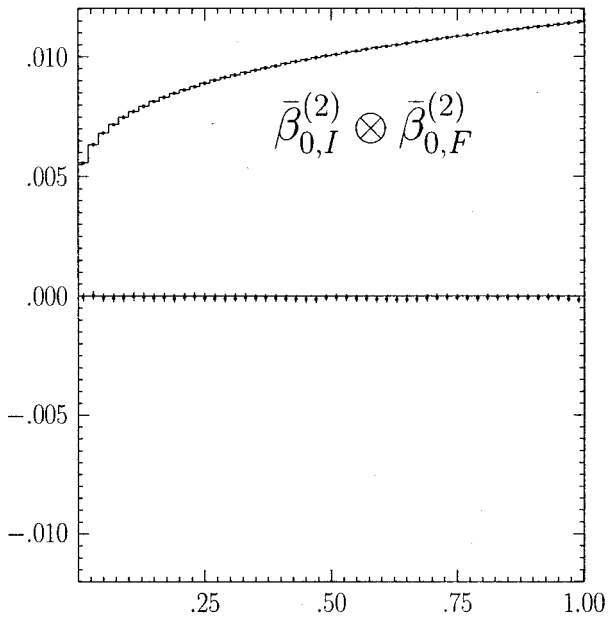

FIG. 10. The comparison between the $\mathcal{KK}$ MC and the $\mathcal{O}(\alpha^2)_{prag}$ IEX formula of Eq. (181) for the constant Born cross section (200 GeV). The difference between the $\mathcal{KK}$ MC in the EEX mode and the semianalytical formula divided by the Born cross section is plotted with a dotted line, as a function of the $v_{\max}$ cutoff on the total energy of all of the ISR and FSR photons. We also include the integrated cross section divided by the Born cross section, and multiplied by a factor of 10^{-2}, as dots for the IEX and a line for the MC.

In order to get a clearer picture about the magnitude of the discrepancy between the EEX MC and the IEX formula we use the artificially flat Born cross-section $\sigma^f_{\rm Born}[s(1-u)(1-v)]\to\sigma^f_{\rm Born}(s)$ in both. The results of the comparison are presented in Fig. 10. Following our expectation, the difference is well below 0.1% for the entire range of the photon energy cutoff $v_{\max}$.

The situation does not look as good when we switch on the s dependence in the Born cross section. In Fig. 11(a) we see the relevant comparison. At the CMS energy of 189 GeV the position of the Z radiative return is at $v=0.75$ and we clearly see a worsening there with respect to the previous case in Fig. 10 where the discrepancy is now almost 0.2% (0.4% in terms of $\sigma_{\rm Born}$). The situation is even more dramatic in the last bin, which corresponds to $v_{\max}=1-4m_\mu^2/s$ and here the discrepancy between the $\mathcal{O}(\alpha^2)_{prag}$ IEX and the $\mathcal{O}(\alpha^2)_{prag}$ MC EEX is -2% of the total cross section, that is -7% in terms of the Born cross section. This is, of

[22]We could present results of the numerical tests (which we have done) for the ISR alone. However, they look very much like the simultaneous ISR and FSR results, so we decided not to present them as figures.

course, due to the Z resonance and $1/s$ behavior of the Born cross section at very low s (especially for the case of the $\mu\bar{\mu}$ channel shown in Fig. 11). In order to be sure that the above effect is not due to some technical problem in the MC integration, we had to improve our IEX formula and upgrade the analytical phase-space integration for the ISR to the level of $\mathcal{O}(\alpha^3)_{prag}$. We show the comparison with the $\mathcal{O}(\alpha^3)_{prag}$ IEX for the same EEX $\mathcal{O}(\alpha^2)_{prag}$ MC in Fig. 11(b). Now the difference is reduced to less than 0.1% everywhere, and in the last bin it is reduced from -2% to $+0.2\%$, as expected. The additional terms of the $\mathcal{O}(L^1\alpha^2)$ and $\mathcal{O}(L^3\alpha^3)$ are shown in Table I at the end of this section. We do not show the details of the phase-space integration that provides these two additional terms. The method is generally rather similar to the one used in this section and in Ref. [13].

2. Beta-bar-one: $\overline{\beta}_1$

In the following step our aim is to calculate analytically the ISR contribution to the total cross section from $\overline{\beta}_{1I}^{(2)}$ as given by

$$\begin{aligned}\sigma=&\sum_{n=0}^{\infty}\frac{1}{n!}\int\frac{d^3q_1}{q_1^0}\frac{d^3q_2}{q_2^0}\int\prod_{j=1}^{n}\frac{d^3k_j}{k_j^0}\tilde{S}_I(p_1,p_2;k_j)[1-\Theta(\Omega_I;k_j)]\exp[Y(\Omega_I)]\\&\times\sum_{j=1}^{n}\overline{\beta}_{1I}^{(2)}(X,p_1,p_2,q_1,q_2,k_j)/\tilde{S}_I(k_j)\,\delta^{(4)}\left(p_1+p_2-q_1-q_2-\sum_{j=1}^{n}k_j\right)\\=&\sum_{n=0}^{\infty}\frac{1}{n!}\int\frac{d^3q_1}{q_1^0}\frac{d^3q_2}{q_2^0}\int\prod_{j=1}^{n}\frac{d^3k_j}{k_j^0}\tilde{S}_I(p_1,p_2;k_j)[1-\Theta(\Omega_I;k_j)]\exp[Y(\Omega_I)]\frac{d^3k}{k^0}\\&\times[1-\Theta(\Omega_I;k)]\delta^{(4)}\left(p_1+p_2-q_1-q_2-k-\sum_{j=1}^{n}k_j\right)\overline{\beta}_{1I}^{(2)}(q_1+q_2,p_1,p_2,q_1,q_2,k).\end{aligned}\tag{182}$$

We start again from the EEX $\mathcal{O}(\alpha^2)_{prag}$ matrix element for the initial-state bremsstrahlung and we shall perform the phase-space integration also in the $\mathcal{O}(\alpha^2)_{prag}$. We integrate first over the final-state fermion four-momenta:

$$\begin{aligned}&\int\frac{d^3q_1}{q_1^0}\frac{d^3q_2}{q_2^0}\delta^{(4)}(p_1+p_2-q_1-q_2-k)\\&\quad\times\overline{\beta}_{1I}^{(2)}(q_1+q_2,p_1,p_2,q_1,q_2,k)\\&=B_1^{(2)}(p_1,p_2,k)\sigma^{\mathrm{Born}}[(q_1+q_2)^2],\end{aligned}\tag{183}$$

where

$$\begin{aligned}B_1^{(2)}(p_1,p_2,k)=&\frac{\alpha}{4\pi^2}\frac{2p_1p_2}{(kp_1)(kp_2)}W_e(\hat{\alpha},\hat{\beta})\\&\times[1+\Delta_I^{(1)}(\hat{\alpha},\hat{\beta})]\frac{1}{2}\{(1-\hat{\alpha})^2+(1-\hat{\beta})^2\}\\&-\tilde{S}_I(p_1,p_2,k)(1+\delta_I^{(1)}),\end{aligned}\tag{184}$$

and obtain

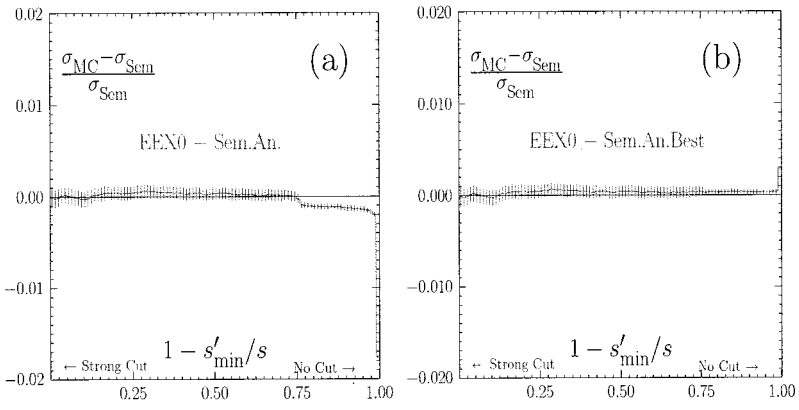

FIG. 11. The comparison between the $\mathcal{KK}$ MC and the IEX $\mathcal{O}(\alpha^2)_{prag}$ formula of Eq. (181) for the s-dependent Born cross section at 189 GeV. The difference between the $\mathcal{KK}$ MC in the EEX mode and the IEX formula divided by the IEX formula is plotted as a function of the $v_{\max}$ cutoff on the total energy of all of the ISR and FSR photons.

$$\sigma=\int_0^1 dv\exp(\delta_{YFS}+\gamma\ln\varepsilon)\sum_{n=0}^{\infty}\frac{1}{n!}\int_{k_j^0>\varepsilon\sqrt{s}/2}\prod_{j=1}^{n}\frac{d^3k_j}{k_j^0}\tilde{S}_I(p_1,p_2;k_j)$$
$$\times\int_{k_j^0>\varepsilon\sqrt{s}/2}\frac{d^3k}{k^0}B_1^{(2)}(p_1,p_2,k)\sigma^{\rm Born}[s(1-v)]\delta\left(v-\frac{1}{s}\left(P-\sum_j k_j-k\right)^2\right)$$
$$\equiv\int_0^1 dv\,\rho_1^{(2)}(v)\sigma^{\rm Born}[s(1-v)]. \tag{185}$$

In the calculation of $\rho_1^{(2)}$ we could follow the first of the methods employed for $\overline{\beta}_0$. Let us describe it briefly, without going into the details of the calculation. We calculate the first two nonzero integrals that are $\mathcal{O}(\alpha)$ and $\mathcal{O}(\alpha^2)$. The first one of $\mathcal{O}(\alpha)$ has to be calculated keeping both the leading $\mathcal{O}(L\alpha)$ and the subleading term $\mathcal{O}(L^0\alpha)$. This can be done following the well-known $\mathcal{O}(\alpha)$ analytical calculations [15]. The $\mathcal{O}(\alpha^2)$ integral with two real photons can be treated in the LL approximation, i.e., keeping only the $\mathcal{O}(L^2\alpha^2)$ terms. This can be done by introducing collinear peaks in the photon angles as demonstrated in the case of $\overline{\beta}_0$. Both integrals are connected due to the infrared regulation with ε. The first one is proportional to $\exp(\gamma\ln\varepsilon)\simeq 1+\gamma\ln\varepsilon$, and the term $\gamma\ln\varepsilon$ from the first one cancels the IR divergence in the second one (independently of the LL approximation). As it is in the case of $\overline{\beta}_0$ one has to pay attention to the subtle ''edge effects'' in the ε regularization.[23]

Let us describe in detail the second method in which the soft photons provide the convenient IR regulation. The main $\mathcal{O}(\alpha)$ contribution comes from the configuration in which we have $k^0\simeq v\sqrt{s}/2$ and one or more soft photons. This part has to be calculated exactly in $\mathcal{O}(\alpha)$. We split, as before,

$$\rho_1^{(2)}(v)=f_1^{(2)}(v)+d_1^{(2)}(v) \tag{186}$$

in such a way that $d_1^{(2)}(v)$ vanishes in $\mathcal{O}(\alpha)$—it can therefore be calculated in the second-order LL while $f_1^{(2)}(v)$ is simple enough to be calculated exactly in the $\mathcal{O}(\alpha)$. We define

$$f_1^{(2)}(v)=\exp(\delta_{YFS})\int\frac{d^3k}{k^0}\exp(\gamma\ln\varepsilon)\sum_{n=0}^{\infty}\frac{1}{n!}\int_{k_j^0>\varepsilon\sqrt{s}/2}\prod_{j=1}^{n}\frac{d^3k_j}{k_j^0}\tilde{S}_I(k_j)\delta\left(v-\frac{2}{s}P\cdot\left(\sum_j k_j+k\right)\right)B_1^{(1)}(p_1,p_2,k)$$
$$=\exp(\delta_{YFS})\int\frac{d^3k}{k^0}f\left(\gamma,v-\frac{2}{s}P\cdot k\right)B_1^{(1)}(p_1,p_2,k), \tag{187}$$

where

$$B_1^{(1)}(p_1,p_2,k)=\frac{\alpha}{4\pi^2}\frac{2p_1p_2}{(kp_1)(kp_2)}W_e(\hat{\alpha},\hat{\beta})\frac{1}{2}\{(1-\hat{\alpha})^2+(1-\hat{\beta})^2\}-\tilde{S}_I(p_1,p_2,k). \tag{188}$$

The remarkable feature of $f_1^{(2)}$ is that we could integrate over the spectator photons exactly. Note that the ε regulator has disappeared from the k integral. In the next step we integrate *exactly* over photon angles following the old $\mathcal{O}(\alpha)$ calculations and we are left with a single integral over the photon energy $x=2k^0/\sqrt{s}$, with the strongest singularity $(v-x)^{\gamma-1}$ being nicely regularized by the soft photons

$$f_1^{(2)}(v)=\exp(\delta_{YFS})F(\gamma)\int_0^v dx\,\gamma(v-x)^{\gamma-1}\gamma\left[-1+\frac{1}{2}x\right]$$
$$=\exp(\delta_{YFS})F(\gamma)\gamma v^{\gamma}\left[-1+\frac{1}{2}v-\frac{1}{2}\gamma v\right]+\mathcal{O}(\gamma^3). \tag{189}$$

Now we shall calculate the remaining part $d_1^{(2)}$ of $\rho_1^{(2)}$. Since it vanishes at $\mathcal{O}(\alpha)$ we may calculate it in the LL approximation. Although it is not strictly necessary, we treat the photons gently (as in the $\overline{\beta}_0$ example), so that we do not use the crude collinear approximation. As before, we split the photon angular integration into the forward and backward hemispheres and we integrate immediately over the final fermion momenta

[23]Generally, the calculation for $\overline{\beta}_1$ is more difficult than for $\overline{\beta}_0$ and $\overline{\beta}_2$, because this is the only case in $\mathcal{O}(\alpha^2)$ where we deal with the simultaneous emission of real and virtual photons.

$$d_1^{(2)}(v)=\exp(\gamma\ln\varepsilon)\sum_n\sum_{n'}\frac{1}{n!}\frac{1}{n'!}2\int_{\theta<\pi/2}\frac{d^3k}{k^0}\exp(\delta_{YFS})\prod_{i=1}^{n}\int_{\theta_i>\pi/2}\frac{d^3k_i^+}{k_i^{+0}}\tilde{S}_I(k_i^+)\Theta\left(k_i^{+0}-\varepsilon\sqrt{\frac{s}{2}}\right)$$
$$\times\prod_{j=1}^{n'}\int_{\theta_j<\pi/2}\frac{d^3k_j^-}{k_j^{-0}}\tilde{S}_I(k_j^-)\Theta\left(k_j^{-0}-\varepsilon\sqrt{\frac{s}{2}}\right)\left\{\left[\delta\left(v-1+\frac{(P-k-K^+-K^-)^2}{s}\right)\right.\right.$$
$$\left.-\delta\left(v-\frac{2P\cdot(k+K^++K^-)}{s}\right)\right]B_1^{(1)}(p_1,p_2,k)+\delta\left(v-1+\frac{1}{s}(P-k-K^+-K^-)^2\right)[B_1^{(2)}(p_1,p_2,k)$$
$$\left.-B_1^{(1)}(p_1,p_2,k)]\right\}. \tag{190}$$

Using the collinear replacement $K^{\pm}=(K^{\pm 0},0,0,\pm|K^{\pm 0}|)$ in δ's allows us to integrate over the spectator multiple photons

$$d_1^{(2)}(v)=\int_0^1dv_+\int_0^1dv_-\int_{\theta<\pi/2}\frac{d^3k}{k^0}\exp(\delta_{YFS})f\left(\frac{\gamma}{2},v_+\right)f\left(\frac{\gamma}{2},v_-\right)\{[\delta(v-1+(1-x-v_+)(1-v_-))$$
$$-\delta(v-x-v_+-v_-)]B_1^{(1)}(p_1,p_2,k)+\delta(v-1+(1-x-v_+)(1-v_-))[B_1^{(2)}(p_1,p_2,k)-B_1^{(1)}(p_1,p_2,k)]\}, \tag{191}$$

where $x=2k^0/\sqrt{s}$ and the other notation is the same as it is in the $\overline{\beta_0}$ case. Integration over the photon angles leads to

$$d_1^{(2)}(v)=\int_0^1dv_+\int_0^1dv_-\int_0^1dx\exp(\delta_{YFS})f\left(\frac{\gamma}{2},v_+\right)f\left(\frac{\gamma}{2},v_-\right)\{[\delta(v-1+(1-x-v_+)(1-v_-))-\delta(v-x-v_+-v_-)]\gamma b_1(x)$$
$$+\delta(v-1+(1-x-v_+)(1-v_-))\gamma^2b_2(x)\},$$
$$b_1(x)=-1+\frac{1}{2}x,\quad b_2(x)=-1+\frac{1}{2}x-\frac{1}{8}[1+(1-x)^2]\frac{\ln(1-x)}{x}. \tag{192}$$

Let us quickly show the calculation of the part proportional to the difference of the δ's, which is somewhat more tricky. We convolute b_1 first with the photons in the same hemisphere and next with the photons from the opposite hemisphere:

$$d_{1A}^{(2)}(v)=\int dVdv_-[\delta(v-1+(1-V)(1-v_-))-\delta(v-V-v_-)]\exp(\delta_{YFS})f\left(\frac{\gamma}{2},v_-\right)$$
$$\times\int dxdv_+\delta(V-x-v_+)f\left(\frac{\gamma}{2},v_+\right)\gamma b_1(x)$$
$$=\exp(\delta_{YFS})F^2\left(\frac{\gamma}{2}\right)\gamma v^{\gamma-1}\int_0^1dyy^{(1/2)\gamma}(1-y)^{(1/2)\gamma-1}\{(1-vy)^{-(1/2)\gamma}-1\}\left[-1+\frac{vy}{2}\left(1-\frac{\gamma}{2}\right)\right]$$
$$=\exp(\delta_{YFS})F(\gamma)\gamma v^{\gamma}\left(-1+\frac{1}{2}v\right)\left(-\frac{1}{2}\gamma\ln(1-v)\right)+\mathcal{O}(\gamma^3). \tag{193}$$

The remaining part of $d_1^{(2)}$ is easier to calculate because it is explicitly of $\mathcal{O}(\gamma^2)$:

$$d_{1B}^{(2)}(v)=\exp(\delta_{YFS})F(\gamma)\gamma v^{\gamma}\gamma\left\{\frac{1}{2}\left(-1+\frac{1}{2}v\right)\right.$$
$$\left.-\frac{1}{8}[1+(1-v)^2]\frac{\ln(1-v)}{v}\right\}+\mathcal{O}(\gamma^3). \tag{194}$$

The contribution from the initial-state $\overline{\beta_1}$ with an $\mathcal{O}(\alpha^2)_{prag}$ QED matrix element and with an $\mathcal{O}(\alpha^2)_{prag}$ analytical integration over the multiphoton phase-space (see Fig. 12) reads

$$\rho_1^{(2)}(v)=\exp(\delta_{YFS})F(\gamma)\gamma v^{\gamma-1}\left\{\frac{1}{2}\left(-1+\frac{1}{2}v\right)\right.$$
$$\left.+\gamma\left[-\frac{1}{2}v-\frac{1}{4}v^2+\frac{1}{8}[-1+3(1-v)^2]\ln(1-v)\right]\right\}$$
$$+\mathcal{O}(\gamma^3). \tag{195}$$

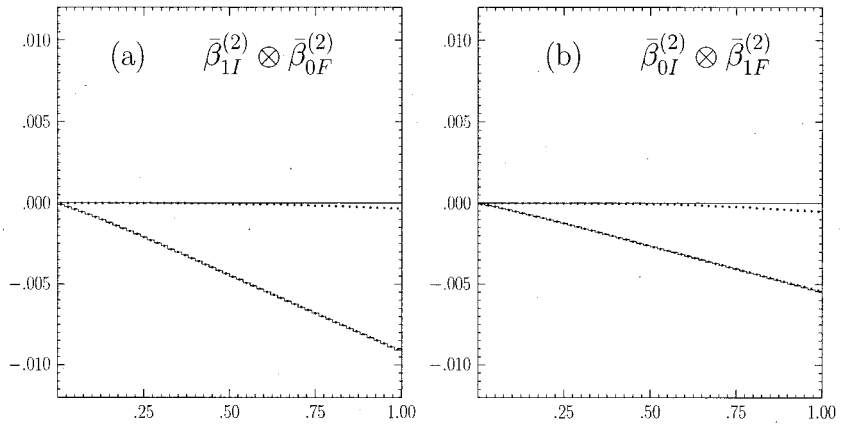

FIG. 12. The comparison between the results of the $\mathcal{KK}$ MC and the IEX $\mathcal{O}(\alpha^2)_{prag}$ formulas for the integrated cross section as a function of the cutoff parameter $v_{\max}$ on the ISR and FSR photons. Presented are the $\mathcal{KK}$ MC (solid line) and the IEX (line with open circles) results for: (a) the ISR $\bar{\beta}_{1I}^{(2)}$ and the FSR $\bar{\beta}_{0F}^{(2)}$, (b) the FSR $\bar{\beta}_{1F}^{(2)}$ and the ISR $\bar{\beta}_{0I}^{(2)}$, multiplied by a factor of 0.1 (in order to fit into the scale). The difference between the $\mathcal{KK}$ MC and the IEX results is shown as a dotted curve. The center-of-mass energy is 189 GeV. The final-state fermion is a muon.

The contribution with an $\mathcal{O}(\alpha^1)_{prag}$ QED matrix element and with an analytical $\mathcal{O}(\alpha^2)_{prag}$ multiphoton phase-space integration is obtained by retaining only $d_{1A}^{(2)}$ and it reads

$$\rho_1^{(1)}(v)=\exp(\delta_{YFS})F(\gamma)\gamma v^{\gamma-1}\left\{\frac{1}{2}\left(-1+\frac{1}{2}v\right)+\gamma\left[-\frac{1}{2}v^2-\frac{1}{2}\left(-1+\frac{1}{2}v\right)\ln(1-v)\right]\right\}+\mathcal{O}(\gamma^3). \tag{196}$$

3. Beta-bar-two: $\bar{\beta}_2$

In the following step, our aim is to calculate analytically the contribution to the total cross section from $\bar{\beta}_{2I}^{(2)}$ as given by

$$\sigma_2=\sum_{n=0}^{\infty}\frac{1}{n!}\int\frac{d^3q_1}{q_1^0}\frac{d^3q_2}{q_2^0}\int\prod_{j=1}^{n}\frac{d^3k_j}{k_j^0}\tilde{S}_I(p_1,p_2;k_j)\times[1-\Theta(\Omega_I;k_j)]\exp[Y(\Omega_I)]\times\sum_{n\geqslant j>k\geqslant 1}\frac{\bar{\beta}_{2II}^{(2)}(X,p_1,p_2,q_1,q_2,k_j,k_k)}{\tilde{S}_I(k_j)\tilde{S}_I(k_k)}\delta^{(4)}\times\left(p_1+p_2-q_1-q_2-\sum_{j=1}^{n}k_j\right). \tag{197}$$

This contribution is in a sense more trivial than the previous two: since it is pure $\mathcal{O}(\alpha^2)$, it has no IR singularity in the two-photon phase-space integral.

We can calculate the contribution from $\bar{\beta}_2$ with the same methods as in the case of $\bar{\beta}_0$ or $\bar{\beta}_1$. The integral is reorganized easily such that the integration over the photon mo-

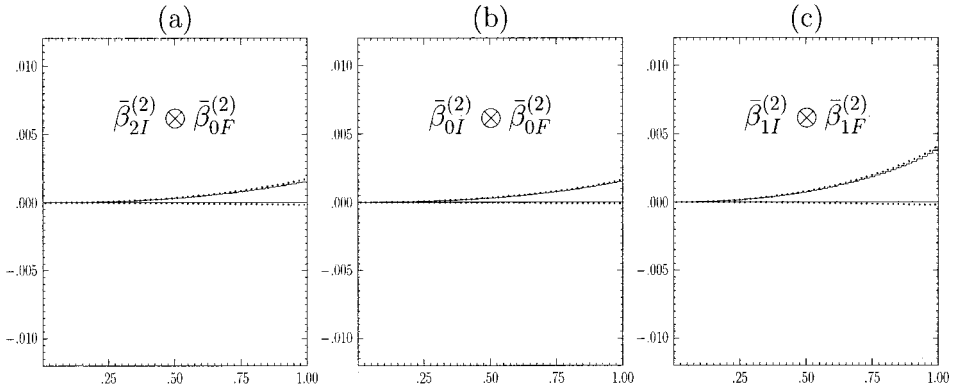

FIG. 13. The comparison between the $\mathcal{KK}$ MC and the IEX $\mathcal{O}(\alpha^2)_{prag}$ formulas for the integrated cross section as a function of the cutoff parameter $v_{\max}$ on the ISR and FSR photons. Presented are the $\mathcal{KK}$ MC (solid line) and IEX (line with open circles) results for: (a) the ISR $\bar{\beta}_{2I}^{(2)}$ and the FSR $\bar{\beta}_{0F}^{(2)}$, (b) the FSR $\bar{\beta}_{2F}^{(2)}$ and the ISR $\bar{\beta}_{0I}^{(2)}$ (c) the ISR $\bar{\beta}_{1I}^{(2)}$ and the FSR $\bar{\beta}_{1F}^{(2)}$. The difference between the $\mathcal{KK}$ MC and the IEX results is also included (dots). The center-of-mass energy is 189 GeV. The final-state fermion is a muon.

menta in the $\overline{\beta}_{2II}^{(2)}$ is isolated and we are able to integrate over final-state fermion momenta, bringing the integral to the standard form

$$\sigma_2 = \int_0^1 dv\, \rho_2^{(2)}(v)\, \sigma^{\mathrm{Born}}[s(1-v)]. \tag{198}$$

The function $\rho_2^{(2)}(v)$ can be calculated in the LL approximation with either of our two methods (keeping an additional spectator photon or not); after integration over the photon angles, the integral boils down to the following integral over the longitudinal photon momenta, separately for the cases with two collinear and two anticollinear photons

$$\begin{aligned}
\rho_2^{(2)}(v) = & \int_0^1 dv_- dv_+ \frac{\gamma^2}{4} \delta(v - v_+ - v_-) \left[\frac{1}{2v_+v_-} \chi(v_+) \chi\left(\frac{v_-}{1-v_+} \right) + \frac{1}{2v_+v_-} \chi(v_-) \chi\left(\frac{v_+}{1-v_-} \right) \right. \\
& \left. - \frac{1}{v_+} \omega(v_-) - \frac{1}{v_-} \omega(v_+) - \frac{1}{v_+v_-} \right] + \int_0^1 dv_- dv_+ \frac{\gamma^2}{4} \delta[v - 1 + (1-v_+)(1-v_-)] \\
& \times \left[\frac{1}{v_+v_-} \chi(v_+) \chi(v_-) - \frac{1}{v_+} \omega(v_-) - \frac{1}{v_-} \omega(v_+) - \frac{1}{v_+v_-} \right] \\
= & \gamma^2 \frac{1}{4} v,
\end{aligned} \tag{199}$$

where $\chi(x) = [1 + (1-x)^2]/2$ and $\omega(x) = -1 + x/2$.

Eventually, by keeping the additional soft photons in the calculation, we obtain our final result for the initial-state $\mathcal{O}(\alpha^2)_{prag}$ contribution from $\overline{\beta}_2$ in a more elegant form

$$\rho_2^{(2)}(v) = \exp(\delta_{YFS}) F(\gamma)\, \gamma v^{\gamma - 1} \left\{ \frac{1}{4} \gamma v^2 \right\} + \mathcal{O}(\gamma^3). \tag{200}$$

We have compared numerically the above formula with the $\mathcal{KK}$ MC in the case that the FSR is switched off and have found an agreement to better than 0.1%. In Fig. 13(a) we present the comparison in which, as it is in the case of the previous $\overline{\beta}$'s, the FSR is switched on. In Fig. 13(a) we compare the convolution of the ISR $\overline{\beta}_{2I}^{(2)}$ and the FSR $\overline{\beta}_{0F}^{(2)}$:

$$\begin{aligned}
\sigma^{(2)}_{\overline{\beta}_2^{(2)} \otimes \overline{\beta}_0^{(2)}} = & \int_0^{v_{\max}} dv \int_0^{v/(1-u_{\max})} du\, \sigma^f_{\mathrm{Born}}[s(1-u) \\
& \times (1-v)] \rho^{(2)}_{I\overline{\beta}_2^{(2)}}(v)\, \rho^{(2)}_{F\overline{\beta}_0^{(2)}}(u).
\end{aligned} \tag{201}$$

The above IEX result is compared with the $\mathcal{KK}$ MC results, and they agree within 0.2%. In Fig. 13(b) we show the analogous comparison for the convolution of the FSR $\overline{\beta}_{2F}^{(2)}$ and the ISR $\overline{\beta}_{0I}^{(2)}$ (anticipating the IEX results for FSR $\overline{\beta}_{2F}^{(2)}$ to be found in the next section) and we find a similar agreement. Finally, there is another, more trivial contribution in the $\overline{\beta}^{(2)}$ family, which corresponds to the case with one real photon emitted in the initial state and one real photon emitted in the final state. This case does not require a separate analytical phase-space integration effort, because the relevant IEX formula involves the convolution of the already known expression for the ISR $\overline{\beta}_{1I}^{(2)}$ and the FSR $\overline{\beta}_{1F}^{(2)}$. The corresponding numerical comparison of the IEX formula and the EEX MC is shown in Fig. 13(c). In fact the IEX matrix element was deliberately constructed in such a way (factorizing virtual corrections) that it results in the above convolution-type IEX formula.

4. Summary on IEX for ISR

The entire initial-state $\mathcal{O}(\alpha^2)_{prag}$-integrated cross section is obtained by combining the contributions from all of the three $\overline{\beta}$'s, and it reads

$$\begin{aligned}
\sigma_I^{(2)} = & \int_0^1 dv\, \rho_I^{(2)}(v)\, \sigma^{\mathrm{Born}}[s(1-v)], \\
\rho_I^{(2)}(v) = & \exp(\delta_{YFS}) F(\gamma)\, \gamma v^{\gamma - 1} \left\{ 1 + \frac{\gamma}{2} + \frac{\gamma^2}{8} \right. \\
& + v\left(-1 + \frac{1}{2} \right) \\
& \left. + \gamma \left[-\frac{v}{2} - \frac{1 + 3(1-v)^2}{8} \ln(1-v) \right] \right\} \\
& + \mathcal{O}(\gamma^3) + \mathcal{O}(\gamma\alpha).
\end{aligned} \tag{202}$$

This ISR formula has been obtained as a result of the *ad hoc* exponentiation (interpolation) in Ref. [7] and was used there as a numerical parametrization/test of the cross section from the Monte Carlo program YFS2. It is now *derived* starting

TABLE I. Contributions to the function $\rho_I(v)=d_S+\Delta_H(v)$ from $\overline{\beta}_k, k=0,1,2$. The ISR matrix element is at $\mathcal{O}(\alpha^r)_{prag}$ with YFS/EEX exponentiation, $r=0,1,2$, as marked in the first column. The phase-space integration is done analytically always within $\mathcal{O}(\alpha^2)_{prag}$, except for the $\mathcal{O}(\alpha^0)_{prag}$ case in the first row, where the phase-space integration is done in $\mathcal{O}(\alpha^3)_{prag}$.

		d_S	$\Delta_H(v)$
$\mathcal{O}(\alpha^0)$	$\overline{\beta}_0$	1	$-\frac{1}{4}\gamma\ln(1-v)-\frac{1}{2}\frac{\alpha}{\pi}\ln^2(1-v)+0\gamma^2$
$\mathcal{O}(\alpha^1)$	$\overline{\beta}_0$	$1+\frac{\gamma}{2}$	$-\frac{1}{4}\gamma\ln(1-v)$
	$\overline{\beta}_1$	0	$v\left(-1+\frac{v}{2}\right)+\gamma\left[-\frac{v^2}{2}-\frac{v(2-v)}{4}\ln(1-v)\right]$
	All	$1+\frac{\gamma}{2}$	$v\left(-1+\frac{v}{2}\right)+\gamma\left[-\frac{v^2}{2}-\frac{(1-v)^2}{4}\ln(1-v)\right]$
$\mathcal{O}(\alpha^2)$	$\overline{\beta}_0$	$1+\frac{\gamma}{2}+\frac{\gamma^2}{8}$	$-\frac{1}{4}\gamma\ln(1-v)$
	$\overline{\beta}_1$	0	$v\left(-1+\frac{v}{2}\right)+\gamma\left[-\frac{v}{2}-\frac{v^2}{4}-\frac{-1+3(1-v)^2}{8}\ln(1-v)\right]$
	$\overline{\beta}_2$	0	$+\gamma\frac{v^2}{4}$
	All	$1+\frac{\gamma}{2}+\frac{\gamma^2}{8}$	$v\left(-1+\frac{v}{2}\right)+\gamma\left[-\frac{v}{2}-\frac{1+3(1-v)^2}{4}\ln(1-v)\right]$
$\mathcal{O}(\alpha^2)-\mathcal{O}(\alpha^1)$		$\frac{\gamma^2}{8}$	$+\gamma\left[-\frac{1+(1-v)^2}{8}\ln(1-v)\right]$

from YFS exclusive exponentiation by means of direct phase-space integration.[24]

Summarizing our IEX calculations for the ISR, we have obtained through the analytical integration over the ISR multiphoton phase-space the inclusive exponentiated cross section for the IEX matrix elements in the $\mathcal{O}(\alpha^0)_{prag}$, $\mathcal{O}(\alpha^1)_{prag}$, and $\mathcal{O}(\alpha^2)_{prag}$ for each $\overline{\beta}_i$, $(i=0,1,2)$ separately. The phase-space integration was always done analytically within the $\mathcal{O}(\alpha^2)_{prag}$. All results from the above extensive study are summarized in Table I, where we have listed the two functions d_S and $\Delta_H(v)$ in the following formula (the notation is recalled for the convenience of the reader):

$$\sigma_I=\int_0^1 dv\,\rho_I(v)\,\sigma^{\rm Born}[s(1-v)], \tag{203}$$

$$\rho_I(v)=\exp(\delta_{YFS})F(\gamma)\,\gamma v^{\gamma-1}[d_S+\Delta_H(v)],$$

$$\delta_{YFS}=\frac{\gamma}{4}+\frac{\alpha}{\pi}\left(-\frac{1}{2}+\frac{\pi^2}{3}\right),$$

$$\gamma=2\frac{\alpha}{\pi}\left(\ln\frac{s}{m_e^2}-1\right),\quad F(\gamma)=\frac{\exp(-C\gamma)}{\Gamma(1+\gamma)}.$$

C. Semianalytical formulas for FSR

The calculation of the $\mathcal{O}(\alpha^2)_{prag}$ IEX formula for the FSR, with the $u_{\max}$ cutoff, that is $u=1-s'/s<u_{\max}$, is quite similar to that in the ISR case and we do not enter into the details. We only discuss the basic differences between the ISR and FSR cases and present the final result.

If we switch off the ISR completely, then the FSR-integrated cross section for the $\mathcal{O}(\alpha^r)_{prag}$, $r=0,1,2$, EEX matrix element reads

$$\sigma_F(u_{\max})=\sigma_{\rm Born}\int_0^{u_{\max}} du\,\rho_F(u),$$

$$\rho_F(u)=\exp(\delta_{YFS})F(\gamma_f)\,\gamma_f u^{\gamma_f-1}[d'_S+\Delta'_H(u)],$$

[24] *Ad hoc* exponentiation is of course easier to do and, in Ref. [44], even the $\mathcal{O}(\alpha^3)_{prag}$ formula for the initial-state bremsstrahlung was given, but the derivation method presented here is much better founded and the result does not depend on any kind of interpolation or guesswork.

TABLE II. Contributions to the function $\rho_F(u)=d'_S+\Delta'_H(u)$ from $\overline{\beta}_k, k=0,1,2$. The FSR matrix element is at $\mathcal{O}(\alpha^r)_{prag}$ with YFS/EEX exponentiation, $r=0,1,2$, as marked in the first column. The phase-space integration is done analytically, always in $\mathcal{O}(\alpha^2)_{prag}$.

		d'_S	$\Delta'_H(u)$
$\mathcal{O}(\alpha^0)$	$\overline{\beta}_0$	1	$-\frac{1}{4}\gamma_f\ln(1-u)$
$\mathcal{O}(\alpha^1)$	$\overline{\beta}_0$	$1+\frac{\gamma_f}{2}$	$-\frac{1}{4}\gamma_f\ln(1-u)$
	$\overline{\beta}_1$	0	$u\left(-1+\frac{u}{2}\right)+\gamma_f\left[-\frac{u^2}{2}+\frac{u(2-u)}{2}\ln(1-u)\right]$
	All	$1+\frac{\gamma_f}{2}$	$u\left(-1+\frac{u}{2}\right)+\gamma_f\left[-\frac{u^2}{2}+\frac{-1+4u-2u^2}{4}\ln(1-v)\right]$
$\mathcal{O}(\alpha^2)$	$\overline{\beta}_0$	$1+\frac{\gamma_f}{2}+\frac{\gamma_f^2}{8}$	$-\frac{1}{4}\gamma_f\ln(1-u)$
	$\overline{\beta}_1$	0	$u\left(-1+\frac{u}{2}\right)+\gamma_f\left[-\frac{u}{2}-\frac{u^2}{4}+\frac{2+6u-3u^2}{8}\ln(1-u)\right]$
	$\overline{\beta}_2$	0	$+\gamma_f\left(\frac{u^2}{4}-\frac{u(2-u)}{4}\ln(1-u)\right)$
	All	$1+\frac{\gamma_f}{2}+\frac{\gamma_f^2}{8}$	$u\left(-1+\frac{u}{2}\right)+\gamma_f\left[-\frac{u}{2}+\frac{u(2-u)}{8}\ln(1-u)\right]$
$\mathcal{O}(\alpha^2)-\mathcal{O}(\alpha^1)$		$\frac{\gamma_f^2}{8}$	$+\gamma_f\left[\frac{2-6u+3u^2}{8}\ln(1-u)\right]$

$$\delta'_{YFS}=\frac{\gamma_f}{4}-\frac{1}{2}\gamma_f\ln(1-u)+\frac{\alpha}{\pi}\left(-\frac{1}{2}+\frac{\pi^2}{3}\right),$$

$$\gamma_f=2\frac{\alpha}{\pi}\left(\ln\frac{s}{m_f^2}-1\right), \tag{204}$$

where the functions d'_S and $\Delta'_H(u)$, obtained with an analytical integration of the phase-space using the $\mathcal{O}(\alpha^2)_{prag}$ approximation, are listed in Table II.

The main difference and complication in the phase-space analytical integration with respect to the case of ISR are that the YFS form factor δ'_{YFS} depends in the case of the FSR on the integration variable u. This is why the terms of $\mathcal{O}(L^2\alpha^2)$ are different in the two cases. In Table II we show separately the contributions from each $\overline{\beta}$. Note that in the case of the FSR we did not integrate the phase-space for $\overline{\beta}_0$ at the $\mathcal{O}(\alpha^3)_{prag}$ analytically, as we did in the case of the ISR. (It was not necessary in order to reach the precision level of 0.2%.) We have checked numerically the agreement of the $\mathcal{KK}$ MC with Eq. (204) separately for each type of $\overline{\beta}$, with the ISR switched off (plots are not shown). We have already presented, in this section, the complete set of numerical results in the case that the ISR is switched off for each combination of the ISR and FSR $\overline{\beta}$'s.

D. Semianalytical IEX for ISR and FSR

The last numerical test, which we show in Fig. 14, is the case in which we switch on all of the ISR and FSR $\overline{\beta}$'s listed in both Tables I and II:

$$\sigma_{\rm tot}=\int_0^{v_{\max}}dv\int_0^{v/(1-u_{\max})}du \times\sigma^f_{\rm Born}[s(1-u)(1-v)]\rho_F(u)\rho_I(v). \tag{205}$$

It is done for the constant Born cross section, the case with the variable cross section will be shown in the next section. We use the IEX formula of the pure $\mathcal{O}(\alpha^2)_{prag}$ type [without $\mathcal{O}(\alpha^3)_{prag}$ improvements for the ISR]. The overall agreement between the IEX formula and the $\mathcal{KK}$ MC is within the advertized 0.2%. When looking into all previous figures in this and the previous subsection, it is interesting to note that this difference does not come from one particular combination of the ISR and FSR $\overline{\beta}$'s, but from several of them.

The reader may wonder why we elaborate so much in this section on the IEX semi-analytical formula, which is related

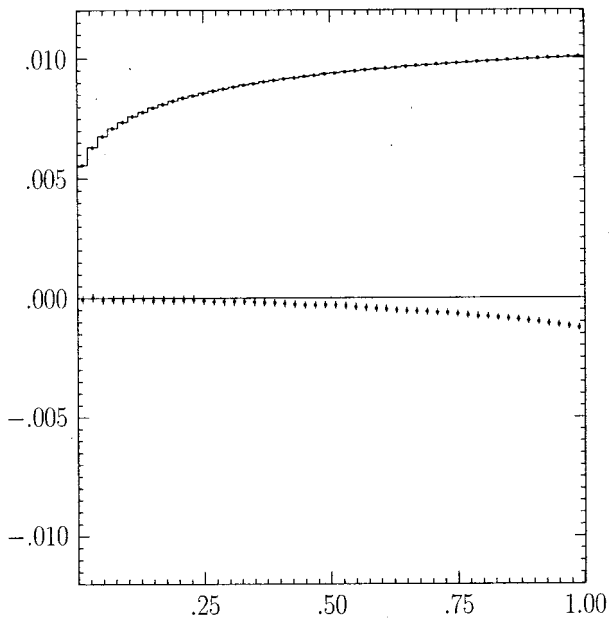

FIG. 14. The comparison between the $\mathcal{KK}$ MC and the IEX $\mathcal{O}(\alpha^2)_{prag}$ formula. The difference between the $\mathcal{KK}$ MC in EEX mode and the IEX formula divided by the Born cross section is plotted with the dotted line, as a function of the cutoff $v_{\max}$ on the total energy of the ISR and FSR photons. Included also is $10^{-2}\times\sigma(v_{\max})/\sigma_{\mathrm{Born}}$, as the dotted line for the IEX formula and the solid line for the MC.

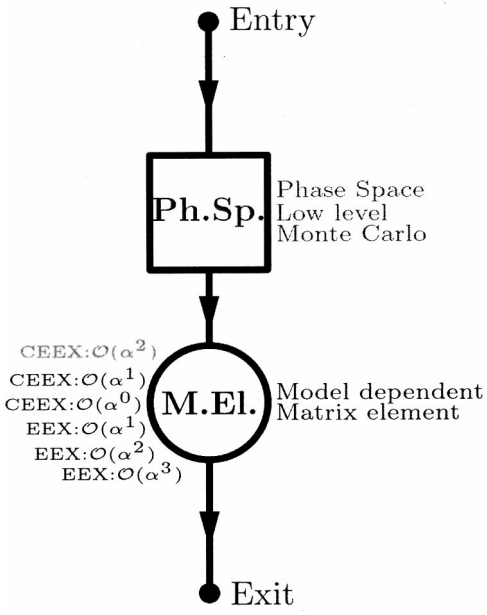

FIG. 15. General structure of the $\mathcal{KK}$ Monte Carlo program.

to the EEX type of matrix element in the $\mathcal{KK}$ MC if in fact the main matrix element in the $\mathcal{KK}$ MC is now CEEX. One reason is that historically the EEX was the first available example of exclusive exponentiation, and the IEX semianalytical formula was developed in parallel, providing a valuable cross-check of the MC. Another reason is that at this stage, as we shall see in the next section, both the IEX and the EEX provide a reference calculation and valuable test for the CEEX. The precision of the present $\mathcal{O}(\alpha^2)_{prag}$ IEX is limited, but it could be improved to the full $\mathcal{O}(\alpha^3)_{prag}$ if necessary. A more important limitation in the present $\mathcal{O}(\alpha^2)_{prag}$ IEX as a test of the CEEX model is the absence of the ISR⊗FSR interference. We believe that this effect can be included in the semianalytical IEX if necessary.[25] The *ad hoc* variant of the $\mathcal{O}(\alpha^1)$ exponentiation, including the ISR⊗FSR interference, is already available in Refs. [22,23].

VI. NUMERICAL RESULTS AND TESTS

In this section we shall mainly present the numerical results from the $\mathcal{KK}$ MC in which the standard model amplitudes for the process $e^-e^+\to f\bar{f}+n\gamma$ of the Secs. II (EEX) and III (CEEX) are implemented. The analytical results of Sec. V will also be exploited to obtain numerical results from the semianalytical program $\mathcal{KK}$sem. These results are mainly for the $\mu^-\mu^+$ final state. For more results on the quark final states and other interesting numerical results from the $\mathcal{KK}$ MC we refer the reader to the forthcoming proceedings of the LEP2 Monte Carlo Workshop [45].

The general structure of the $\mathcal{KK}$MC code is depicted in Fig. 15. The program is divided into two distinct parts (levels): (a) the phase-space Monte Carlo integration engine with common-importance sampling for the entire family of QED distributions (EEX and CEEX); (b) the collection (library) of programs for the SM/QED spin amplitudes and differential distributions, at various orders, with various styles of exponentiation. In this work we do not enter into a description of the MC integration algorithm in the universal MC integration engine. The Monte Carlo method of phase-space integration is fully documented (for the first time) in Ref. [1], and some aspects of the phase-space parametrization are documented in the forthcoming Ref. [46]. Here we regard this low-level MC program as a black box, capable to integrate the phase-space exactly (up to a statistical error).

Life, however, is not that simple, and a numerical program, which ''in principle'' is doing something ''exactly/rigorously,'' may still give imprecise results because of programming bugs and numerical instabilities, especially when they are in a program as complicated as the $\mathcal{KK}$ MC is. This is why we always introduce the concept of the *technical precision* of a given program/calculation (see below). The basic aim of the numerical exercises we present in this section is the determination of the total *theoretical precision* associated with our calculation of standard model predictions for experimental observables (although we limit the discussion to the QED part of the SM for most of our discussion). As far as observables are concerned, we shall concentrate mainly on the total cross section and charge asymmetry at LEP1, LEP2, and linear collider energies.

What are the technical and physical precisions? We define

[25]See the following section for a simple semianalytical formula for the ISR⊗FSR interference in the soft limit.

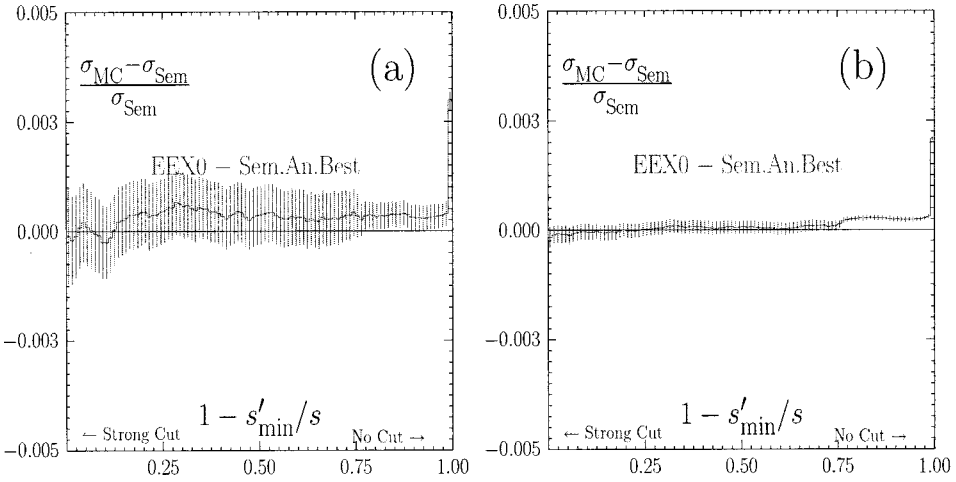

FIG. 16. Evaluation of the technical precision of the $\mathcal{KK}$ Monte Carlo using a simplified QED multiphoton distribution. The difference of the $\mathcal{KK}$ MC result and semianalytical result divided by the semianalytical result is plotted as a function of $v_{\max}=1-s'_{\min}/s$. Results are shown for the $\mu^+\mu^-$ final state at $\sqrt{s}=189$ GeV. In case (a) the phase-space limit $v_{\max}=1-4m_\mu^2/s$ is taken; the last bin represents the entire phase-space. In case (b) $v_{\max}=0.999$.

the *technical precision* as the total uncertainty related to pure numerical problems such as programming bugs, numerical instabilities, numerical approximation, etc. In our case the question of the technical precision will mainly concern the MC integration engine. It is important to determine it at an early stage of the work and it should be generally much better than the physical precision. On the other hand, the physical precision is the total uncertainty related to the neglected higher orders in the coupling constant α or in other expansion parameters such as the inverse of the big-log $1/L$, or the ratio of the width to the mass Γ/M for a narrow resonance. For the physical precision we note that the above truncations are done in the spin amplitudes and/or the differential cross section. If some of them are done in the phase-space integration, we tend to associate them with the technical precision (as phase-space integration is a technical problem).

We start this section with the basic discussion of the technical precision; we then proceed to a subsection elaborating on the physical precision for the EEX matrix element, based on the comparisons between the $\mathcal{KK}$ MC and semianalytical results; later, we discuss the physical precision for the case of the full CEEX matrix element. In this section we also present numerical results and a rather complete discussion of the effects due to the ISR-FSR interference in the fermion-pair production process.

We note that it would be good to include also more numerical tests at lower energies, ~ 10 GeV, and at very high energies ~ 1 TeV, and some more tests specific to spin effects. However, the basic pattern of the spin correlations in the double τ decay was already cross-checked in Ref. [2].

A. Basic test of the technical precision

The best way to determine the technical precision is to compare the results of two or even more independent calculations that implement the same physics model but differ in the technical details of the actual implementation like the method of phase-space integration, independent coding, etc. The two best possible methods are (a) to compare two independent Monte Carlo calculations or (b) to compare Monte Carlo results with results of a semi-analytical calculation. Method (a) is generally better, because it can be done for arbitrary kinematical selections (cuts) and for the simplified QED matrix element, while method (b) is limited to a simple or absent kinematical selection. In the following we shall use method (b).

For our basic test of the technical precision we use the simplest possible variant of the QED model, that is of the type $\mathcal{O}(\alpha^0)_{\rm EEX}$ defined in Sec. II. For this type of QED matrix element we were able to integrate analytically the total cross section in Sec. V. The relevant formula can be read from the first row in Tables I and II. For the sake of completeness we write down the complete expression explicitly:

$$\sigma^f_{\rm SAN}=\int_0^{v_{\max}} dv\,\sigma^f_{\rm Born}[s(1-u)(1-v)]\rho_I^{(0)}(v)\rho_F^{(0)}(u),$$

$$\rho_I^{(0)}(v)=F(\gamma_e)\exp\left[\frac{1}{4}\gamma_e+\frac{\alpha}{\pi}\left(-\frac{1}{2}+\frac{\pi^2}{3}\right)\right]\gamma_e v^{\gamma_e-1}\times\left(1-\frac{1}{4}\gamma_e\ln(1-v)-\frac{1}{2}\frac{\alpha}{\pi}\ln^2(1-v)+0\ \gamma_e^2\right), \tag{206}$$

$$\rho_F^{(0)}(u)=F(\gamma_f)\exp\left[\frac{1}{4}\gamma_f-\frac{1}{2}\gamma_f\ln(1-u)+\frac{\alpha}{\pi}\left(-\frac{1}{2}+\frac{\pi^2}{3}\right)\right]\gamma_f u^{\gamma_f-1}\left(1-\frac{1}{4}\gamma_f\ln(1-u)\right).$$

As we remember the coefficient in front of the $\mathcal{O}(L^3\alpha^3)$ term is zero, as marked explicitly. It was essential to calculate analytically and introduce the ISR term of $\mathcal{O}(L^1\alpha^2)$ because it amounts numerically to several percent for the cross section located close to $v=1$.

In Fig. 16 we present the comparison of the $\mathcal{KK}$ MC with the semianalytical formula of Eq. (206). The difference between the MC result and the semianalytical result is divided by the semianalytical result and, as we see, the difference is remarkably small. The comparison is done for the $\mu^+\mu^-$

final state at $\sqrt{s}=189$ GeV, as a function of $v_{\max}$. In the last point (bin) the entire phase-space is covered, $v_{\max}=1-4m_\mu^2/s$.

The conclusion from the above exercise is that we control the phase-space integration at the level of 2×10^{-4} for $v_{\max}<0.999$, including the Z radiative return, and at the level of 3×10^{-3} for no cuts at all.

The possible loophole in this estimate of the precision is that it may break down when we cut on the transverse momenta of the real photons, or switch to a more sophisticated QED model. The second circumstance is very unlikely as the phase-space and the actual SM model matrix element are split into completely separate modules in the program. The question of cuts on the transverse momenta of the real photons requires further discussion. Here, it has to be stressed that in our MC the so-called big-logarithm

$$L=\ln\left(\frac{s}{m_f^2}\right)-1 \tag{207}$$

is the *result of the phase-space integration* and if this integration were not correct then we would witness the breakdown of the IR singularity cancellation and the fermion mass singularity cancellation for the FSR. We do not see anything like that at the 0.02% precision level. In addition there is a wealth of comparisons with many *independent codes* of the phase-space integration for $n_\gamma=1,2,3$ real photons, with and without cuts on the photon p_T. It should be remembered that the multiphoton phase-space integration module/code in the $\mathcal{KK}$ MC has been unchanged for the last 10 years. For the ISR it is based on the YFS2 algorithm of Ref. [7] and for the FSR on the YFS3 algorithm of Ref. [9]; these modules/codes were part of the KORALZ [10] multiphoton MC from the very beginning, already at the time of the LEP1 1989 workshop [40], and they were continuously tested since then. The phase-space integration for $n_\gamma=1$ was tested very early by the authors of YFS2/YFS3 against the older MC programs MUSTRAAL [16] and KORALB [35] and with analytical calculations, at the precision level of $<0.1\%$, with and without cuts on the photon p_T. The phase-space integration for $n_\gamma=2,3$ with cuts on the photon p_T was tested very many times over the years by the authors of YFS2/YFS3/KORALZ, and independently by all four LEP Collaborations, using other integration programs such as COMPHEP, GRACE [61,62] and others, in the context of the search of the anomalous 2γ and 3γ events. Another important series of tests was done in Ref. [47] for the ISR $n_\gamma=1,2$ photons (with cuts sensitive to the p_T of the photons), comparing KORALZ/YFS2 with the other independent MC's for the $\nu\bar{\nu}\gamma(\gamma)$ final states. Typically, these tests, in which the QED matrix element was programmed in several independent ways, showed agreement at the level of 10% for the cross section for $n_\gamma=2$, which was of the order of 0.1% of the Born cross section, or 0.2–0.5 % for $n_\gamma=1$, which was of the order of 1% of the Born cross section, so they never invalidated our present technical precision of 0.02% in terms of the Born cross section (or the total cross section in terms of the Z-inclusive cut).

We therefore conclude that the technical precision of the $\mathcal{KK}$ MC due to the phase-space integration is 0.02% of the integrated cross section, for any cuts on the photon energies, Z inclusive and Z exclusive, stronger than[26] $M_{inv}(f\bar{f})>0.1\sqrt{s}$ and any mild cut on the transverse photon energies due to any typical realistic experimental cuts. For the cross sections with a single photon tagged, it is about 0.2–0.5 % and with two photons tagged it is $\sim10\%$ of the corresponding integrated cross section. These conclusions are based on the comparisons with at least six other independent codes.

B. Physical precision, the case of EEX

We now start the presentation of the numerical results from the $\mathcal{KK}$ MC run in the EEX mode with the semianalytical calculations based on the results in Sec. V. Note that the EEX matrix element of Sec. II is very similar to (basically the same as) the one implemented since many years in the KORALZ program [10]. We do this for two reasons: (a) these tests were historically the first (they existed, unpublished, for many years, giving us confidence that the KORALZ/YFS3 program provides correct results) and (b) they are now still useful as a reference calculation for the newer CEEX scheme. They will also allow us to introduce some notations and to introduce gradually the reader to the subject of the discussion on the theoretical precision of our results. Of course, we shall remember that in the case of the EEX we do not include the ISR-FSR interferences (IFI).

In Fig. 17 we show the dependence of the total cross section on the cut on the total photon energy (ISR+FSR). The comparison is done for the $\mu^+\mu^-$ final state at $\sqrt{s}=189$ GeV, as a function of $v_{\max}$. In the last point (bin) the *entire phase-space* is covered, i.e., $v_{\max}=1-4m_\mu^2/s$. The very striking (and well-known) phenomenon is that the total cross section due to the huge ISR correction is almost three times the Born cross section, in the absence of any kinematical cuts. Part of this ISR contribution is located close to $v=1$, $s'\sim4m_\mu^2/s$; let us call it the $\gamma\gamma^*$ process. This amounts to as much as the Born cross section itself, $\sigma_{\gamma\gamma^*}\sim\sigma_{\rm Born}$, while the dominant part of the cross section $\sigma_{\rm ZRR}\sim2\sigma_{\rm Born}$ is concentrated close to $v=1-M_Z^2/s\sim0.75$, and is associated with the so-called ''Z radiative return'' (ZRR) process, that is the resonant production of the Z, after the emission of a rather hard ISR photon, which is usually lost in the beam pipe. In the experiment the $\gamma\gamma^*$ process is almost always eliminated from the data, and the ZRR process is also not very often included in the data sample. The typical experimental cut is situated somewhere in the range $0.1<v_{\max}<0.3$. As we see in Fig. 17(a), the total QED correction $[\sigma(v_{\max})-\sigma_{\rm Born}]/\sigma_{\rm Born}$ is in this case quite close to zero, in fact it is slightly negative.

In Fig. 17(b) we compare the $\mathcal{KK}$ MC calculation with the semianalytical expression based on the phase-space integration in Sec. V. In the MC calculation we use the

[26]It downgrades to 0.5% for $M_{inv}(\mu\bar{\mu})\geqslant2m_\mu$, i.e., for full phase-space.

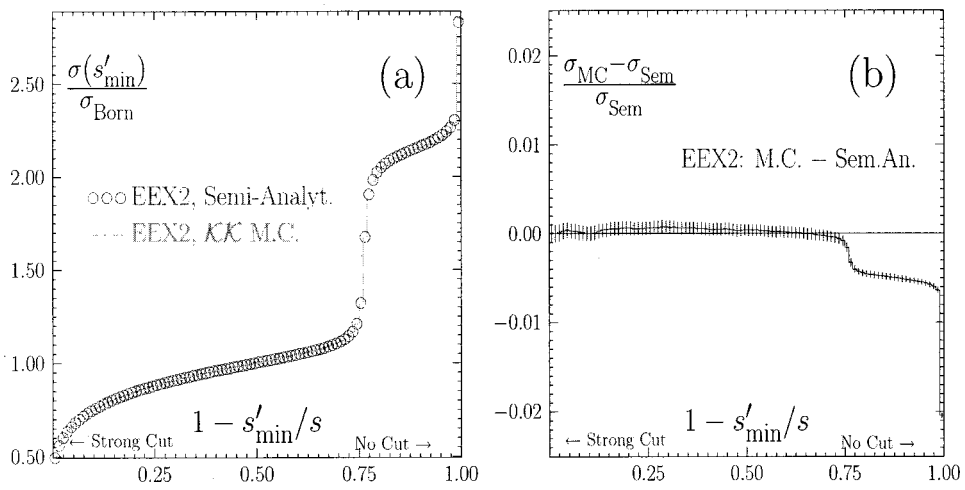

FIG. 17. The process $e^-e^+ \to f\bar{f}$, for $f=\mu^-$, at $\sqrt{s}=189$ GeV. ISR and FSR are on, IFI=ISR×FSR interference is off, EW corrections are off. The total cross-section $\sigma(s'>s'_{\min})$ where $s'=m^2_{f\bar{f}}$.

second-order EEX type of QED model EEX2 $\equiv \mathcal{O}(1,\alpha,\alpha L,\alpha^2 L^2)_{\rm EEX}$, defined in Sec. II. The semianalytical formula used in Fig. 17(b) is also in the class EEX2. It is defined as follows:

$$\sigma^f_{\rm SAN}=\int_0^{v_{\max}} dv\,\sigma^f_{\rm Born}[s(1-u)(1-v)]\rho_I^{(2)}(v)\rho_F^{(2)}(u), \tag{208}$$

where the distributions $\rho_I^{(2)}$ and $\rho_F^{(2)}$ are from Tables I and II.

What kind of lesson can we draw from Fig. 17(b)? We treat the result in Fig. 17(b) as an indication that the contribution from the QED (non-IFI) photonic corrections to the combined physical and technical precision in the EEX2-class integrated cross section for the standard cut $v_{\max}\sim 0.2$ is about 0.2%, for the ZRR process it is 0.7%, and for the $\gamma\gamma$* process it is 3%. We are here talking about the technical precision of the coding of the EEX2 matrix element, not associated with the phase-space integration (covered in the previous section).

In Fig. 18 we make an attempt at estimating the physical precision of the QED model in the EEX class. Specifically, we look into the difference between the EEX2 (as defined above) and the EEX1, with the EEX1 being the $\mathcal{O}(\alpha^1)_{\rm EEX}$ of Sec. II, EEX1$\equiv\mathcal{O}(1,\alpha,\alpha L)_{\rm EEX}$. This is plotted in Fig. 18(a) both from the $\mathcal{KK}$ MC and the semianalytical formula. Taking conservatively (see the discussion below) half of the difference between the EEX2 and the EEX1 as an estimate of the physical precision of the EEX2, we arrive at similar estimates of about 0.2% for the standard cut $v_{\max}\sim 0.2$, 0.7% for the ZRR process and up to 3% for the $\gamma\gamma$* process.

The other useful piece of information comes from Fig. 18(b), where we plot the difference EEX3−EEX2, with EEX3$\equiv\mathcal{O}(1,\alpha,\alpha L,\alpha^2L^2,\alpha^3L^3)_{\rm EEX}$; this provides direct insight into the neglected third-order LL contributions. As we see it is always below 3×10^{-4}. (This estimate will also be useful for the case of CEEX.) If the $\mathcal{O}(L^3\alpha^3)$ correction is of this size, then the main contribution to the above estimate of the theoretical error necessarily comes from the $\mathcal{O}(L^1\alpha^2)$ corrections.

In fact the absence of the $\mathcal{O}(\alpha^2L^1)$ corrections in both the EEX2 and the EEX1 is the main deficiency of the above tests, so that they cannot directly pin down the size of this contribution. Keeping this limitation in mind, from the test above we nevertheless estimate tentatively the combined physical and technical precision in the integrated EEX3-class cross section of the $\mathcal{KK}$ MC to be 0.2% for the standard cut $v_{\max}\sim 0.2$, 0.7% for the ZRR process, and about 1.5% for the $\gamma\gamma$* process. The caveat of this exercise is that we know

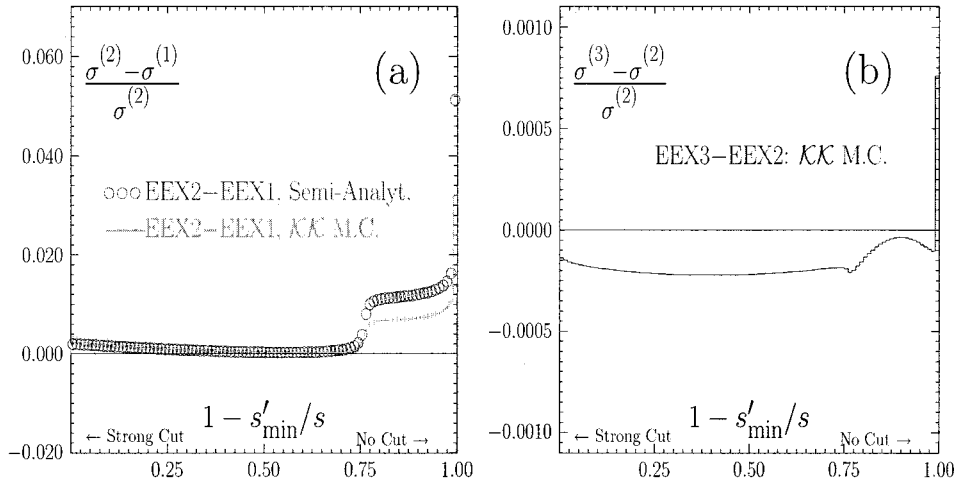

FIG. 18. An attempt at estimating the physical precision for EEX: $\mathcal{O}(\alpha^2)$ and $\mathcal{O}(\alpha^3)$. The process, energy, and definition of cuts are the same as in Fig. 17.

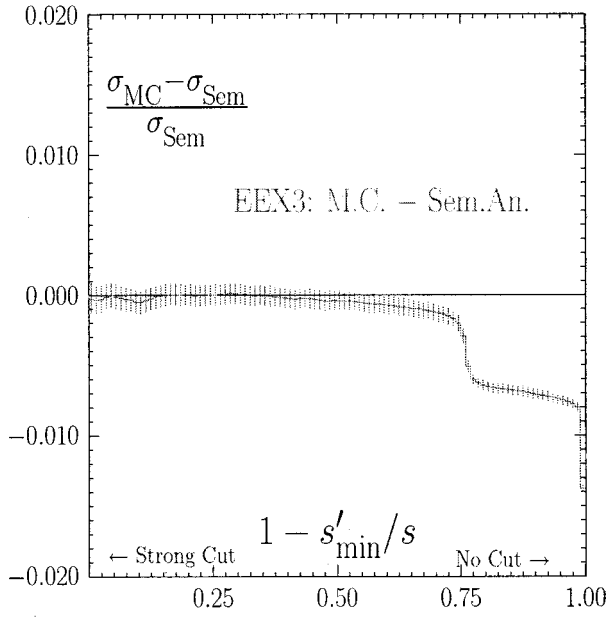

FIG. 19. The final attempt at estimating the physical precision for EEX3: the difference between EEX3 from the $\mathcal{KK}$ MC and the semi-analytical EEX3best, see the definition in the text. The process, energy and definition of the cuts are the same as in Fig. 17.

retrospectively the QED non-IFI component of the precision on the KORALZ/YFS3 Monte Carlo at LEP2 energies because the EEX of KORALZ and the EEX of the $\mathcal{KK}$ MC are practically the same.[27] The above exercise does help indeed, in spite of the fact that the neglected IFI contribution to the integrated cross section is of the order of 1%, because KORALZ in the nonexponentiated $\mathcal{O}(\alpha)$ mode can calculate the IFI separately; see the discussion in the following subsections.

Let us finally make an ultimate effort to estimate the total precision, staying all the time within the EEX model. As we have already noted the most important missing contribution seems to be the $\mathcal{O}(L^1\alpha^2)$, most probably the ISR part of it. In the semianalytical formula for the total cross section we are able to add it, since it is known from Ref. [18]. We may add the $\mathcal{O}(L^3\alpha^3)$ corrections as well and, in this way, we replace the $\rho_I^{(2)}$ by the $\rho_I^{(3)}$ of Ref. [44], which is the true $\mathcal{O}(\alpha^3)_{prag}$ for the ISR (according to the terminology explained in the Introduction) and $\mathcal{O}(\alpha^2)_{prag}$ for the FSR (non-IFI). Let us call it EEX3best $\equiv \mathcal{O}(1,\alpha,\alpha L,\alpha^2L^2,\alpha^2L^1,\alpha^3L^3)_{\rm EEX}$. The difference between the semianalytical EEX3best and the EEX3 from the $\mathcal{KK}$ MC is plotted in Fig. 19. As we see, this final test confirms the previous estimate of the physical precision of the EEX type of matrix element.

C. Physical precision, the case of CEEX

The quantitative determination of the *physical precision* should be based on the comparison of calculations in two consecutive orders in the expansion parameters, for instance by comparing results from the $\mathcal{O}(\alpha^r)$ and $\mathcal{O}(\alpha^{r-1})$ calculations, or the $\mathcal{O}(L^r\alpha^n)$ versus the $\mathcal{O}(L^{r-1}\alpha^n)$ calculations, etc. For example, when only the Born and $\mathcal{O}(\alpha^1)$ results are available, one should take the difference between the two (or some fraction of it) as an estimate of the physical precision. The above conservative recipe gives a solid estimate of the physical precision and we shall employ it as our basic method in the following. In most cases in the literature, however, authors try to *estimate* the *uncalculated* higher order effects with some ''rule of thumb.'' For instance in the case when Born and $\mathcal{O}(\alpha^1)$ results are known, they take $\frac{1}{2}L(\alpha/\pi)$ as an estimate of the missing/uncalculated $\mathcal{O}(\alpha^2)$ corrections. This has to be done with care because one may easily overlook some ''enhancement factor.'' For example the cross section close to a resonance can be modified by additional powers of the big logarithm $\ln\Gamma/M$. In most cases these ''enhancement factors'' are already seen in the $\mathcal{O}(\alpha^1)$ calculation so it is not difficult to trace them.

We are in a rather comfortable situation because for the QED ''photonic'' corrections we have at our disposal the $\mathcal{O}(\alpha^0)$, $\mathcal{O}(\alpha^1)$, and $\mathcal{O}(\alpha^2)$ calculations (at least for the ISR, where they are the biggest). We can therefore afford to take half of the difference between the $\mathcal{O}(\alpha^1)$ and $\mathcal{O}(\alpha^2)$ calculations as a conservative estimate of the physical precision due to QED ''photonic'' corrections. We also profit from the fact that the exponentiation considerably speeds up the convergence of the perturbative series by the ''advanced summation'' of certain classes of corrections to infinite order, and by not introducing additional spurious cutoff parameters dividing real emissions into soft and hard ones, which are typical of the calculations without exponentiation (see the discussion on the famous k_0 parameter in the 1989 LEP workshop [40]).

Let us mention that we omit, in our estimates of the physical precision, from the discussion the $\mathcal{O}(\alpha^2)$ effects due to an additional fermion pair, either real or virtual. We do it because: (a) there are many MC programs that implement the production of the four-fermion final states (often with the additional ISR) and (b) in the experiment this contribution can be eliminated at an early stage from the data in the experimental data analysis aimed at single fermion-pair production, see for example Ref. [48]. In fact this point is still under debate; see the proceedings of the LEP2 Monte Carlo workshop [45]. It was proposed that in the final combined LEP2 data the so-called nonsinglet initial-state and final-state secondary pair contribution will be kept in the data, as it is done by OPAL, see Refs. [49–51]. We have recently included the virtual corrections of the ''vacuum polarization'' type with the fermionic bubble in the $\mathcal{O}(\alpha^2)$ photonic contributions to the vertex corrections in the yet unpublished version 4.14 of the $\mathcal{KK}$ MC. This is done while keeping in mind the combined results of the $\mathcal{KK}$ MC with those of the other MC programs for the four-fermion production process, such as KORALW [52]. The tandem of the $\mathcal{KK}$ MC and KORALW programs will be able to realize any possible scenario of the treatment of the soft/light pair corrections in the LEP2 data.

In Fig. 20 we present the numerical results on which we base our quantitative estimate of the physical precision due

[27]The version 4.02 of KORALZ and its earlier versions have EEX implemented differently from $\mathcal{KK}$ MC.

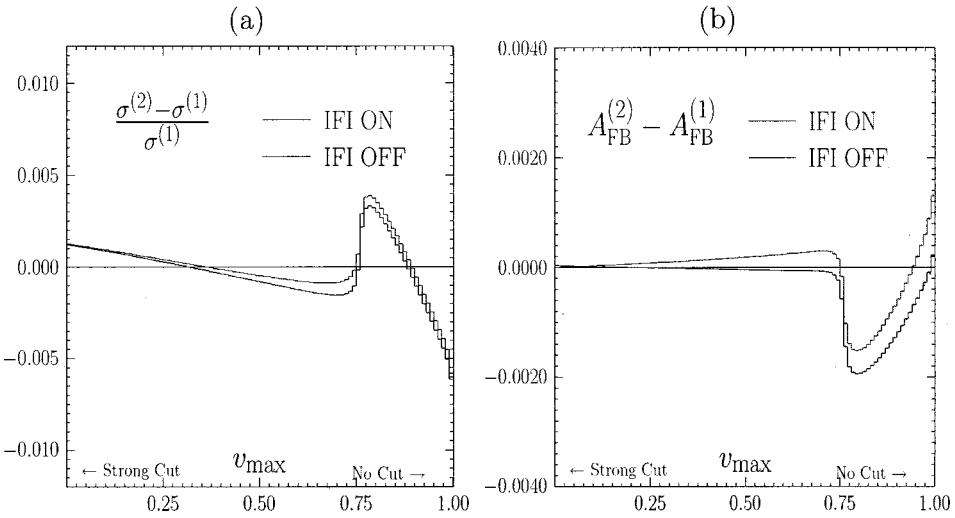

FIG. 20. Evaluation of the physical precision for the total cross section and charge asymmetry. The difference between the $\mathcal{O}(\alpha^2)_{\mathrm{CEEX}}$ and $\mathcal{O}(\alpha^1)_{\mathrm{CEEX}}$ is plotted as a function of $v_{\max}=1-s'_{\min}/s$. Results are shown for the $\mu^+\mu^-$ final state at $\sqrt{s}=189$ GeV.

to the photonic QED corrections. In this figure, we plot the difference between the $\mathcal{O}(\alpha^2)_{\mathrm{CEEX}}$ and the $\mathcal{O}(\alpha^1)_{\mathrm{CEEX}}$ results for the total cross section and charge asymmetry at 189 GeV as a function of the cut on the total energy emitted by all ISR and FSR photons in the $\mu^+\mu^-$ final state. The cut is formulated with the $s'>s'_{\min}$ or equivalently $v<v_{\max}$ condition, where s' is the effective mass squared of the $\mu^+\mu^-$ pair and $v=1-s'/s$, as usual. One should remember that the actual experimental cut is around $v_{\max}\sim 0.2$ (eliminating the Z radiative return) in the case of the standard data analysis, and sometimes around $v_{\max}\sim 0.9$ in the case when the Z radiative return is admitted in the data. The ''kink'' around $v_{\max}\sim 0.75$ is at the position of the Z radiative return. In either case, whether we admit or eliminate the Z radiative return, that is for $v_{\max}\sim 0.9$, the difference between the $\mathcal{O}(\alpha^2)_{\mathrm{CEEX}}$ and $\mathcal{O}(\alpha^1)_{\mathrm{CEEX}}$ results for the total cross section is below 0.4%, and the corresponding difference is below 0.002 for the charge asymmetry.

Taking *conservatively* half of this difference between the $\mathcal{O}(\alpha^2)_{\mathrm{CEEX}}$ and the $\mathcal{O}(\alpha^1)_{\mathrm{CEEX}}$ results as an estimate of the neglected $\mathcal{O}(\alpha^3)_{\mathrm{CEEX}}$ and higher orders we conclude that the physical precision due to the photonic QED corrections of our $\mathcal{O}(\alpha^2)_{\mathrm{CEEX}}$ calculation, for all possible cutoffs in the $0<v_{\max}<0.9$ range, is 0.2% in the total cross reaction and 0.001 in the charge asymmetry. This estimate would even be a factor of 2 better, if we restricted ourselves to the most typical cutoff range of $0.1<v_{\max}<0.3$. The above estimate will be confirmed by more auxiliary tests in the following.

As we see, we have improved on the physical precision estimate with respect to the previous estimates for the EEX model—in addition we do include IFI all of the time. For the respective precision of the ZRR process we now quote, for the integrated cross section, 0.2% instead of the previous 0.7%, and for the analogous $\gamma\gamma^*$ process precision we have something like 0.3% instead of the previous 1.5%. These we interpret as the results of the inclusion of the $\mathcal{O}(L\alpha^2)$ ISR correction in our CEEX spin amplitudes.

We have to stress very strongly that the estimate of the physical precision depends on the type of observable (we took σ and A_{FB}), the type of final state (we took the μ pair final state; for the quark-pair final states, the QED FSR effects are smaller, because of the smaller electric charges of quarks), and on many other input parameters, for example, on the total CMS energy. The great thing about the Monte Carlo is that the type of evaluation we proposed and implemented in this section [half of difference $\mathcal{O}(\alpha^2)-\mathcal{O}(\alpha^1)$] can be repeated for any observable, any final state, and any energy. For example, in Fig. 21 we repeat our evaluation of the physical precision for σ and A_{FB} at a linear collider energy of 500 GeV. As we see the resulting precision is worse, negligibly for a mild cut of the order of $v_{\max}<0.5$ and significantly by a factor of almost 2 for the Z radiative return, which is now placed close to $v=0.95$.

D. Absolute predictions, more on the physical/technical precision

In this section we shall present the SM absolute predictions for the total cross section and charge asymmetry at LEP2 (189 GeV) and at the linear collider (500 GeV). We compare them with our own semianalytical program $\mathcal{KK}$sem, with KORALZ [10], and in some cases with ZFITTER [5]. They may not improve our basic estimates of the technical and physical precision from the previous sections, but they can confirm them (or disprove them).

In Table III we show numerical results for the total cross section $\sigma(v_{\max})$ and charge asymmetry $A_{\mathrm{FB}}(v_{\max})$ as a function of the cut $v_{\max}$ on the total photon energy (the cutoff parameter $v_{\max}$ is defined as in the previous subsection). Generally, in Table III we show results with the ISR-FSR interference (IFI) switched on and off. The $\mathcal{KK}$sem semianalytical program (part of the $\mathcal{KK}$ MC package) provides the *reference results* for σ and A_{FB}, see the first column in Table III, which are without the IFI and are obtained from using the EEX3best formula defined in Sec. VI B. For the

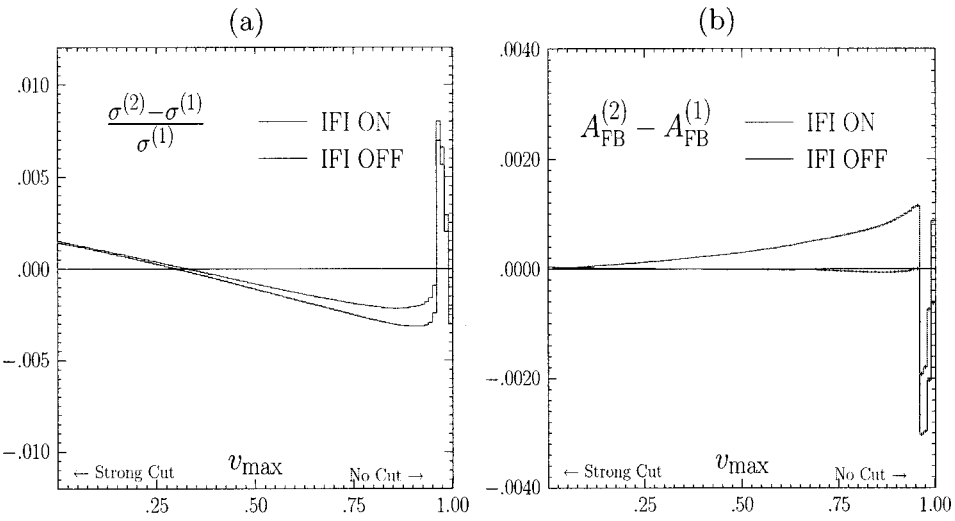

FIG. 21. Evaluation of the physical precision for the total cross section and charge asymmetry at $\sqrt{s}=500$ GeV. The difference between $\mathcal{O}(\alpha^2)_{\mathrm{CEEX}}$ and $\mathcal{O}(\alpha^1)_{\mathrm{CEEX}}$ is plotted as a function of $v_{\max}=1-s'_{\min}/s$ in the $\mu^+\mu^-$ final state.

charge asymmetry we use the convolution-type semianalytical formula of Eq. (208). (In fact we use this formula separately for the cross section in the forward and backward hemispheres and then we calculate A_{FB} from these partial integrals.) The results from the $\mathcal{KK}$ MC in Table III are shown for two types of QED matrix element: the $\mathcal{O}(\alpha^2)_{\mathrm{CEEX}}$ with and without IFI. In addition, the results we include from KORALZ are for the $\mathcal{O}(\alpha^1)$ matrix element with and without IFI, which will be discussed in the next section.

As tables with lists of numbers are difficult to comprehend, we present the essential results of Table III in Fig. 22, where they are all plotted as a difference with the *reference* results of our semianalytical program $\mathcal{KK}$sem. (In other words the results from $\mathcal{KK}$sem are exactly on the x axis.)

In the case with the IFI switched on, $\mathcal{KK}$sem cannot be used as a cross-check of the $\mathcal{KK}$ MC. Remembering that the IFI in KORALZ in the $\mathcal{O}(\alpha^1)$ mode (without exponentiation) is very well tested, we combine the $\mathcal{O}(\alpha^1)$ IFI contribution with the CEEX result without the IFI. Such a hybrid solution denoted in Fig. 22 as ''CEEX2+IFI at $\mathcal{O}(\alpha^1)$'' is used as our primary test of the full CEEX matrix element with IFI switched on. The above procedure is done separately for cross sections in the forward and backward hemispheres such that the prediction for charge asymmetry is also available.

It is worth mentioning that the above hybrid solution was already successfully used in Refs. [53,54] for the study of the IFI contribution at the Z peak, imposing a strong acollinearity cut. It is also implemented in a semianalytical form in

TABLE III. Absolute predictions for the total cross section and charge asymmetry. They are for the $\mu^+\mu^-$ final state at $\sqrt{s}=189$ GeV. The results are plotted as a function of the cutoff on the total photon energy $v_{\max}=1-s'_{\min}/s$. The ''reference'' σ and A_{FB} in first column are from the $\mathcal{KK}$sem semi-analytical program. We have used a Higgs boson mass of 100 GeV and a top mass of 175 GeV as input parameters.

$v_{\max}$	$\mathcal{KK}$sem refer.	$\mathcal{O}(\alpha^3)_{\mathrm{EEX3}}$	$\mathcal{O}(\alpha^2)_{\mathrm{CEEX}}$ int OFF	$\mathcal{O}(\alpha^2)_{\mathrm{CEEX}}$	KORALZ	KORALZ interf.
			$\sigma(v_{\max})$ [pb], $\mathcal{KK}$ MC and KORALZ 1st order			
0.01	1.6712±0.0000	1.6687±0.0020	1.6690±0.0020	1.7679±0.0024	0.9639±0.0009	0.1610±0.0009
0.10	2.5198±0.0000	2.5164±0.0023	2.5170±0.0023	2.5967±0.0027	2.1919±0.0010	0.0880±0.0010
0.30	3.0616±0.0000	3.0565±0.0024	3.0581±0.0024	3.1190±0.0029	2.7690±0.0010	0.0545±0.0010
0.50	3.3747±0.0000	3.3682±0.0025	3.3713±0.0025	3.4203±0.0029	3.0565±0.0010	0.0385±0.0010
0.70	3.7225±0.0000	3.7131±0.0025	3.7200±0.0025	3.7596±0.0030	3.3649±0.0010	0.0246±0.0010
0.90	7.1434±0.0000	7.0904±0.0024	7.1496±0.0024	7.1789±0.0030	6.3558±0.0010	0.0210±0.0010
0.99	7.6145±0.0000	7.5511±0.0024	7.6254±0.0024	7.6542±0.0029	6.7004±0.0010	0.0213±0.0010
			$A_{\mathrm{FB}}(v_{\max})$, $\mathcal{KK}$ MC and KORALZ 1st order			
0.01	0.5654±0.0000	0.5650±0.0014	0.5650±0.0014	0.6111±0.0016	0.5765±0.0013	0.1201±0.0013
0.10	0.5664±0.0000	0.5660±0.0011	0.5660±0.0011	0.5922±0.0012	0.5784±0.0006	0.00324±0.0006
0.30	0.5692±0.0000	0.5687±0.0009	0.5686±0.0009	0.5856±0.0011	0.5818±0.0005	0.0164±0.0005
0.50	0.5744±0.0000	0.5738±0.0009	0.5737±0.0009	0.5863±0.0010	0.5868±0.0005	0.0112±0.0005
0.70	0.5864±0.0000	0.5852±0.0008	0.5852±0.0008	0.5947±0.0009	0.5972±0.0004	0.0078±0.0004
0.90	0.3105±0.0000	0.3115±0.0004	0.3096±0.0004	0.3170±0.0005	0.3260±0.0002	0.0037±0.0002
0.99	0.2851±0.0000	0.2867±0.0004	0.2843±0.0004	0.2912±0.0004	0.3039±0.0002	0.0024±0.0002

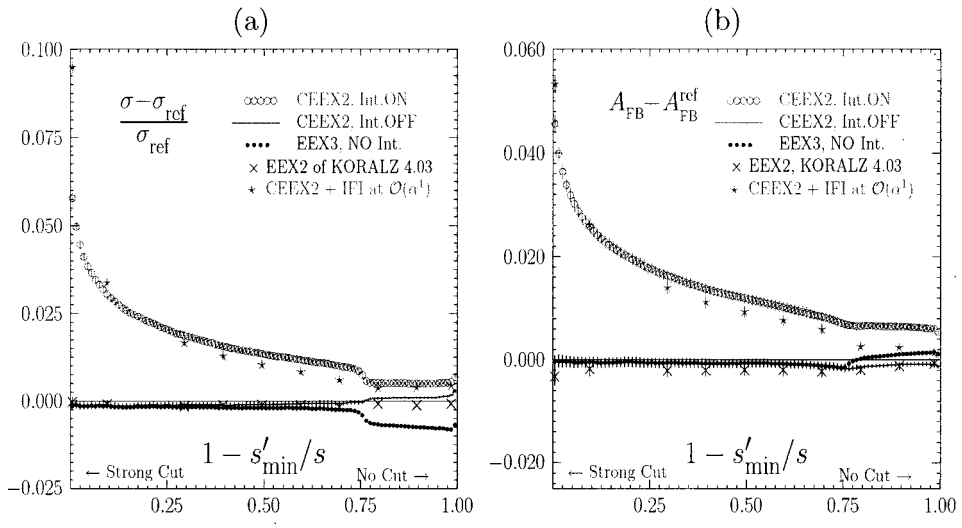

FIG. 22. Absolute predictions for the total cross section and charge asymmetry. They are for the $\mu^+\mu^-$ final state at $\sqrt{s}=189$ GeV. The results are plotted as a function of the cutoff on the total photon energy $v_{\rm max}=1-s'_{\rm min}/s$.

ZFITTER 6.x. On general grounds, we expect this recipe to be rather good, because the IFI correction itself at $\mathcal{O}(\alpha^1)$ does not contain any large mass logarithms, is relatively small, and can be handled additively.

In Fig. 22 we also show the numerical results from the $\mathcal{KK}$ MC in the EEX3 mode (no IFI) and from KORALZ in the EEX2 mode (no IFI), which are not included in Table III.

Let us now comment on the results in Fig. 22. The EEX3 from the $\mathcal{KK}$ MC differs from the EEX3best of the $\mathcal{KK}$sem (no IFI in either) by about 0.7% for the ZRR process, as we have already seen, and we interpret this difference as the result of the missing $\mathcal{O}(L^1\alpha^2)$. The EEX2 of KORALZ 4.03 is closer to the EEX3best of the $\mathcal{KK}$sem for the ZRR process—we do not see any contradiction in this since the implementations of the EEX in KORALZ and the $\mathcal{KK}$ MC differ in the details [causing a difference of $\mathcal{O}(L^1\alpha^2)$ in the integrated cross section].

In the case with the IFI switched off, the CEEX2 result, corresponding exactly to the $\mathcal{O}(\alpha^2)_{\rm CEEX}$, defined in Sec. III, as implemented in the $\mathcal{KK}$ MC 4.13, agrees very well with the EEX3best of the $\mathcal{KK}$sem. This result is compatible with the total theoretical precision of 0.2% for the integrated cross section, even including the ZRR process.

In the case with the IFI switched on, the hybrid solution ''CEEX2+IFI at $\mathcal{O}(\alpha^1)$'' also agrees with the full CEEX2 result, confirming the total theoretical precision of 0.2% for the integrated cross section, including the ZRR process.

For the charge asymmetry in Fig. 22, the situation is quite similar. The IFI effect is up to 4% for strong cuts. In the case with the IFI switched off, the CEEX2 result agrees with the EEX3best of the $\mathcal{KK}$sem to within 0.2%. When the IFI is included, the CEEX2 agrees with the hybrid solution rather well, to within 0.4%. Note that in the above Monte Carlo exercise we have used the symmetric definition of the scattering angle θ^* of Ref. [55] (which is close to what is used in the LEP experiments).

Summarizing, the numerical results in Fig. 22 establish our basic estimate of the theoretical precision of the $\mathcal{KK}$ MC, due to QED effects, at LEP2 energies of about 0.2% for the total cross section and 0.2–0.4 % (depending on the cutoffs) for the charge asymmetry. Finally, we examine the analogous results from the $\mathcal{KK}$ MC at 500 GeV in Fig. 23. In this case we include only results from the $\mathcal{KK}$ MC and $\mathcal{KK}$sem. The pattern of agreement is, up to a factor of 2, the same as at 189 GeV.

E. Initial–final-state interference

The control of the initial–final-state interference correction down to the precision of 0.2% in the integrated cross-section and in the charge asymmetry is rather important—this is why we dedicate this section to a more detailed study of this QED correction. In particular we would like to answer the following questions.

(1) How big is the ISR⊗FSR interference in σ_{tot}, A_{FB}?
(2) Do we know the ISR⊗FSR at $\mathcal{O}(\alpha^1)$?
(3) Do we know the ISR⊗FSR beyond $\mathcal{O}(\alpha^1)$?
(4) How sensitive is the ISR⊗FSR to cutoff changes?

KORALZ is the best starting point and reference for the problem of calculating the ISR⊗FSR. In Fig. 24 we show results from the $\mathcal{O}(\alpha^1)$ KORALZ (no exponentiation) for the $\mu^+\mu^-$ final state at $\sqrt{s}=189$ GeV. The angular distributions from KORALZ, in pure $\mathcal{O}(\alpha^1)$ (without exponentiation), were verified very precisely at the level of $\sim 0.01\%$ using a special analytical calculation, see Ref. [55], so we know the ISR⊗FSR at $\mathcal{O}(\alpha^1)$ very precisely. As we see, the ISR ⊗FSR contribution to the integrated cross section is about 3% and its contribution is about 0.03 to $A_{\rm FB}$. This is definitely above the ultimate experimental error tag for the combined LEP2 data at the end of the LEP2 operation. The energy cut on the total photon energy is fixed in the results of Fig. 24 to just one value, $v<v_{\rm max}=0.1$ (where $v_{\rm max}=1-s'/s$ is defined as usual). This is close to the usual value in the experimental LEP2 data analysis. We introduce also the angular cut $|\cos\theta|<\cos\theta_{\rm max}$ and vary the value of $\cos\theta_{\rm max}$, see Fig. 24(b), where the value used in the experimental

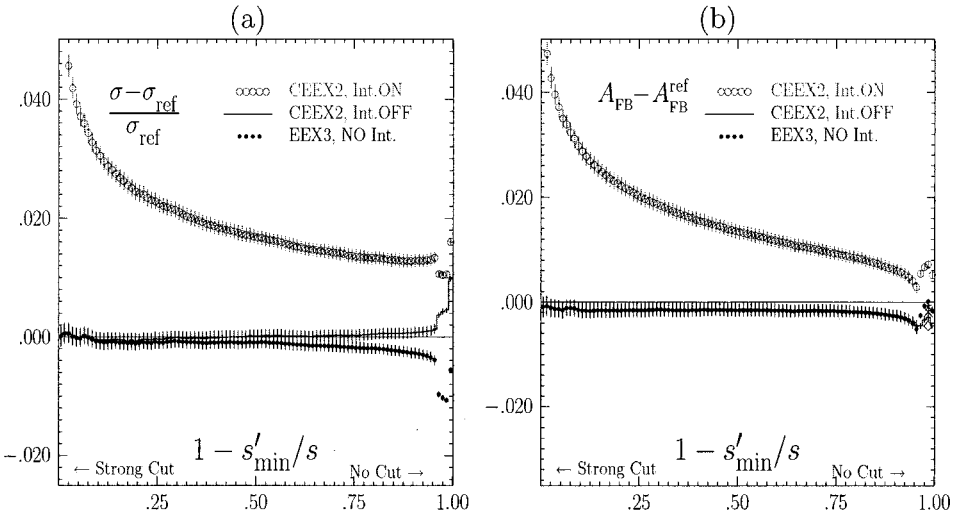

FIG. 23. Total cross section and charge asymmetry for the $\mu^+\mu^-$ final state at $\sqrt{s}=500$ GeV. The results are analogous to those in Fig. 22.

LEP2 data analysis is around $\cos\theta_{\rm max}=0.9$; this corresponds to two bins before the last one in Fig. 24(b) (the last point in the plot is for $\cos\theta_{\rm max}=1$). In this way we have already answered the first two questions from the above list.

In Fig. 25 we present similar results from the $\mathcal{KK}$ MC, which will help us to answer whether we know the ISR $\otimes$FSR beyond $\mathcal{O}(\alpha^1)$ and to inspect in more detail the dependence on cutoffs. In Fig. 25(a),(b) we essentially repeat the exercise of Fig. 24, finding out the ISR$\otimes$FSR contribution to the angular distribution and $A_{\rm FB}$ for the same energy cut using $\mathcal{KK}$ MC instead of KORALZ. As we see, the results change slightly, the ISR$\otimes$FSR effect is about 20–30 % smaller. We attribute this mainly to (a) a different (better) treatment of the ISR in the $\mathcal{KK}$ MC and (b) the exponentiation of the ISR$\otimes$FSR effect in the $\mathcal{KK}$ MC. As is well known, in $\mathcal{O}(\alpha^1)$, the ISR$\otimes$FSR contributes like $4Q_eQ_f(\alpha/\pi)\ln(1-\cos\theta)/(1+\cos\theta)$ to the angular distribution—this even causes the angular distribution to be negative close to $\cos\theta=-1$. In the CEEX exponentiation the above singularity is summed up to infinite order and the angular distribution near $|\cos\theta|=1$ is no longer singular. (This kind of exponentiation will be implemented in the next version of ZFITTER, see [45] for the first numerical results.) The typical experimental cut $|\cos\theta|<0.9$ eliminates most of the above trouble anyway—what is probably more important is the correct ''convolution'' of the IR-finite $\mathcal{O}(\alpha^1)$ ISR $\otimes$FSR with the $\mathcal{O}(\alpha^2)$ ISR. In the $\mathcal{KK}$ MC, this is done in a maximally clean way from the theoretical/physical point of view (at the amplitude level) while in the semianalytical programs like ZFITTER [5] this is done in a more *ad hoc* manner. Let us remind the reader that we still lack the genuine IR-finite $\mathcal{O}(\alpha^2)$ corrections in the ISR$\otimes$FSR class from diagrams like 2-boxes and 5-boxes, see Sec. III. These contributions are most likely negligible, of the order of $\mathcal{O}(L^1\alpha^2)$ at most.

In Fig. 25(c),(d) we make the energy cut looser, $v_{\rm max}=0.9$, thus admitting the ZRR into the available phase-space. As a result, the relative ISR$\otimes$FSR decreases by a factor of 3, simply because it gets ''diluted'' in the integrated cross section, which is larger by a factor of 3 while ZRR does not contribute to the ISR$\otimes$FSR because of its narrow-resonance character, as we already discussed at length in Sec. III. The

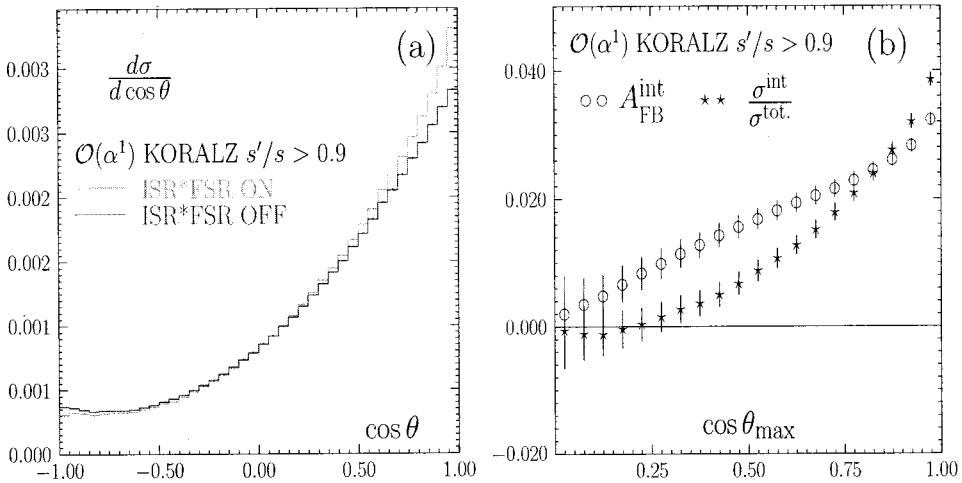

FIG. 24. Results from the $\mathcal{O}(\alpha^1)$ KORALZ (no exponentiation) for the $\mu^+\mu^-$ final state at $\sqrt{s}=189$ GeV. The energy cut is on s'/s, where $s'=m_{ff}^2$. The angular cut is $|\cos\theta|<\cos\theta_{\rm max}$. The scattering angle is the $\theta=\theta^*$ of Ref. [55].

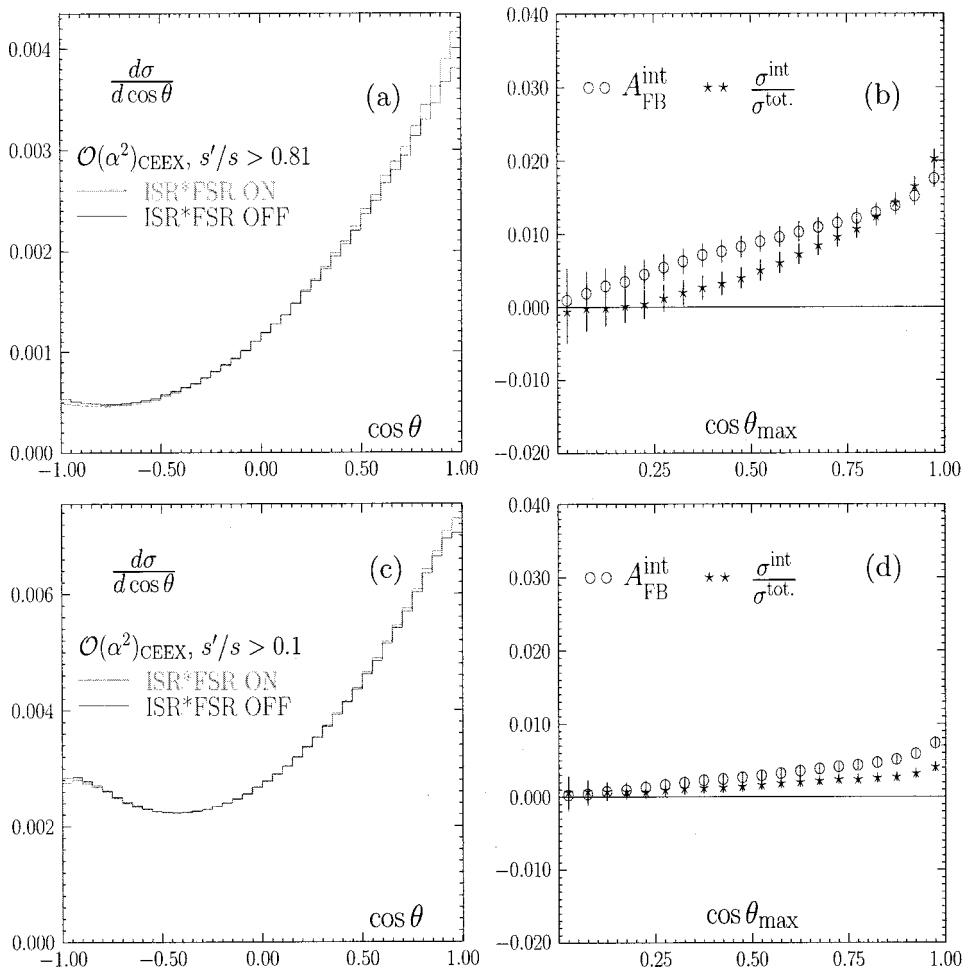

FIG. 25. Results from the $\mathcal{O}(\alpha^2)$ $\mathcal{KK}$ MC for the $\mu^+\mu^-$ final state at $\sqrt{s}=189$ GeV. The energy cut is on s'/s, where $s'=m_{ff}^2$. The angular cut is $|\cos\theta|<\cos\theta_{\rm max}$. The scattering angle is the $\theta=\theta^*$ of Ref. [55].

fact that the ZRR does not contribute to the ISR⊗FSR can be seen explicitly in Fig. 26 where we plot the ISR⊗FSR contribution to $A_{\rm FB}$ ''binperbin,'' that is calculated in each bin separately. As we see the contribution from the ZRR,

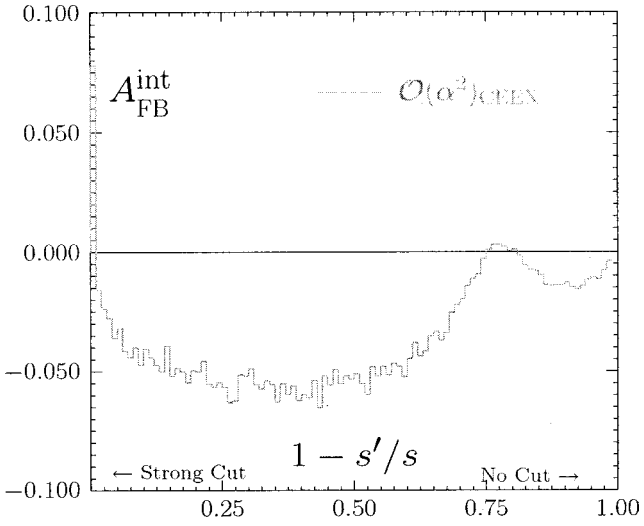

FIG. 26. The ISR⊗FSR contribution to $A_{\rm FB}$ ''binperbin.''

which at this energy (189 GeV) is located at $v=0.75$, is very small, smaller than the contributions from all of the other v's where there is no Z resonance.

In the above exercises, and also in the following, we always use the energy cut on the $v=1-s'/s$ variable defined in terms of the effective mass of the ''bare'' final fermions, that is without any attempt at combining them with the collinear FSR photons. This is experimentally well justified for the μ-pair final states but not for τ-pairs or quarks. It is possible, and in fact rather easy, to define a ''propagator'' or ''reduced'' s_p' that takes into account the loss of energy due to ISR but not FSR. In other words, the s_p' effective mass-squared sums up FSR photons. One can ask the following legitimate question: If we would cut not on the ''bare'' final fermion variable s', but instead on the ''propagator'' s_p', would perhaps the estimate of the ISR⊗FSR contribution then be dramatically different, for instance would it be much smaller? In Fig. 27 we show a numerical exercise in which we employ the energy cut in terms of $v_p=1-s_p'/s$. One can construct such an s_p' by looking into the angles of the outgoing fermions. This type of variable was used in Ref. [55]. In Fig. 27 we use the definition of s_p' of ALEPH [56]. As we see in this figure, the result is not dramatically different from

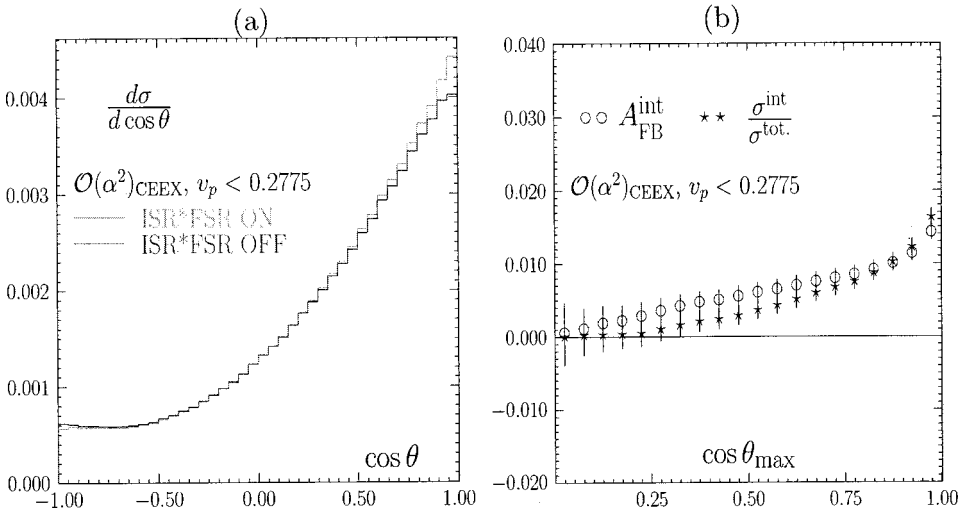

FIG. 27. Results from the $\mathcal{O}(\alpha^1)$ $\mathcal{KK}$ MC for the $\mu^+\mu^-$ final state at $\sqrt{s}=189$ GeV. The energy cut is on $v_p=1-s'/s$, where s' is an estimate of the ''propagator eff. mass'' as defined by ALEPH. The angular cut is $|\cos\theta|<\cos\theta_{\rm max}$. The scattering angle is the $\theta=\theta^*$ of Ref. [55].

what we have seen in Fig. 25. The magnitude of the ISR $\otimes$FSR contribution is close to what we could see if we applied the same value of the energy cut for the ''bare'' s' (as we have checked independently).

We shall now examine the dependence of the ISR$\otimes$FSR contribution on the energy cut $v_{\rm max}$ in more detail. In Fig. 28 we show the ISR$\otimes$FSR contribution to $A_{\rm FB}$ as a function of the energy cut $v_{\rm max}$ at two energies (a) 189 GeV and (b) $\sqrt{s}=M_Z$ at the Z peak. No cut is applied on $\cos\theta$. In addition to the $\mathcal{KK}$ MC results, we show the results from the $\mathcal{O}(\alpha^1)$ mode of KORALZ and from ZFITTER.[28] At 189 GeV and for the typical energy cut $0.2<v_{\rm max}<0.3$, all three programs agree very well. This cut is relatively ''inclusive,'' so that exponentiation effects are not so important and the ISR is eliminated in a ''gentle'' way (the total cross section is close to the Born value). For stronger cuts $v_{\rm max}<0.2$ we see a large (factor of 2) discrepancy between the results from the $\mathcal{KK}$ MC and both KORALZ and ZFITTER, because of the lack of exponentiation in KORALZ and ZFITTER (in ZFITTER the ISR $\otimes$FSR is taken without exponentiation and combined with the ISR ''additively''). We also observe the discrepancy of about 0.2% for the ZRR between the $\mathcal{KK}$ MC on the one hand and both KORALZ and ZFITTER on the other hand. Our guess is that it is due to the difference in the method of combining the ISR$\otimes$FSR with the second-order ISR (of course, we believe that the CEEX method of doing it at the amplitude level is the best one can do). In Fig. 28(b) we see, first of all, the well-known phenomenon of the strong suppression of the ISR$\otimes$FSR contribution at the resonance, especially for a loose cutoff. Even for a strong cut, $v_{\rm max}$

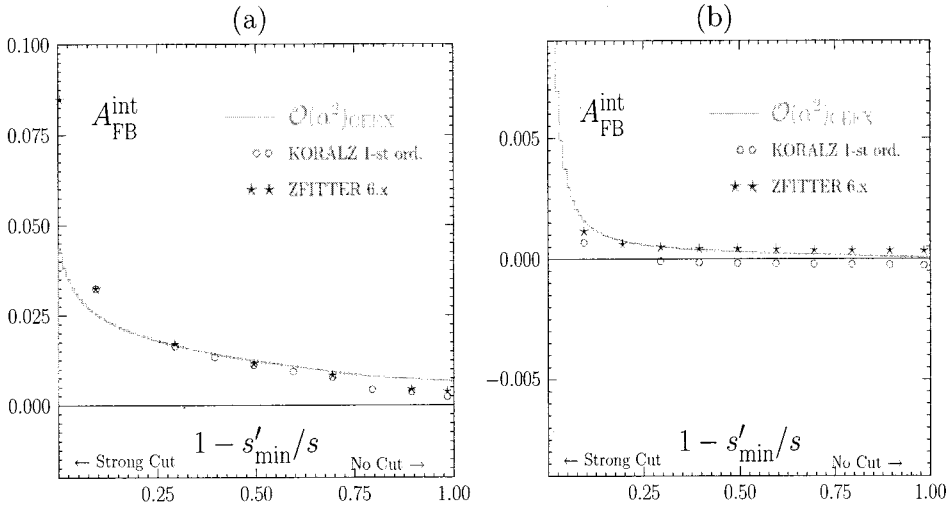

FIG. 28. The s'-cut dependence of δA_{FB}. No θ-cut.

[28]We thank D. Bardin for providing us the results from ZFITTER.

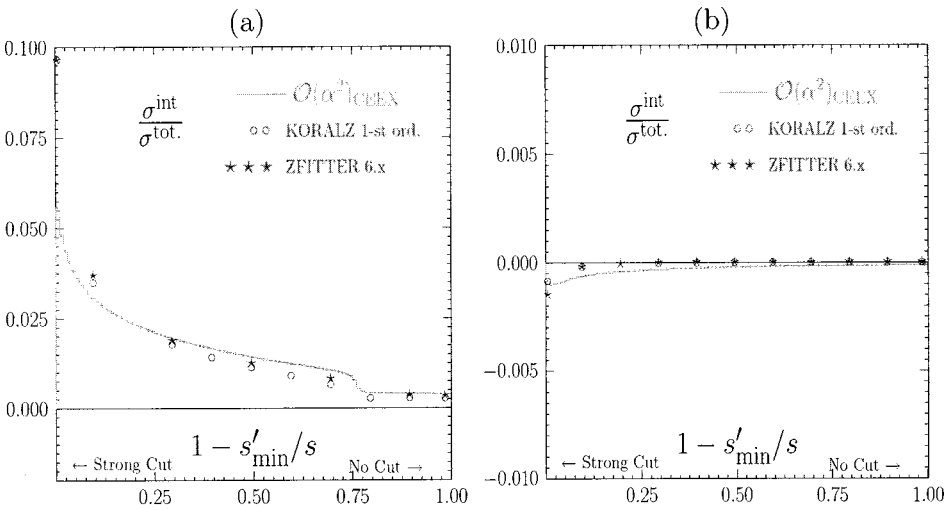

FIG. 29. The s'-cut dependence of $\delta\sigma$. No θ-cut.

$=0.1$, the ISR⊗FSR contribution is about 0.01, a factor of about 30 smaller than it is in the off-resonance case. Here, the $\mathcal{KK}$ MC agrees rather well with KORALZ and ZFITTER. The differences are generally[29] up to 0.0015.

In Fig. 29(a) we examine the ISR⊗FSR contribution to the integrated cross section as a function of the energy cut $v_{\rm max}$. At 189 GeV and for the typical energy cut $0.1<v_{\rm max}<0.6$, all three programs agree reasonably well, KORALZ and ZFITTER are generally closer to each other than to the $\mathcal{KK}$ MC. After admitting the ZRR, $v_{\rm max}>0.8$, all three programs agree even better. For a very strong cut, $v_{\rm max}<0.1$, KORALZ and ZFITTER differ dramatically from the $\mathcal{KK}$ MC because of the lack of exponentiation in KORALZ and ZFITTER for the IFI. In Fig. 29(b), we see again the strong suppression of the ISR⊗FSR contribution at the resonance, especially for the loose cutoff. The suppression is cutoff dependent and generally stronger for KORALZ and ZFITTER than for the $\mathcal{KK}$ MC. Most of the comments that we made on the ISR⊗FSR contribution to $A_{\rm FB}$ apply also here.

Finally, in Fig. 30 we go back to the vicinity of the Z peak (LEP1) and we show the magnitude of the ISR⊗FSR contribution to the integrated cross section as a function of the CMS energy, for the $\mu^-\mu^+$ final state and for all five quark final states taken together (the so-called hadronic cross section) from the $\mathcal{KK}$ Monte Carlo. No angular cut or energy cut is applied (the full phase-space). For the $\mu^-\mu^+$ final state, we also include results from the $\mathcal{O}(\alpha^1)$ KORALZ and ZFITTER/TOPAZ0 [5,41]. The results on quarks are multiplied by a factor of 10 to be visible, because the ISR⊗FSR contribution in this case is small. It is not only suppressed by the smallness of the quark charge, but we also have partial cancellation among the up- and down-type quarks, see Ref. [55]. However, the ISR⊗FSR contribution to the hadronic cross section has to be known much more precisely (a factor ~ 3) because it is measured much more precisely, thanks to higher statistics. In Fig. 30 we see that the suppression of the ISR⊗FSR is much weaker as we go away from the center of the resonance, and it changes the resonance curve in such a way that it affects the fitted mass of the Z. The actual size of the shift of M_Z was studied in Ref. [57], and it was found to be 0.15 MeV. Results of the $\mathcal{KK}$ MC are smaller by about 10–20 % than the $\mathcal{O}(\alpha^1)$ estimates of KORALZ and ZFITTER, away from the Z peak. This is compatible with the 10–20 % size of the $\mathcal{O}(L^2\alpha^2)$ ISR corrections with respect to $\mathcal{O}(L^1\alpha^1)$ corrections, which are included in the $\mathcal{KK}$ MC and are not included in KORALZ, and apparently are also not included in ZFITTER/TOPAZ0 (which agree very well with KORALZ). Our last comment concerns the reliability of our estimate for the ISR⊗FSR contribution in the absence of the correct implementation of the simultaneous emission of the FSR photon and the FSR gluon. We think that through the usual arguments, see Ref. [57], we can neglect considering the emission of the FSR single gluon, as long as we stick to a very inclusive cross section, such as the total cross section in Fig. 30. For stronger angular cuts, or events with a definite jet multiplicity, we would need to improve our calculation.

We summarize the results of this section on the ISR⊗FSR as follows.

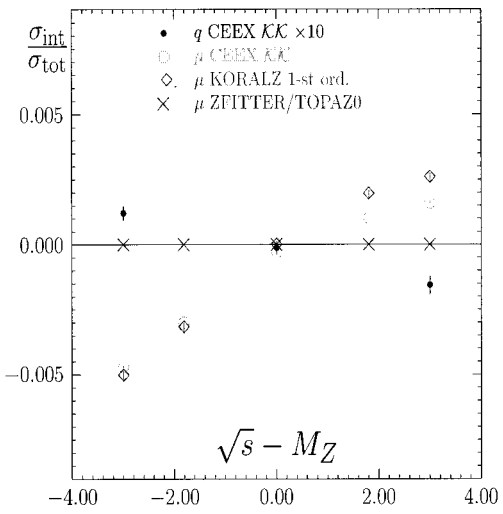

FIG. 30. Back on the Z peak.

[29]The difference between KORALZ and ZFITTER should perhaps be smaller, since both are $\mathcal{O}(\alpha^1)$? The difference could be due to the angle definition.

(1) For a typical experimental energy cut of 0.3 the ISR $\otimes$ FSR interference is about 1.5% in σ_{tot} and A_{FB}.

(2) For the energy cut of 0.1, it is a factor of 2 larger.

(3) The cut $|\cos\theta|<0.9$ makes it 25% smaller.

(4) The $\mathcal{O}(\alpha^1)$ ISR$\otimes$FSR interference is under total control, using KORALZ and $\mathcal{KK}$ Monte Carlo for arbitrary cuts.

(5) Effects beyond $\mathcal{O}(\alpha^1)$ are negligible [$<20\%$ of the $\mathcal{O}(\alpha^1)$], except when the energy cut is stronger than 0.1.

(6) The ISR$\otimes$FSR interference at the Z radiative return is very small, as expected.

(7) Changing from s' to the propagator Q^2 in the energy cut has no effect.

F. Total theoretical precision

Let us summarize the total theoretical precision.

(1) For the most typical cutoff range $0.1<v_{\max}<0.3$, excluding the Z radiative return, we quote for CEEX a total precision of 0.2% for LEP2 and for the LC at 0.5 TeV.

(2) For a cutoff including ZRR we quote 0.2% total precision for LEP2 and 0.4% total precision for the LC at 0.5 TeV.

(3) For $\gamma\gamma^*$ we quote 0.3% at LEP2 (there is no firm result for the LC).

In the above estimates the technical component of the error was significantly below the physical one. The restrictions to be applied are as follows: no light-fermion pairs (pure photonic QED); no EW component.

VII. OUTLOOK AND SUMMARY

The most important new features in the present CEEX are the ISR-FSR interference, the second-order subleading corrections, and the exact matrix element for two hard photons. This already makes CEEX a unique source of SM predictions for the LEP2 and the LC physics programs. Note that for these programs the electroweak correction library has to be reexamined at LC energies. The most important omission in the present version is the absence of the neutrino and electron channels. Let us stress that the present program is an excellent starting platform for the construction of the second-order Bhabha MC generator based on CEEX exponentiation. We hope to be able to include the Bhabha and neutrino channels soon, possibly in the next version. The other important directions for the development are the inclusion of the exact matrix element for three hard photons, together with virtual corrections up to $\mathcal{O}(\alpha^3L^3)$ and the emission of the light fermion pairs. The inclusion of the W^+W^- and $t\bar{t}$ final states is still in a further perspective.

ACKNOWLEDGMENTS

Two of us (S.J. and B.F.L.W.) would like to thank the CERN EP and TH Divisions. We are grateful to all four LEP Collaborations and their members for support. In particular we would like to thank Dr. D. Schlatter of ALEPH for continuous support and help. One of us (S.J.) would like to thank the DESY Directorate for its generous support in the critical stage of the beginning of this project. We would like to express our gratitude to W. Płaczek, E. Richter-Wąs, M. Skrzypek, and S. Yost for valuable comments. This work was supported in part by Polish Government Grants Nos. KBN 2P03B08414 and KBN 2P03B14715; the U.S. DOE Contracts Nos. DE-FG05-91ER40627 and DE-AC03-76SF00515; the Maria Skłodowska-Curie Joint Fund II PAA/DOE-97-316, and the Polish–French Collaboration within IN2P3 through LAPP Annecy.

APPENDIX: BASIC KS/GPS SPINORS AND PHOTON POLARIZATIONS

The arbitrary massless spinor $u_\lambda(p)$ of momentum p and chirality λ is defined according to the KS methods [24,25]. In the following we closely follow the notation of Ref. [2] (in particular we also use $\zeta=\zeta_\downarrow$). In the above framework every spinor is transformed out of the two *constant basic* spinors $u_\lambda(\zeta)$, of opposite chirality $\lambda=\pm$, as follows:

$$u_\lambda(p)=\frac{1}{\sqrt{2p\zeta}}\not{p}u_{-\lambda}(\zeta),\quad u_+(\zeta)=\not{\eta}u_-(\zeta),$$
$$\eta^2=-1,\quad (\eta\zeta)=0. \tag{A1}$$

The usual relations hold: $\not{\zeta}u_\lambda(\zeta)=0$, $\omega_\lambda u_\lambda(\zeta)=u_\lambda(\zeta)$, $u_\lambda(\zeta)\bar{u}_\lambda(\zeta)=\not{\zeta}\omega_\lambda$, $\not{p}u_\lambda(p)=0$, $\omega_\lambda u_\lambda(p)=u_\lambda(p)$, $u_\lambda(p)\bar{u}_\lambda(p)=\not{p}\omega_\lambda$, where $\omega_\lambda=\frac{1}{2}(1+\lambda\gamma_5)$. Spinors for the massive particle with four-momentum p (with $p^2=m^2$) and spin projection $\lambda/2$ are defined similarly:

$$u(p,\lambda)=\frac{1}{\sqrt{2p\zeta}}(\not{p}+m)u_{-\lambda}(\zeta),$$
$$v(p,\lambda)=\frac{1}{\sqrt{2p\zeta}}(\not{p}-m)u_\lambda(\zeta), \tag{A2}$$

or, equivalently, in terms of massless spinors

$$u(p,\lambda)=u_\lambda(p_\zeta)+\frac{m}{\sqrt{2p\zeta}}u_{-\lambda}(\zeta),$$
$$v(p,\lambda)=u_{-\lambda}(p_\zeta)-\frac{m}{\sqrt{2p\zeta}}u_\lambda(\zeta), \tag{A3}$$

where $p_\zeta\equiv\hat{p}\equiv p-\zeta m^2/(2\zeta p)$ is the light-cone projection ($p_\zeta^2=0$) of the p obtained with the help of the constant auxiliary vector ζ.

The above definition is supplemented in Ref. [2] with the precise prescription of the spin quantization axes, the translation from spin amplitudes to density matrices (also in vector notation), and the methodology of connecting production and decay for unstable fermions. We collectively call these rules the global positioning of spin (GPS). Thanks to these we are able to easily introduce polarizations for beams and implement polarization effects for final fermion decays (of τ-leptons, t-quarks), for the first time also in the presence of the emission of many ISR and FSR photons.

The GPS rules determining the spin quantization frame for the $u(p,\pm)$ and $v(p,\pm)$ of Eq. (A3) are summarized as follows.

(a) In the rest frame of the fermion, take the z axis along $-\vec{\zeta}$.

(b) Place the x axis in the plane defined by the z axis from the previous point and the vector $\vec{\eta}$, in the same half-plane as $\vec{\eta}$.

(c) With the y-axis, complete the right-handed system of coordinates. The rest frame defined in this way we call the GPS frame of the particular fermion.

See Ref. [2] for more details. In the following we shall assume that polarization vectors of beams and of outgoing fermions are defined in their corresponding GPS frames.

The inner product of the two massless spinors is defined as follows:

$$s_+(p_1,p_2)\equiv\overline{u}_+(p_1)u_-(p_2),$$
$$s_-(p_1,p_2)\equiv\overline{u}_-(p_1)u_+(p_2)=-[s_+(p_1,p_2)]^*. \tag{A4}$$

The above inner product can be evaluated using the Kleiss-Stirling (KS) expression

$$s_+(p,q)=2(2p\zeta)^{-1/2}(2q\zeta)^{-1/2}[(p\zeta)(q\eta)-(p\eta)(q\zeta) - i\epsilon_{\mu\nu\rho\sigma}\zeta^\mu\eta^\nu p^\rho q^\sigma] \tag{A5}$$

in any reference frame. In particular, in the laboratory frame we typically use $\zeta=(1,1,0,0)$ and $\eta=(0,0,1,0)$, which leads to the following ''massless'' inner product

$$s_+(p,q)=-(q^2+iq^3)\sqrt{(p^0-p^1)/(q^0-q^1)} + (p^2+ip^3)\sqrt{(q^0-q^1)/(p^0-p^1)}. \tag{A6}$$

Equation (A3) immediately provides us also with the *inner product* for massive spinors

$$\overline{u}(p_1,\lambda_1)u(p_2,\lambda_2)=S(p_1,m_1,\lambda_1,p_2,m_2,\lambda_2),$$
$$\overline{u}(p_1,\lambda_1)v(p_2,\lambda_2)=S(p_1,m_1,\lambda_1,p_2,-m_2,-\lambda_2), \tag{A7}$$
$$\overline{v}(p_1,\lambda_1)u(p_2,\lambda_2)=S(p_1,-m_1,-\lambda_1,p_2,m_2,\lambda_2),$$
$$\overline{v}(p_1,\lambda_1)v(p_2,\lambda_2)=S(p_1,-m_1,-\lambda_1,p_2,-m_2,-\lambda_2),$$

where

$$S(p_1,m_1,\lambda_1,p_2,m_2,\lambda_2) = \delta_{\lambda_1,-\lambda_2}s_{\lambda_1}(p_{1\zeta},p_{2\zeta}) + \delta_{\lambda_1,\lambda_2}\left(m_1\sqrt{\frac{2\zeta p_2}{2\zeta p_1}}+m_2\sqrt{\frac{2\zeta p_1}{2\zeta p_2}}\right). \tag{A8}$$

In our spinor algebra we shall exploit the completeness relations

$$\not{p}+m=\sum_\lambda u(p,\lambda)\overline{u}(p,\lambda),\quad \not{p}-m=\sum_\lambda v(p,\lambda)\overline{v}(p,\lambda),$$
$$\not{k}=\sum_\lambda u(k,\lambda)\overline{u}(k,\lambda),\quad k^2=0. \tag{A9}$$

For a circularly polarized photon with four-momentum k and helicity $\sigma=\pm1$ we adopt the KS choice (see also Ref. [58]) of the polarization vector[30]

$$[\epsilon^\mu_\sigma(\beta)]^*=\frac{\overline{u}_\sigma(k)\gamma^\mu u_\sigma(\beta)}{\sqrt{2}\overline{u}_{-\sigma}(k)u_\sigma(\beta)},$$
$$[\epsilon^\mu_\sigma(\zeta)]^*=\frac{\overline{u}_\sigma(k)\gamma^\mu \mathrm{u}_\sigma(\zeta)}{\sqrt{2}\overline{u}_{-\sigma}(k)\mathrm{u}_\sigma(\zeta)}, \tag{A10}$$

where β is an arbitrary light-like four-vector $\beta^2=0$. The second choice with $\mathrm{u}_\sigma(\zeta)$ (not exploited in [24]) often leads to simplifications in the resulting photon emission amplitudes. Using the Chisholm identity[31]

$$\overline{u}_\sigma(k)\gamma_\mu u_\sigma(\beta)\gamma^\mu=2u_\sigma(\beta)\overline{u}_\sigma(k)+2u_{-\sigma}(k)\overline{u}_{-\sigma}(\beta), \tag{A11}$$

$$\overline{u}_\sigma(k)\gamma_\mu \mathrm{u}_\sigma(\zeta)\gamma^\mu=2\mathrm{u}_\sigma(\zeta)\overline{u}_\sigma(k)-2u_{-\sigma}(k)\overline{\mathrm{u}}_{-\sigma}(\zeta), \tag{A12}$$

we get two useful expressions, equivalent to Eq. (A10):

$$[\not{\epsilon}_\sigma(k,\beta)]^*=\frac{\sqrt{2}}{\overline{u}_{-\sigma}(k)u_\sigma(\beta)}[u_\sigma(\beta)\overline{u}_\sigma(k) + u_{-\sigma}(k)\overline{u}_{-\sigma}(\beta)] \tag{A13}$$

$$[\not{\epsilon}_\sigma(k,\zeta)]^*=\frac{\sqrt{2}}{\sqrt{2\zeta k}}[\mathrm{u}_\sigma(\zeta)\overline{u}_\sigma(k)-u_{-\sigma}(k)\overline{\mathrm{u}}_{-\sigma}(\zeta)].$$

In the evaluation of photon emission spin amplitudes, we shall use the following important building blocks—the elements of the ''transition matrices'' U and V defined as

[30]Contrary to other papers on Weyl spinor techniques [24,59], we keep here the explicitly complex conjugation in ϵ. This conjugation is canceled by another, following Feynman rules, but only for outgoing photons, not for a beam photon, as in the Compton process, see Ref. [60].

[31]For $\beta=\zeta$ the identity is slightly different because of the additional minus sign in the ''line-reversal'' rule, i.e., $\overline{u}_\sigma(k)\gamma^\mu \mathrm{u}_\sigma(\zeta) = -\overline{\mathrm{u}}_{-\sigma}(\zeta)\gamma^\mu u_{-\sigma}(k)$, in contrast to the usual $\overline{u}_\sigma(k)\gamma^\mu u_\sigma(\beta)= +\overline{u}_{-\sigma}(\beta)\gamma^\mu u_{-\sigma}(k)$.

$$\overline{u}(p_1,\lambda_1)\not{\epsilon}^*_\sigma(k,\beta)u(p_2,\lambda_2)=U\left(\begin{matrix}k\\ \sigma\end{matrix}\right)\left[\begin{matrix}p_1p_2\\ \lambda_1\lambda_2\end{matrix}\right]=U^\sigma_{\lambda_1,\lambda_2}(k,p_1,m_1,p_2,m_2),$$
$$\overline{v}(p_1,\lambda_1)\not{\epsilon}^*_\sigma(k,\zeta)v(p_2,\lambda_2)=V\left(\begin{matrix}k\\ \sigma\end{matrix}\right)\left[\begin{matrix}p_1p_2\\ \lambda_1\lambda_2\end{matrix}\right]=V^\sigma_{\lambda_1,\lambda_2}(k,p_1,m_1,p_2,m_2). \tag{A14}$$

In the case of $u_\sigma(\zeta)$ the above transition matrices are rather simple:[32]

$$U^+(k,p_1,m_1,p_2,m_2)=\sqrt{2}\begin{bmatrix}\sqrt{\frac{2\zeta p_2}{2\zeta k}}s_+(k,\hat{p}_1), & 0\\ m_2\sqrt{\frac{2\zeta p_1}{2\zeta p_2}}-m_1\sqrt{\frac{2\zeta p_2}{2\zeta p_1}}, & \sqrt{\frac{2\zeta p_1}{2\zeta k}}s_+(k,\hat{p}_2)\end{bmatrix}, \tag{A15}$$

$$U^-_{\lambda_1,\lambda_2}(k,p_1,m_1,p_2,m_2)=[-U^+_{\lambda_2,\lambda_1}(k,p_2,m_2,p_1,m_1)]^*, \tag{A16}$$

$$V^\sigma_{\lambda_1,\lambda_2}(k,p_1,m_1,p_2,m_2)=U^\sigma_{-\lambda_1,-\lambda_2}(k,p_1,-m_1,p_2,-m_2). \tag{A17}$$

The more general case with $u_\sigma(\beta)$ looks a little bit more complicated:

$$U^+(k,p_1,m_1,p_2,m_2)=\sqrt{\frac{2}{s_-(k,\beta)}}\times\begin{bmatrix}s_+(\hat{p}_1,k)s_-(\beta,\hat{p}_2)+m_1m_2\sqrt{\frac{2\zeta\beta}{2\zeta p_1}\frac{2\zeta k}{2\zeta p_2}} & m_1\sqrt{\frac{2\zeta\beta}{2\zeta p_1}}s_+(k,\hat{p}_2)+m_2\sqrt{\frac{2\zeta\beta}{2\zeta p_2}}s_+(\hat{p}_1,k)\\ m_1\sqrt{\frac{2\zeta k}{2\zeta p_1}}s_-(\beta,\hat{p}_2)+m_2\sqrt{\frac{2\zeta k}{2\zeta p_2}}s_-(\hat{p}_1,\beta) & s_-(\hat{p}_1,\beta)s_+(k,\hat{p}_2)+m_1m_2\sqrt{\frac{2\zeta\beta}{2\zeta p_1}\frac{2\zeta k}{2\zeta p_2}}\end{bmatrix}, \tag{A18}$$

with the same relations (A16) and (A17).

In the above the following numbering of elements in matrices U and V was adopted

$$\{(\lambda_1,\lambda_2)\}=\begin{bmatrix}(++) & (+-)\\ (-+) & (--)\end{bmatrix}. \tag{A19}$$

When analyzing (multi) bremsstrahlung amplitudes we shall also often employ the following compact notation:

$$U\left[\begin{matrix}pkp\\ \lambda_1\sigma\lambda_2\end{matrix}\right]=U^\sigma_{\lambda_1,\lambda_2}(k,p_1,m_1,p_2,m_2),$$

$$V\left[\begin{matrix}pkp\\ \lambda_1\sigma\lambda_2\end{matrix}\right]=V^\sigma_{\lambda_1,\lambda_2}(k,p_1,m_1,p_2,m_2). \tag{A20}$$

When analyzing the soft real photon limit we shall exploit the following important *diagonality* property:[33]

$$U\left[\begin{matrix}pkp\\ \lambda_1\sigma\lambda_2\end{matrix}\right]=V\left[\begin{matrix}pkp\\ \lambda_1\sigma\lambda_2\end{matrix}\right]=b_\sigma(k,p)\,\delta_{\lambda_1\lambda_2}, \tag{A21}$$

$$b_\sigma(k,p)=\sqrt{2}\frac{\overline{u}_\sigma(k)\not{p}u_\sigma(\zeta)}{\overline{u}_{-\sigma}(k)u_\sigma(\zeta)}=\sqrt{2}\sqrt{\frac{2\zeta p}{2\zeta k}}s_\sigma(k,\hat{p}), \tag{A22}$$

which also holds in the general case of $u_\sigma(\beta)$, where

$$b_\sigma(k,p)=\frac{\sqrt{2}}{s_{-\sigma}(k,\beta)}\left(s_{-\sigma}(\beta,\hat{p})s_\sigma(\hat{p},k)+\frac{m^2}{2\zeta\hat{p}}\sqrt{(2\beta\zeta)(2\zeta k)}\right). \tag{A23}$$

[32]Our U and V matrices are not the same as the M matrices of Ref. [25], but rather are products of several of those.

[33]Let us also keep in mind the relation $b_{-\sigma}(k,p)=-[b_\sigma(k,p)]^*$, which can save time in the numerical calculations.

[1] S. Jadach, Z. Wąs, and B.F.L. Ward, Comput. Phys. Commun. **130**, 260 (2000); source version 4.13 available from http://home.cern.ch/jadach

[2] S. Jadach, B.F.L. Ward, and Z. Wąs, hep-ph/9905452.

[3] S. Jadach, B.F.L. Ward, and Z. Wąs, Phys. Lett. B **449**, 97 (1999).

[4] S. Jadach and B. Ward, in *Electroweak Physics*, Proceedings of Sussex University Conference, edited by N. Dombey and F. Boudjema (Plenum, London, 1989).

[5] D. Bardin *et al.*, Comput. Phys. Commun. **133**, 229 (2001).

[6] S. Jadach and B.F.L. Ward, Phys. Rev. D **38**, 2897 (1988).

[7] S. Jadach and B.F.L. Ward, Comput. Phys. Commun. **56**, 351 (1990).

[8] D.R. Yennie, S. Frautschi, and H. Suura, Ann. Phys. (N.Y.) **13**, 379 (1961).

[9] S. Jadach and B.F.L. Ward, Phys. Lett. B **274**, 470 (1992).

[10] S. Jadach, B.F.L. Ward, and Z. Wąs, Comput. Phys. Commun. **79**, 503 (1994).

[11] S. Jadach, E. Richter-Was, B.F.L. Ward, and Z. Wąs, Comput. Phys. Commun. **70**, 305 (1992).

[12] S. Jadach *et al.*, Comput. Phys. Commun. **102**, 229 (1997).

[13] S. Jadach and B.F.L. Ward, Acta Phys. Pol. B **28**, 1907 (1997).

[14] D. Bardin *et al.*, Comput. Phys. Commun. **59**, 303 (1989).

[15] F.A. Berends and R. Kleiss, Nucl. Phys. **B177**, 237 (1981).

[16] F.A. Berends, R. Kleiss, and S. Jadach, Comput. Phys. Commun. **29**, 185 (1983).

[17] F. Berends, R. Kleiss, and S. Jadach, Nucl. Phys. **B202**, 63 (1982).

[18] F. Berends, W. Van Neerven, and G. Burgers, Nucl. Phys. **B297**, 429 (1988).

[19] S. Jadach, E. Richter-Wąs, B.F.L. Ward, and Z. Wąs, Phys. Rev. D **44**, 2669 (1991).

[20] E. Richter-Wąs (private communication); and (unpublished).

[21] E. Richter-Wąs, Z. Phys. C **61**, 323 (1994).

[22] M. Greco, G. Pancheri-Srivastava, and Y. Srivastava, Nucl. Phys. **B101**, 234 (1975).

[23] M. Greco, G. Pancheri-Srivastava, and Y. Srivastava, Nucl. Phys. **B171**, 118 (1980); **B197**, 543(E) (1982).

[24] R. Kleiss and W.J. Stirling, Nucl. Phys. **B262**, 235 (1985).

[25] R. Kleiss and W.J. Stirling, Phys. Lett. B **179**, 159 (1986).

[26] S. Jadach and Z. Wąs, Acta Phys. Pol. B **15**, 1151 (1984); **16**, 483(E) (1985).

[27] S. Jadach, Z. Wąs, R. Decker, and J.H. Kühn, Comput. Phys. Commun. **76**, 361 (1993).

[28] S. Jadach, Acta Phys. Pol. B **16**, 1007 (1985).

[29] G. Burgers (private communication).

[30] S. Jadach, W. Płaczek, and B.F.L. Ward, Phys. Lett. B **390**, 298 (1997). The Monte Carlo program BHWIDE is available from http://hephp01.phys.utk.edu/pub/BHWIDE

[31] S. Jadach, W. Płaczek, M. Skrzypek, and B.F.L. Ward, Phys. Rev. D **54**, 5434 (1996).

[32] S. Jadach *et al.*, Phys. Lett. B **417**, 326 (1998).

[33] Z. Wąs, Acta Phys. Pol. B **18**, 1099 (1987).

[34] R.W. Brown, R. Decker, and E.A. Paschos, Phys. Rev. Lett. **52**, 1192 (1984).

[35] S. Jadach and Z. Wąs, Comput. Phys. Commun. **36**, 191 (1985).

[36] V.A. Smirnov and O.L. Veretin, Nucl. Phys. **B566**, 469 (2000).

[37] R. Barbieri, J. Mignaco, and E. Remiddi, Nuovo Cimento Soc. Ital. Fis., A **11**, 824 (1972).

[38] G. Burgers, Phys. Lett. **164B**, 167 (1985).

[39] F. Berends, G. Burgers, and W. Van Neerven, Phys. Lett. B **177**, 1191 (1986).

[40] Z-PHYSICS at LEP1, edited by G. Altarelli, R. Kleiss, and C. Verzegnassi (CERN Report No. 89-08, Geneva, 1989), 3 vols.

[41] G. Montagna, O. Nicrosini, F. Piccinini, and G. Passarino, Comput. Phys. Commun. **117**, 278 (1999).

[42] J. Jackson and D. Scharre, Nucl. Instrum. Methods **128**, 13 (1975).

[43] E. Kuraev and V. Fadin, Yad. Fiz. **41**, 733 (1985) [Sov. J. Nucl. Phys. **41**, 466 (1985)].

[44] S. Jadach, M. Skrzypek, and B. Ward, Phys. Lett. B **257**, 173 (1991).

[45] M. Kobel *et al.*, ''Report of the two-fermion working group of the LEP2 Monte Carlo Workshop, 2000,'' hep-ph/0007180.

[46] S. Jadach (unpublished).

[47] P. Colas, R. Miquel, and Z. Wąs, Phys. Lett. B **246**, 541 (1990).

[48] DELPHI Collaboration, P. Abreu *et al.*, Eur. Phys. J. C **11**, 383 (1999).

[49] K. Ackerstaff *et al.*, Eur. Phys. J. C **2**, 441 (1998).

[50] G. Abbiendi *et al.*, Eur. Phys. J. C **6**, 1 (1999).

[51] OPAL Collaboration, G. Abbiendi *et al.*, Eur. Phys. J. C **13**, 553 (2000).

[52] S. Jadach *et al.*, Comput. Phys. Commun. **119**, 272 (1999).

[53] P. Holt, Z. Phys. C **72**, 31 (1996).

[54] P. Holt, Acta Phys. Pol. B **25**, 689 (1997).

[55] S. Jadach and Z. Wąs, Phys. Rev. D **41**, 1425 (1990).

[56] D. Buskulic *et al.*, Phys. Lett. B **378**, 373 (1996).

[57] S. Jadach *et al.*, Phys. Lett. B **465**, 254 (1999).

[58] Z. Xu, D.-H. Zhang, and L. Chang, Nucl. Phys. **B291**, 392 (1987).

[59] CALKUL Collaboration, F.A. Berends *et al.*, Phys. Lett. **103B**, 124 (1981); **105B**, 215 (1981); **114B**, 203 (1982); Nucl. Phys. **B206**, 53 (1982); **B206**, 61 (1982); **B239**, 382 (1984).

[60] A. Góngora and R.G. Stuart, Z. Phys. C **42**, 617 (1989).

[61] A. Pukhov *et al.*, ''CompHEP: A package for evaluation of Feynman diagrams and integration over multi-particle phase space. User's manual for version 33,'' hep-ph/9908288.

[62] T. Ishikawa, T. Kaneko, K. Kato, S. Kawabata, Y. Shimizu, and H. Tanaka, ''GRACE Manual,'' KEK Report No. 92-19, 1993.